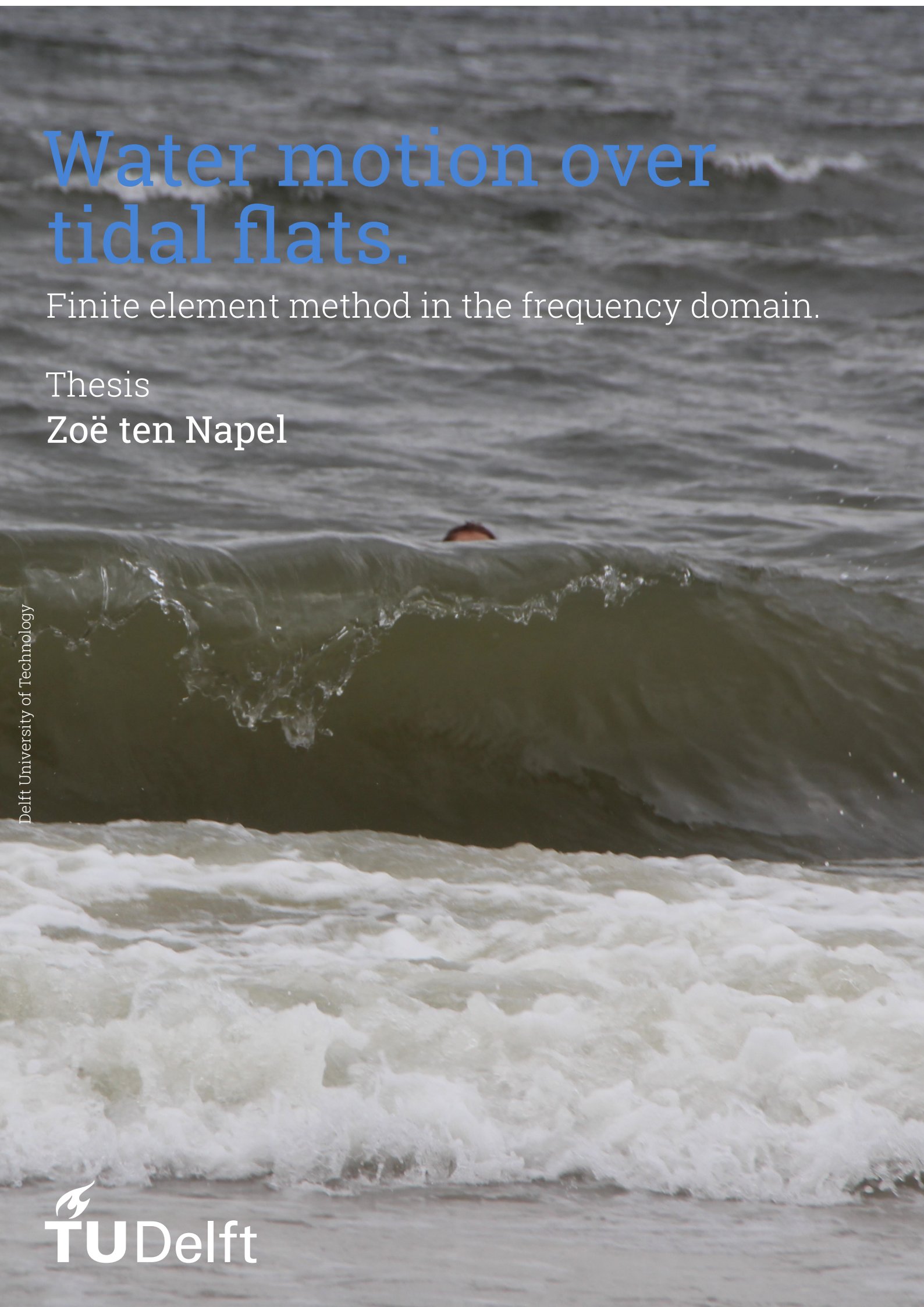

# Water motion over tidal flats.

Finite element method in the frequency domain.

Thesis

**Zoë ten Napel**

Delft University of Technology

TU Delft

# Water motion over tidal flats.

## Finite element method in the frequency domain.

by

Zoë ten Napel

to obtain the degree of Master of Science
at the Delft University of Technology,
to be defended publicly on Friday June 9, 2023 at 15:00.

Student number: 4590341

Project duration: September 1, 2022 – June 9, 2023

Thesis committee: Prof. dr. H.M. Schuttelaars, TU Delft, supervisor
Prof. dr. ir. M.B. van Gijzen, TU Delft

*This thesis is confidential and cannot be made public until June 8, 2023.*



TU Delft

# Preface

*Before diving into the mathematics, I would like to acknowledge how this thesis came about and thank the people who made it possible.*
*While writing this thesis, there were times that the tide was too high, much higher than physically expected. Both in the water motion predictions as in my mental abilities, I often thought 'the tide is high'. However, with the support of my professor, friends and family and the great lyrics of Atomic Kittens, I kept holding on.*
*First of all, I would like to thank my supervisors Henk and Martin. Their positive feedback and support, made this research fun even when I was hopelessly stuck. I would especially like to thank Henk. Henk, I am grateful to your endless pushes in the right direction even when I was being too stubborn to start simple. Our meetings on Monday morning, not only provided me with the necessary caffeine, but also with the motivation and knowledge I needed for a productive week.*
*As my time as a student comes to an end, I would like to commmemorate all my friends I met over the years. There are too many to all thank individually, but they are the reason that I believe coming to Delft is the best choice I ever made. Thank you for being there, being my family and my partners in crime. While we might not see each other as much as we did in the years to come, I trust there are many more adventures to come.*
*In particular, I would like to thank Giulia. While we both studied applied mathematics, our extreme differences in speciality and subjects of our theses proved for interesting study sessions. I believe we could have made a successful sitcom. Thank you for having the best study faces, listening to my frustrations and motivating me when I needed it.*
*Last but surely not least, I would like to thank my family. Your love and support has allowed me to develop into the person I am. Thank you for being there and listening to all my highs and lows.*
*Reflecting on my time in Delft, I will miss it immensely, but I look forward to the next chapter.*

*Zoë ten Napel*
*Delft, June 2023*

# Abstract

Tidal flats are important coastal ecosystems that support a diverse range of plants and animals. Accurate prediction of water motion over tidal flats is crucial for the design of coastal infrastructure, hazard assessment, environmental management and oceanography research. Defina [1] derived a new set of shallow water equations that allow for water motion prediction in partially dry domains. Existing methods for predicting water motion are limited by numerical stability and accuracy, and require high-quality input data. Using the periodic behaviour of tides, this thesis introduces a new method in the frequency domain. The method is tested and compared to a fully numerical solution. The results of the linearised classical shallow water equations encourage future research required for the statistical shallow water equations that allow partially dry domains.

# Contents

# Nomenclature

## Abbreviations

| Abbreviation | Definition |
|---|---|
| RANS | Reynolds-Averaged Navier-Stokes |
| NAP | Normaal Amsterdams Peil |

## Operators

| Symbol | Name | Definition |
|---|---|---|
| $\nabla$ | Gradient | $\left(\frac{\partial}{\partial x}, \frac{\partial}{\partial y}, \frac{\partial}{\partial y}\right)^T$ |
| $\Delta$ | Laplace Operator | $\frac{\partial^2}{\partial x^2} + \frac{\partial^2}{\partial y^2} + \frac{\partial^2}{\partial z^2}$ |

## Symbols

| Symbol | Definition | Unit |
|---|---|---|
| $u$ | Velocity | [m/s] |
| $p$ | Pressure | [kg/s$^2$ m] |
| $\nu$ | Kinematic viscosity | [m$^2$/s] |
| $\rho$ | Density | [kg/m$^3$] |
| $g$ | Gravitational force | [m/s$^2$] |
| $K_s$ | Strickler coefficient | [s/m$^3$] |

# 1

# Introduction

Tidal flats are areas of land that are intermittently submerged and exposed due to the ebb and flow of tides. These areas are characterised by their dynamic nature, with water levels constantly changing due to the gravitational pull of the moon and the sun. They are important ecosystems, supporting a diverse array of plants and animals that have adapted to the challenging conditions of living in the intertidal zone. It is of vital importance to understand and predict the water motion over tidal flats.

Accurate predictions of the water motion are essential for many applications.

1. One of the applications of water motion prediction is in the design of coastal infrastructure such as ports, harbours, and breakwaters. Accurate predictions of water motion are essential to ensure that these structures are built to withstand the forces of waves and tides, protecting ships and cargo from damage.
2. Also, an accurate water motion prediction is important for coastal hazard assessment, in order to predict the impacts of storm surges and tsunamis. Accurate predictions can help inform evacuation planning and emergency response, potentially saving lives and reducing damage to infrastructure.
3. In addition, understanding water motion is important for the management of coastal ecosystems. Changes in water motion can affect the distribution of sediment, which can impact the habitats of aquatic species. Predicting changes in water motion due to climate change can also inform management strategies for preserving coastal ecosystems and protecting biodiversity.
4. Furthermore, water motion prediction plays a role in oceanography research, such as understanding the transport of pollutants, nutrients, and planktonic organisms. The cyanobacteria present in tidal flats possess the ability to convert atmospheric nitrogen into a usable form for other organisms inhabiting these areas. Much of this escapes to the surrounding areas, and the daily ebb and flow of the tides takes these nutrients into coastal waters [2]. Accurate predictions of water motion are necessary to develop models that can predict the behaviour of these substances in the ocean, which can have important implications for human health and the environment.

In summary, water motion prediction is essential for a wide range of practical applications and for informing decision making, reducing risk, and helping protect coastal communities and ecosystems. In coastal regions, such as estuaries and tidal inlet systems, accurately predicting water motion on tidal flats is crucial to understanding the overall behaviour of tides and the effects they have on the ecology and economy of these regions.

Unfortunately, water motion on tidal flats is difficult to predict due to its small water depths and drying and flooding processes. First, most existing methods to predict water motion are restricted to solely wet domains. Additionally, problems arise with respect to numerical stability and accuracy. Most existing water motion prediction methods are numerical methods consisting of space and time discretisation. One of the main limitations is the need for many discretisation steps in both space and time. Accurate results require a more refined grid in space. In turn, to obtain stable results, many discretisation steps in time are required. These methods are computationally intensive and require powerful computers and software, which can be costly and limit their accessibility. Another limitation is that the models are only as good as the input data and assumptions made. High-quality input data,

accurate bathymetry, wind, and current data are required to initialise the model and ensure accurate predictions. Complex phenomena such as turbulence and wave-breaking are difficult to model accurately, and small errors in the initial conditions or boundary conditions can have a significant impact on the accuracy of the predictions.

In 2000, Defina derived shallow water equations specifically designed to be applied to partially dry domains [1]. In these equations, parameters are approximated statistically using physical knowledge. This contrasts previous methods that assume the domain is either wet or dry. These new equations allow for the prediction of water motion on tidal flats.

The other limitations motivate the need for a method that does not require discretisation in time. The periodic behaviour of tides justify methods in the frequency domain. In this thesis a method is developed and tested using discretisation in space within the frequency domain. This facilitates both stability and accuracy, without being computationally intensive.

## Thesis structure

Firstly, the behaviour of tides is described and analysed to justify the description of tides over time in the frequency domain. Chapter 2 provides a physical explanation and analysis of tides. The Wadden Sea is the largest area of connected tidal flats in the world, extending over a length of approximately 500 km [3]. Therefore, examples from this area are used to analyse the tidal behaviour. For later predictions, the most prominent tidal constituents are distinguished. In Chapter 3 and Chapter 4, the equations to model water motion in shallow waters are derived. Chapter 4 distinguishes the classical shallow water equations which are restricted to solely wet domains, and the statistical shallow water equations as described in [1]. In Chapter 5 the classical shallow water equations are linearised and used to predict water motion. Three solution methods are obtained: an analytical solution, a fully numerical solution and a solution in the frequency domain. Finally, in Chapter 6 the statistical shallow water equations are used to predict water motion using a fully numerical method and a finite element method in the frequency domain. Chapter 7 concludes the obtained results discusses possibilities for future research.

# 2

# Tides

This chapter provides a physical explanation and analysis of tides. The first section, Section 2.1, provides an explanation of the driving forces for the tides. In Section 2.2 the tidal signals at two measurement stations at the Wadden Sea are analysed. This section shows which tidal constituents are most important for the water motion over tidal flats and predicts the water motion based on these found frequencies and associated amplitudes and phases. These findings support frequency approximation as a method to predict water motion used in subsequent chapters.

## 2.1 Tidal forcing

Tides are mainly caused by the gravitational forces between the earth, the moon and the sun. These forces combined cause many different types of tides that each play a role in the water motion. In this section we discuss different tidal constituents and how they relate to the celestial motion.

Even though the sun is much larger than the moon, due to the larger distance between the sun and earth, the most dominant tidal signals are caused by the forces between the earth and the moon. The moon has a large gravitational pull on the earth. The moon pulls on each part of the earth, but the strength of this pull varies due to the varying distance between the earth and the moon at different locations. The small blue vectors in Fig. 2.1 show the gravitational pull of the moon on each part of the earth where the vectors indicate the strength and direction of the force. The force on the earth is greater on the parts of the earth which are closer to the moon than on the parts of the earth further away from the moon. Meanwhile, the earth rotates around the center of mass causing centrifugal force, these are indicated by the yellow lines in Fig. 2.1. The forces combined are what cause the tides.

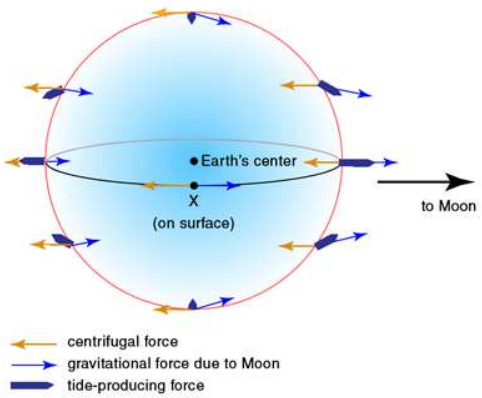


**Fig. 2.1:** Tidal forces between the moon and the earth. The blue vectors show the gravitational forces on the earth due to the gravitational pull of the moon. The yellow vectors show the centrifugal force due to the rotation of the earth. The bold blue vectors show the tide producing forces. Adapted from [4].

Combining the centrifugal forces of the earth with the gravitational forces due to the pull from the moon, results in the tide-producing force. Fig. 2.2 shows only these tide -producing forces. Note that the tides are not caused by water being pulled towards the moon, but rather by water being squeezed towards the sides of the earth. There are two high tides and two low tides during each day. Due to the periodicity of the high and low tides indicated, these tides are called semidiurnal.

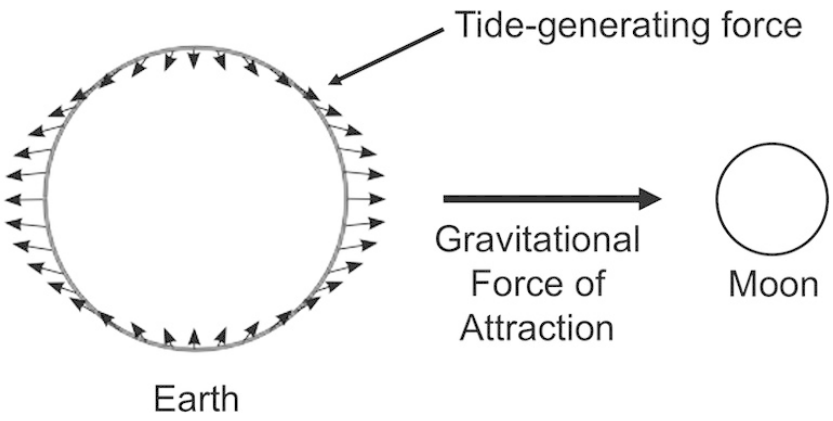


**Fig. 2.2:** Tide producing forces showing two high and low tides a day. The high tides in this figure can be observed at the side of the earth, while the low tides are at the top and bottom of the earth. Courtesy of [5].

Besides the moon, the sun also has a gravitational pull on the earth albeit smaller than the moon due to the larger distance between the sun and the earth, even thought the mass of the sun is much larger than that of the moon. The rotations of the earth and moon relative to the sun cause different periods and therefore different types of forces. Combinations of these forces cause many different types of tides which all have their own frequency. The main tidal constituents are listed in Tab. 2.3. For more details and explanations on their derivation, see Chapter 3 and 4 of [6].

| Name | Symbol | Period (h) | Speed (°/h) |
|---|---|---|---|
| *Higher Harmonics* | | | |
| Shallow water overtides of principal lunar | $M_4$ | 6.210300601 | 57.9682084 |
| Shallow water overtides of principal lunar | $M_6$ | 4.140200401 | 86.9523127 |
| Shallow water terdiurnal | $MK_3$ | 8.177140247 | 44.0251729 |
| Shallow water overtides of principal solar | $S_4$ | 6 | 60 |
| Shallow water quarter diurnal | $MN_4$ | 6.269173724 | 57.4238337 |
| Shallow water overtides of principal solar | $S_6$ | 4 | 90 |
| Lunar terdiurnal | $M_3$ | 8.280400802 | 43.4761563 |
| Shallow water terdiurnal | $2''MK_3$ | 8.38630265 | 42.9271398 |
| Shallow water eighth diurnal | $M_8$ | 3.105150301 | 115.9364166 |
| Shallow water quarter diurnal | $MS_4$ | 6.103339275 | 58.9841042 |
| *Semi-Diurnal* | | | |
| Principal lunar semidiurnal | $M_2$ | 12.4206012 | 28.9841042 |
| Principal solar semidiurnal | $S_2$ | 12 | 30 |
| Larger lunar elliptic semidiurnal | $N_2$ | 12.65834751 | 28.4397295 |
| Larger lunar evectional | $\nu_2$ | 12.62600509 | 28.5125831 |
| Variational | $MU_2$ | 12.8717576 | 27.9682084 |
| Lunar elliptical semidiurnal second-order | $2''N_2$ | 12.90537297 | 27.8953548 |
| Smaller lunar evectional | $\lambda_2$ | 12.22177348 | 29.4556253 |
| Larger solar elliptic | $T_2$ | 12.01644934 | 29.9589333 |
| Smaller solar elliptic | $R_2$ | 11.98359564 | 30.0410667 |
| Shallow water semidiurnal | $2SM_2$ | 11.60695157 | 31.0158958 |
| Smaller lunar elliptic semidiurnal | $L_2$ | 12.19162085 | 29.5284789 |
| Lunisolar semidiurnal | $K_2$ | 11.96723606 | 30.0821373 |
| *Diurnal* | | | |
| Lunar diurnal | $K_1$ | 23.93447213 | 15.0410686 |
| Lunar diurnal | $O_1$ | 25.81933871 | 13.9430356 |
| Lunar diurnal | $OO_1$ | 22.30608083 | 16.1391017 |
| Solar diurnal | $S_1$ | 24 | 15 |
| Smaller lunar elliptic diurnal | $M_1$ | 24.84120241 | 14.4920521 |
| Smaller lunar elliptic diurnal | $J_1$ | 23.09848146 | 15.5854433 |
| Larger lunar evectional diurnal | $\rho$ | 26.72305326 | 13.4715145 |
| Larger lunar elliptic diurnal | $Q_1$ | 26.86835 | 13.3986609 |
| Larger elliptic diurnal | $2Q_1$ | 28.00621204 | 12.8542862 |
| Solar diurnal | $P_1$ | 24.06588766 | 14.9589314 |
| *Long Period* | | | |
| Lunar monthly | $M_m$ | 661.3111655 | 0.5443747 |
| Solar semiannual | $S_{sa}$ | 4383.076325 | 0.0821373 |
| Solar annual | $S_a$ | 8766.15265 | 0.0410686 |
| Lunisolar synodic fortnightly | $M_{sf}$ | 354.3670666 | 1.0158958 |
| Lunisolar fortnightly | $M_f$ | 327.8599387 | 1.0980331 |

**Fig. 2.3:** Main tidal constituents and their characteristics, courtesy of [7].

The semidiurnal, diurnal and long period frequencies follow immediately from tide-producing forces, while the higher harmonics are not directly forced but caused by nonlinear interactions amongst the various tidal constituents.

## 2.2 Tidal analysis

The water motion typically consists of all the tidal constituents discussed in the previous section, but some have a much larger amplitude than others. This means that the water motion can be approximated and predicted by only considering some tidal constituents. In order to get an indication of the most important tidal constituents, the amplitudes corresponding to tidal constituents have to be analysed.
Measurements of the tides around the Wadden Sea have been documented for many years. These measurement focus on the height of the water at a certain place as a function of time. Using these measurements, one can analyse which tidal constituents dominate the tidal signal by calculating the amplitudes and phases of these tidal constituents. We will use Pytides (see [8]) to do this analysis. Pytides uses least-squares analysis to estimate the tidal harmonic constituent amplitudes and phases, which can then be used for long-term tidal predictions. For this analysis it is important to note that the Rayleigh criterion must apply. This criterion requires that all the constituents included in the harmonic analysis of a given time series must be separated by at least one complete period from their neighbouring constituents over the length of data record. Thus the data for analysis needs to include measurements over a long enough time period. For more details on the Rayleigh criterion, see Appendix A. Measurements of a year should be long enough to distinguish the most important constituents. The tide can be described as a combination of tidal constituents such that

$$Tide = \sum_{c \in C} A_c \cos(\omega_c t + \phi_c) \tag{2.1}$$

where $c$ denotes a tidal constituents and $\omega_c$, $A_c$, $\phi_c$ are its corresponding radial frequency, amplitude and phase, respectively. The radial frequency of each constituent is known and can be found in Tab. 2.3

### 2.2.1 Vlieland haven

As an example, analysis of the measurements of Vlieland Haven of the year 2021 have been used to predict the behaviour of January 2022. The data is found on `https://waterinfo.rws.nl/`, it consists of water heights measurements relative to the Normaal Amsterdams Peil (NAP) in centimetres measured every ten minutes. Using Pytides we find the tidal constituents with their corresponding amplitudes and phases, given in Tab. 2.1.

| | Amplitude | Phase | | | |
|---|---|---|---|---|---|
| M2 | 79.1141 | 266.965 | MN4 | 1.75474 | 348.492 |
| S2 | 21.6188 | 334.477 | T2 | 1.06381 | 313.301 |
| N2 | 13.0921 | 246.538 | M8 | 0.907275 | 254.359 |
| O1 | 9.11957 | 231.79 | 2MK3 | 0.80445 | 58.4601 |
| mu2 | 8.07076 | 347.607 | S1 | 0.560613 | 347.539 |
| K1 | 6.93113 | 31.6036 | MK3 | 0.381572 | 238.418 |
| L2 | 6.43188 | 261.165 | M1 | 0.359635 | 303.974 |
| K2 | 6.09486 | 333.157 | Mm | 0.220789 | 312.111 |
| M6 | 5.11405 | 134.184 | S4 | 0.218812 | 194.98 |
| M4 | 5.01637 | 10.4266 | R2 | 0.0936626 | 224.198 |
| nu2 | 4.3869 | 226.398 | Mf | 0.0844112 | 354.33 |
| MS4 | 3.12817 | 82.2713 | S6 | 0.0336934 | 350.095 |
| P1 | 2.88008 | 28.8841 | rho1 | 0.019659 | 338.537 |
| lambda2 | 2.746 | 274.911 | 2Q1 | 0.0155404 | 266.384 |
| Q1 | 2.67429 | 173.915 | J1 | 0.0140702 | 5.50577 |
| 2N2 | 2.45908 | 124.551 | OO1 | 0.0107199 | 39.594 |
| MSF | 2.0709 | 12.1177 | M3 | 0.00532511 | 31.5187 |
| 2SM2 | 1.8293 | 183.05 | Z0 | 1.21336e-15 | 180 |

**Table 2.1:** The tidal constituents and corresponding amplitudes and phases of Vlieland Haven 2021 determined using Pytides, sorted on the highest amplitude.

To validate the results, the amplitudes and phases found for the water heights of 2021 are now used to predict the water heights of 2022. The results of the prediction of the first month of 2022 for Vlieland Haven are given in Fig. 2.4.

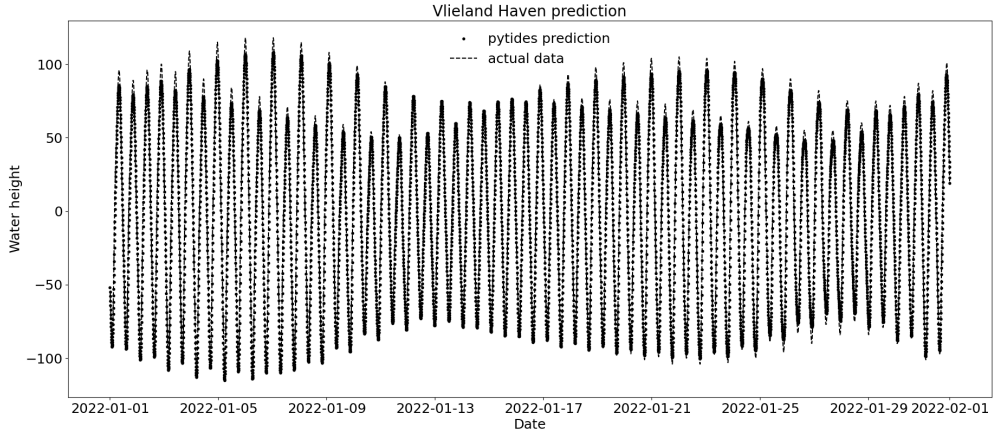


**Fig. 2.4:** Results of the prediction of the water heights for January of 2022, using pytides with the found amplitudes and phases given in Tab. 2.1.

The figure shows little difference between the measured water heights of January of 2022 and the predicted water heights of Vlieland Haven. Indeed, the prediction is quite accurate with a relative squared error of 0.012. This means that for prediction of the water motion, it is sufficient to consider

only the main constituents listed in Tab. 2.3. In this case this still requires 36 constituents, but the large difference in amplitudes given in Tab. 2.1 indicates that even less constituents might be sufficient. This will be tested using another example.

### 2.2.2 Oudeschild

To get a better indication of which constituents dominate tidal motion, we consider another example. Oudeschild is a coastal area in the middle of Texel bordering the Wadden Sea. The large Texel inlet passes this area. Using Pytides analysis of data of the water height measured during the year 2021, we find the tidal constituents with their corresponding amplitudes and phases, given in Tab. 2.2.

| | Amplitude | Phase | | | |
|---|---|---|---|---|---|
| M2 | 61.6982 | 215.068 | 2SM2 | 1.74955 | 126.035 |
| S2 | 16.9179 | 286.749 | M8 | 1.55759 | 77.191 |
| O1 | 10.4331 | 216.497 | T2 | 0.813689 | 257.054 |
| N2 | 9.62795 | 198.56 | S1 | 0.747885 | 340.181 |
| M4 | 9.19854 | 249.686 | 2MK3 | 0.436509 | 8.9238 |
| mu2 | 8.45751 | 297.109 | S4 | 0.413485 | 23.449 |
| K1 | 7.87698 | 19.8629 | M1 | 0.41347 | 279.857 |
| L2 | 5.76104 | 205.75 | MK3 | 0.282059 | 290.385 |
| MS4 | 5.35176 | 312.758 | Mm | 0.239 | 310.329 |
| K2 | 4.82984 | 283.574 | R2 | 0.0718669 | 175.43 |
| M6 | 4.3432 | 15.9295 | Mf | 0.0696008 | 351.348 |
| nu2 | 3.77175 | 171.638 | S6 | 0.0384042 | 224.205 |
| MSF | 3.46192 | 26.7443 | J1 | 0.021633 | 346.246 |
| P1 | 3.36487 | 13.2914 | rho1 | 0.0211328 | 308.682 |
| MN4 | 3.07704 | 227.436 | 2Q1 | 0.0159883 | 255.632 |
| Q1 | 2.97917 | 160.301 | M3 | 0.0137718 | 173.863 |
| lambda2 | 2.48117 | 221.3 | OO1 | 0.0107832 | 344.417 |
| 2N2 | 2.3081 | 72.2713 | Z0 | 0 | 0 |

**Table 2.2:** The tidal constituents and corresponding amplitudes and phases of Oudeschild 2021 determined using Pytides, sorted on the highest amplitude.

To validate the analysis, the amplitudes and phases are used to predict the water heights for January of 2022. Furthermore, the water heights are predicted using only a few constituents. Similar to the results for Vlieland Haven, there is a large difference in amplitudes indicating that the tides are dominated by the first few constituents listed in Tab. 2.2. In Fig. 2.5 the predictions of the water height are shown, considering all found constituents and only the first four constituents. Additionally, Fig. 2.6 shows the accuracy of the water height predictions based on the number of constituents considered.

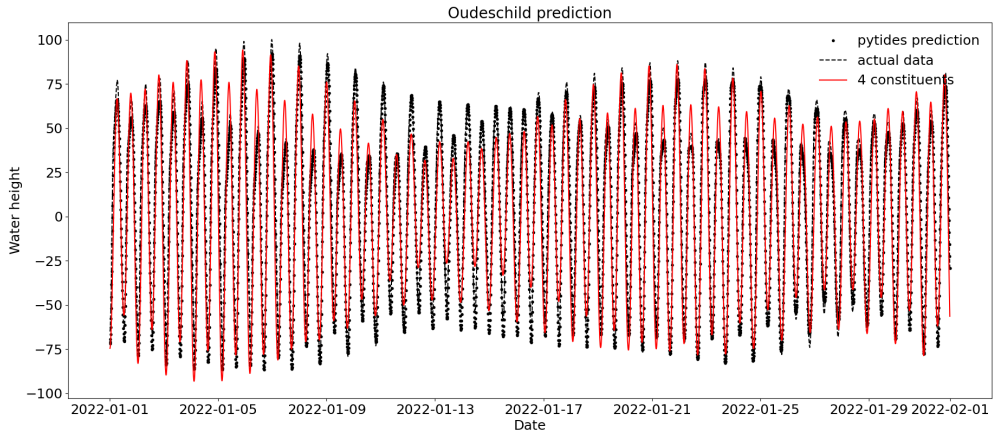


**Fig. 2.5:** Results of the prediction of the water heights for January of 2022, using Pytides with the found amplitudes and phases given in Tab. 2.2.

The relative squared error is 0.038 for the prediction that uses all found constituents and 0.128 for the prediction that only uses the four largest constituents.

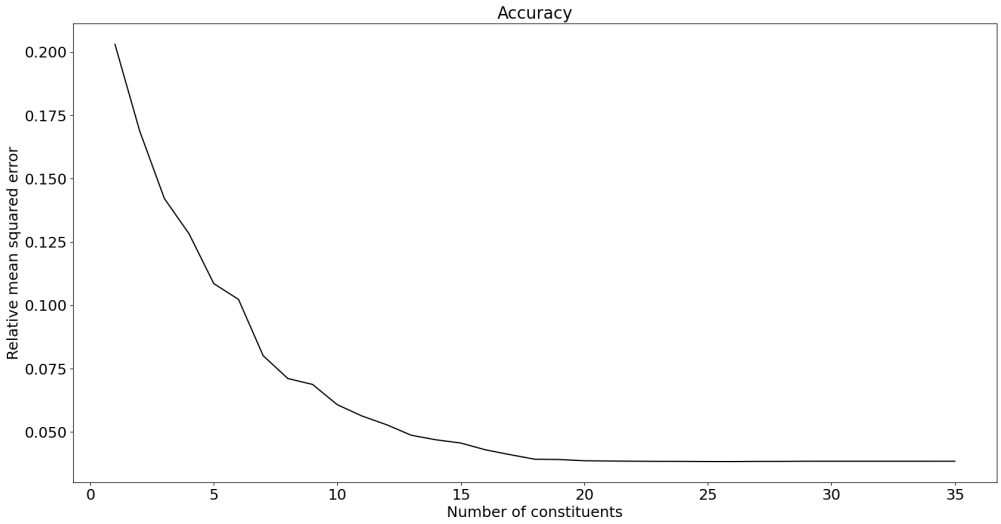


**Fig. 2.6:** Accuracy of the water height predictions depending on the number of considered constituents.

As can be seen in Tab. 2.2, the last 16 constituents have an amplitude smaller than one. Fig. 2.6 shows that including these constituents hardly increases the accuracy of the prediction. Even only considering the largest constituent, gives a prediction with a relative squared error of 0.203.
These examples show that an accurate prediction of water motion can be determined using the tidal constituents. If the amplitudes and phases of the constituents are known, there is no time integration needed to predict the water motion. Furthermore, the large difference in amplitudes of the tidal constituents indicates that the tides are dominated by a few constituents. Even considering a few tidal constituents, leads to accurate predictions of the water motion. These findings motivate a water motion prediction using frequency approximation.

# 3

# Water motion equations

The water motion is typically driven by various forcing terms, namely tides, density differences, wind, etc. In this chapter, the equations describing water motion will be discussed. Section 3.1 discusses the equations describing water motion for general areas. Next, in Section 3.2, the shallow water equations are derived from the general equations.

## 3.1 Water motion

To describe the water motion, the mass and momentum balance equations are used, which are discussed in detail in Section 3.1.1 and Section 3.1.2. Combining these balances results in equations that describe the water motion. In Section 3.1.3 the Coriolis effect is discussed and added to the equations to account for the rotation of the Earth. Finally, since the focus of this thesis will be on turbulence-averaged flow, in Section 3.1.4 Reynolds decomposition is applied to the equations.

### 3.1.1 Mass balance

The fluid flow $\mathbf{u}$ needs to satisfy the mass balance equation. We will use Cartesian coordinates and define $x$, $y$ as the horizontal spatial coordinates and $z$ as the vertical spatial coordinate. The fluid velocity in these coordinates is denoted by $\mathbf{u} = (u_x, u_y, u_z)^T$. The mass balance equation requires that the local storage of the water in volume $\Delta x \Delta y \Delta z$ per unit time needs to be equal to the net import of water in that control volume during time interval $\Delta t$. At low pressures, the variations in density in liquids are negligible and thus the water flow can be approximated as incompressible [9]. Since there is no local production of fluid, the resulting continuity equation reads:

$$\frac{\partial u_x}{\partial x} + \frac{\partial u_y}{\partial y} + \frac{\partial u_z}{\partial z} = 0. \tag{3.1}$$

### 3.1.2 Momentum balance

The momentum balance is obtained by considering the conservation of momentum, including the internal friction and forcing in the water. This results in the Navier Stokes equations, which read:

$$\frac{\partial u_x}{\partial t} + u_x\frac{\partial u_x}{\partial x} + u_y\frac{\partial u_x}{\partial y} + u_z\frac{\partial u_x}{\partial z} = -\frac{1}{\rho}\frac{\partial p}{\partial x} + \nu\left(\frac{\partial^2 u_x}{\partial x^2} + \frac{\partial^2 u_x}{\partial y^2} + \frac{\partial^2 u_x}{\partial z^2}\right), \tag{3.2a}$$

$$\frac{\partial u_y}{\partial t} + u_x\frac{\partial u_y}{\partial x} + u_y\frac{\partial u_y}{\partial y} + u_z\frac{\partial u_y}{\partial z} = -\frac{1}{\rho}\frac{\partial p}{\partial y} + \nu\left(\frac{\partial^2 u_y}{\partial x^2} + \frac{\partial^2 u_y}{\partial y^2} + \frac{\partial^2 u_y}{\partial z^2}\right), \tag{3.2b}$$

$$\frac{\partial u_z}{\partial t} + u_x\frac{\partial u_z}{\partial x} + u_y\frac{\partial u_z}{\partial y} + u_z\frac{\partial u_z}{\partial z} = -\frac{1}{\rho}\frac{\partial p}{\partial z} - g + \nu\left(\frac{\partial^2 u_z}{\partial x^2} + \frac{\partial^2 u_z}{\partial y^2} + \frac{\partial^2 u_z}{\partial z^2}\right), \tag{3.2c}$$

where $\rho$ denotes the fluid density, $p$ denotes the pressure, $\nu$ denotes the kinematic viscosity and $g$ is the gravitational acceleration [10]. Combining that with the continuity equation, we find the full system of

water motion equations

$$\begin{cases} \nabla \cdot \mathbf{u} & = 0, \\ \dfrac{\partial u_x}{\partial t} + \mathbf{u} \cdot \nabla u_x & = -\dfrac{1}{\rho}\dfrac{\partial p}{\partial x} + \nu \Delta u_x, \\ \dfrac{\partial u_y}{\partial t} + \mathbf{u} \cdot \nabla u_y & = -\dfrac{1}{\rho}\dfrac{\partial p}{\partial y} + \nu \Delta u_y, \\ \dfrac{\partial u_z}{\partial t} + \mathbf{u} \cdot \nabla u_z & = -\dfrac{1}{\rho}\dfrac{\partial p}{\partial z} - g + \nu \Delta u_z. \end{cases} \tag{3.3}$$

### 3.1.3 Coriolis parameters

The equations given in Section 3.1.2 are obtained in an inertial frame of reference, while we are interested in the fluid flow with respect to a coordinate system fixed to the rotating earth. The rotational speed with respect to the center of the earth depends on the place on earth. The speed increases for further distance from the center of the earth. The earth rotates at a rate

$$\Omega = 7.29 \times 10^{-5} s^{-1}$$

around the polar axis in a counterclockwise sense looking down from the north pole. The Coriolis parameter is associated with the Coriolis force. For eastward moving particles, the Coriolis force exerts a pull to the south in the northern hemisphere and to the north in the southern hemisphere. Similarly for northward moving particles, it exerts a pull to the east in the northern hemisphere and to the west in the southern hemisphere, etc. It is important to note that the Coriolis force does not initiate a motion and is only a deflecting force on a existing motion [6]. This deflecting force is visualised in Fig. 3.1.

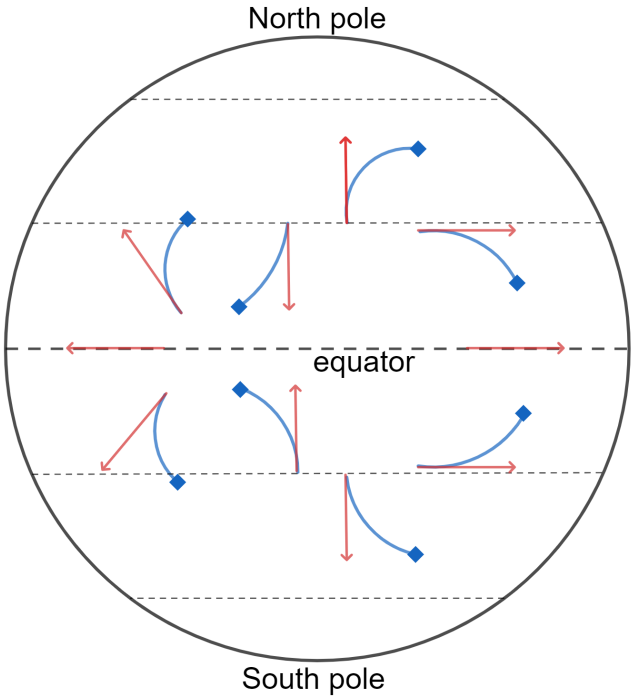


**Fig. 3.1:** The Coriolis effect visualised. The red lines show the expected path and the blue lines show the actual deflected paths due to the Coriolis effect.

As Fig. 3.1 shows, the deflection is largest at the poles and there is no deflection at the equator. We will use an $f$-plane approach to keep things simple. This approach considers smaller areas around a fixed latitude $\theta$. The components of angular velocity of the earth in the local Cartesian system are $\Omega = (\Omega_x, \Omega_y, \Omega_z) = (0, \Omega \cos\theta, \Omega \sin\theta)$, where $\theta$ is the latitude which is positive north of the equator and negative south of the equator. For such an area the Earth's surface can be regarded as fundamentally

flat. The Coriolis acceleration is therefore [11]

$$2\Omega \times u = \begin{vmatrix} e_x & e_y & e_z \\ 0 & 2\Omega\cos\theta & 2\Omega\sin\theta \\ u_x & u_y & u_z \end{vmatrix}. \tag{3.4}$$

This gives the three components of the Coriolis acceleration $(2\Omega u_z \cos\theta - 2\Omega u_y \sin\theta, 2\Omega u \sin\theta, -2\Omega u_x \cos\theta)$. We define the Coriolis parameter $f = 2\Omega\sin\theta$ and the reciprocal Coriolis parameter $f^* = 2\Omega\cos\theta$, and include these in our system Eq. (3.3), resulting in:

$$\begin{cases} \nabla \cdot \mathbf{u} & = 0, \\ \dfrac{\partial u_x}{\partial t} + \mathbf{u}\cdot\nabla u_x + f^* u_z - f u_y & = -\dfrac{1}{\rho}\dfrac{\partial p}{\partial x} + \nu\Delta u_x, \\ \dfrac{\partial u_y}{\partial t} + \mathbf{u}\cdot\nabla u_y + f u_x & = -\dfrac{1}{\rho}\dfrac{\partial p}{\partial y} + \nu\Delta u_y, \\ \dfrac{\partial u_z}{\partial t} + \mathbf{u}\cdot\nabla u_z - f^* u_x & = -\dfrac{1}{\rho}\dfrac{\partial p}{\partial z} - g + \nu\Delta u_z. \end{cases} \tag{3.5}$$

### 3.1.4 Reynolds decomposition

In our model, turbulent eddies will be present, causing small scale motions where the velocities and pressure fluctuate on the turbulent length- and timescale. We are not interested in these turbulent fluctuations, but in the turbulence-averaged flow. To be able to focus on the turbulence averaged flow, we apply the Reynolds decomposition to the system of equations to separate the expectation value from its fluctuations. This results in the Reynolds-averaged Navier-Stokes equations (RANS).
As a first step in this averaging procedure, the velocities $\mathbf{u}$ are split into the time-averaged values $\overline{\mathbf{u}}$ and the fluctuating velocities $\mathbf{u}'$. The decomposition of the velocities and the pressure $p$ can now be written as:

$$u_x = \overline{u}_x + u'_x, \qquad u_y = \overline{u}_y + u'_y, \qquad u_z = \overline{u}_z + u'_z, \qquad p = \overline{p} + p'.$$

The following properties must hold for all turbulent quantities $f$ and $g$:

$$\overline{\overline{f}} = \overline{f}, \qquad \overline{f+g} = \overline{f} + \overline{g}, \qquad \overline{\overline{f}\,g} = \overline{f}\,\overline{g}, \qquad \overline{\frac{\partial f}{\partial s}} = \frac{\partial}{\partial s}\overline{f}, \qquad \overline{\int f ds} = \int \overline{f} ds, \tag{3.6}$$

where $s$ is any of the spatial variables $x, y, z$ or the time variable $t$ [12]. Note that $\overline{f\cdot g} \neq \overline{f}\cdot\overline{g}$. First, the continuity equation Eq. (3.1) is averaged by substituting the velocity decomposition.

$$\frac{\partial \overline{u}_x}{\partial x} + \frac{\partial u'_x}{\partial x} + \frac{\partial \overline{u}_y}{\partial y} + \frac{\partial u'_y}{\partial y} + \frac{\partial \overline{u}_z}{\partial z} + \frac{\partial u'_z}{\partial z} = 0.$$

Taking the time-average of the continuity equation Eq. (3.1) therefore gives

$$\overline{\frac{\partial \overline{u}_x}{\partial x} + \frac{\partial u'_x}{\partial x} + \frac{\partial \overline{u}_y}{\partial y} + \frac{\partial u'_y}{\partial y} + \frac{\partial \overline{u}_z}{\partial z} + \frac{\partial u'_z}{\partial z}} = 0.$$

The time-averaged values of the fluctuating values are defined to be zero. Due to the properties given in Eq. (3.6), it follows that the averaged derivatives of the fluctuations are also zero. Therefore, the Reynolds averaged continuity equation reads

$$\frac{\partial \overline{u}_x}{\partial x} + \frac{\partial \overline{u}_y}{\partial y} + \frac{\partial \overline{u}_z}{\partial z} = 0. \tag{3.7}$$

To simplify the calculations, the advection terms in the momentum equations are slightly rewritten as

$$\mathbf{u}\cdot\nabla u_x = \mathbf{u}\cdot\nabla u_x + u_x\nabla\cdot\mathbf{u} = \frac{\partial u_x^2}{\partial x} + \frac{\partial u_x u_y}{\partial y} + \frac{\partial u_x u_z}{\partial z}, \tag{3.8a}$$

$$\mathbf{u}\cdot\nabla u_y = \mathbf{u}\cdot\nabla u_y + u_y\nabla\cdot\mathbf{u} = \frac{\partial u_x u_y}{\partial x} + \frac{\partial u_y^2}{\partial y} + \frac{\partial u_y u_z}{\partial z}, \tag{3.8b}$$

$$\mathbf{u}\cdot\nabla u_z = \mathbf{u}\cdot\nabla u_z + u_z\nabla\cdot\mathbf{u} = \frac{\partial u_x u_z}{\partial x} + \frac{\partial u_y u_z}{\partial y} + \frac{\partial u_z^2}{\partial z}, \tag{3.8c}$$

since $\nabla\cdot\mathbf{u} = 0$ (continuity). Averaging and substituting the Reynolds decomposition to the advection terms of the $x$ component of the Navier-Stokes equations gives

$$\begin{aligned}
&\overline{\frac{\partial u_x}{\partial t} + \frac{\partial u_x^2}{\partial x} + \frac{\partial u_x u_y}{\partial y} + \frac{\partial u_x u_z}{\partial z}} = \\
&\overline{\frac{\partial \overline{u}_x + u_x'}{\partial t} + \frac{\partial(\overline{u}_x + u_x')^2}{\partial x} + \frac{\partial(\overline{u}_x + u_x')(\overline{u}_y + u_y')}{\partial y} + \frac{\partial(\overline{u}_x + u_x')(\overline{u}_z + u_z')}{\partial z}} = \\
&\frac{\partial \overline{u}_x}{\partial t} + \frac{\partial \overline{u}_x^2}{\partial x} + \frac{\partial \overline{u_x'^2}}{\partial x} + \frac{\partial \overline{u}_x\,\overline{u}_y}{\partial y} + \frac{\partial \overline{u_x' u_y'}}{\partial y} + \frac{\partial \overline{u}_x\,\overline{u}_z}{\partial z} + \frac{\partial \overline{u_x' u_z'}}{\partial z},
\end{aligned} \tag{3.9}$$

where we used that $\overline{\frac{\partial u u'}{\partial x}} = 0$. Similar equations are obtained when applied to Eq. (3.8b) and Eq. (3.8c). This leads to the following system of equations

$$\begin{aligned}
&\frac{\partial \overline{u}_x}{\partial t} + \frac{\partial \overline{u}_x^2}{\partial x} + \frac{\partial \overline{u}_x\,\overline{u}_y}{\partial y} + \frac{\partial \overline{u}_x\,\overline{u}_z}{\partial z} + f^*\overline{u}_z - f\overline{u}_y = \\
&\qquad -\frac{1}{\rho}\frac{\partial \overline{p}}{\partial x} + \frac{\partial}{\partial x}\left(\nu\frac{\partial \overline{u}_x}{\partial x} - \overline{u_x'^2}\right) + \frac{\partial}{\partial y}\left(\nu\frac{\partial \overline{u}_x}{\partial y} - \overline{u_x' u_y'}\right) + \frac{\partial}{\partial z}\left(\nu\frac{\partial \overline{u}_x}{\partial z} - \overline{u_x' u_z'}\right),
\end{aligned} \tag{3.10a}$$

$$\begin{aligned}
&\frac{\partial \overline{u}_y}{\partial t} + \frac{\partial \overline{u}_x\,\overline{u}_y}{\partial x} + \frac{\partial \overline{u}_y^2}{\partial y} + \frac{\partial \overline{u}_y\,\overline{u}_z}{\partial z} + f\overline{u}_x = \\
&\qquad -\frac{1}{\rho}\frac{\partial \overline{p}}{\partial y} + \frac{\partial}{\partial x}\left(\nu\frac{\partial \overline{u}_y}{\partial x} - \overline{u_x' u_y'}\right) + \frac{\partial}{\partial y}\left(\nu\frac{\partial \overline{u}_y}{\partial y} - \overline{u_y'^2}\right) + \frac{\partial}{\partial z}\left(\nu\frac{\partial \overline{u}_y}{\partial z} - \overline{u_y' u_z'}\right),
\end{aligned} \tag{3.10b}$$

$$\begin{aligned}
&\frac{\partial \overline{u}_z}{\partial t} + \frac{\partial \overline{u}_x\,\overline{u}_z}{\partial x} + \frac{\partial \overline{u}_y\,\overline{u}_z}{\partial y} + \frac{\partial \overline{u}_z^2}{\partial z} - f^*\overline{u}_x = \\
&\qquad -\frac{1}{\rho}\frac{\partial \overline{p}}{\partial z} - g + \frac{\partial}{\partial x}\left(\nu\frac{\partial \overline{u}_z}{\partial x} - \overline{u_x' u_z'}\right) + \frac{\partial}{\partial y}\left(\nu\frac{\partial \overline{u}_z}{\partial y} - \overline{u_y' u_z'}\right) + \frac{\partial}{\partial z}\left(\nu\frac{\partial \overline{u}_z}{\partial z} - \overline{u_z'^2}\right).
\end{aligned} \tag{3.10c}$$

This results in the three turbulence-averaged velocities $\overline{u}_x$, $\overline{u}_y$ and $\overline{u}_z$ and six new unknowns, dependent on the turbulent fluctuations $\overline{u_x'^2}$, $\overline{u_y'^2}$, $\overline{u_z'^2}$, $\overline{u_x' u_y'}$, $\overline{u_x' u_z'}$ and $\overline{u_y' u_z'}$. These stresses are a result of the Reynolds decomposition and are therefore called Reynolds stresses. Due to these stresses, the resulting system contains more unknowns than equations. This is known as the Turbulence Closure Problem. To solve this problem, the Reynolds stresses have to be expressed in terms of Reynolds averaged quantities. It is observed that the fluctuations in turbulent flows consist of eddies, consisting of smaller eddies and so on until the fluctuations can be dissipated by the viscosity of the fluid. Therefore, it is reasonable to parameterise the turbulence-averaged effect of fluctuation as an enhanced viscosity. Generally the turbulent motion is many orders of magnitude larger in the horizontal direction than in the vertical direction, due to the water flow occurring mainly in the horizontal direction [13]. Therefore a distinction between two eddy viscosities is made. One eddy visocity is defined for the $x-$ and $y-$direction: the horizontal eddy viscosity $\eta_h$. Another eddy viscosity in the $z-$direction is called the vertical eddy viscosity and is denoted by $\eta_v$. Using these assumptions, the Reynold stresses can be expressed as

$$\overline{u_x'^2} = -2\eta_h\frac{\partial \overline{u}_x}{\partial x}, \qquad \overline{u_y'^2} = -2\eta_h\frac{\partial \overline{u}_y}{\partial x}, \qquad \overline{u_z'^2} = -2\eta_v\frac{\partial \overline{u}_z}{\partial x},$$

$$\overline{u_x' u_y'} = -\eta_h\left(\frac{\partial \overline{u}_x}{\partial y} + \frac{\partial \overline{u}_y}{\partial x}\right), \qquad \overline{u_x' u_z'} = -\eta_v\frac{\partial \overline{u}_x}{\partial z} - \eta_h\frac{\partial \overline{u}_z}{\partial x}, \qquad \overline{u_y' u_z'} = -\eta_v\frac{\partial \overline{u}_y}{\partial z} - \eta_h\frac{\partial \overline{u}_z}{\partial y}.$$

Substituting these eddy viscosities to the time-averaged equations, and applying the continuity equation, gives

$$\frac{\partial \overline{u}_x}{\partial t} + \overline{\mathbf{u}} \cdot \nabla \overline{u}_x + f^* \overline{u}_z - f \overline{u}_y = -\frac{1}{\rho}\frac{\partial \overline{p}}{\partial x} + \frac{\partial}{\partial x}\left(\mu_h \frac{\partial \overline{u}_x}{\partial x}\right) + \frac{\partial}{\partial y}\left(\mu_h \frac{\partial \overline{u}_x}{\partial y}\right) + \frac{\partial}{\partial z}\left(\mu_v \frac{\partial \overline{u}_x}{\partial z}\right), \tag{3.11a}$$

$$\frac{\partial \overline{u}_y}{\partial t} + \overline{\mathbf{u}} \cdot \nabla \overline{u}_y + f \overline{u}_x = -\frac{1}{\rho}\frac{\partial \overline{p}}{\partial y} + \frac{\partial}{\partial x}\left(\mu_h \frac{\partial \overline{u}_y}{\partial x}\right) + \frac{\partial}{\partial y}\left(\mu_h \frac{\partial \overline{u}_y}{\partial y}\right) + \frac{\partial}{\partial z}\left(\mu_v \frac{\partial \overline{u}_y}{\partial z}\right), \tag{3.11b}$$

$$\frac{\partial \overline{u}_z}{\partial t} + \overline{\mathbf{u}} \cdot \nabla \overline{u}_z - f^* \overline{u}_x = -\frac{1}{\rho}\frac{\partial p}{\partial z} - g + \frac{\partial}{\partial x}\left(\mu_h \frac{\partial \overline{u}_z}{\partial x}\right) + \frac{\partial}{\partial y}\left(\mu_h \frac{\partial \overline{u}_z}{\partial y}\right) + \frac{\partial}{\partial z}\left(\mu_v \frac{\partial \overline{u}_z}{\partial z}\right), \tag{3.11c}$$

where $\mu_h = \nu + \eta_h$ and $\mu_v = \nu + \eta_v$. For more details on the derivation of these equations, see Appendix B. To simplify the notation of the equations, we omit the overbar and we define the viscosity matrix

$$D = \begin{pmatrix} \mu_h & 0 & 0 \\ 0 & \mu_h & 0 \\ 0 & 0 & \mu_v \end{pmatrix}.$$

The resulting Reynolds Averaged Navier-Stokes equations can now be written as

$$\begin{cases} \nabla \cdot \mathbf{u} = 0 \\ \dfrac{\partial u_x}{\partial t} + \mathbf{u} \cdot \nabla u_x + f^* u_z - f u_y &= -\dfrac{1}{\rho}\dfrac{\partial p}{\partial x} + \nabla \cdot (D \nabla u_x), \\ \dfrac{\partial u_y}{\partial t} + \mathbf{u} \cdot \nabla u_y + f u_x &= -\dfrac{1}{\rho}\dfrac{\partial p}{\partial y} + \nabla \cdot (D \nabla u_y), \\ \dfrac{\partial u_z}{\partial t} + \mathbf{u} \cdot \nabla u_z - f^* u_x &= -\dfrac{1}{\rho}\dfrac{\partial p}{\partial z} - g + \nabla \cdot (D \nabla u_z). \end{cases} \tag{3.12}$$

### 3.1.5 Boundary conditions

The RANS equations are complemented with boundary conditions. These conditions are determined by the motions of the water particles, defined as the kinematic boundary conditions, and the forces acting on the water particles at the boundary, defined as the dynamic boundary conditions.

Fig. 3.2 shows the vertical boundaries in a cross-sectional view of the water column. The bottom is given at $z = h_b$ with $z = 0$ as the reference level. The free surface is found at $z = \zeta + H$, with $\zeta$ the deviation of the free surface from a constant reference height $H$. The height of the water column is thus given by $H + \zeta - h_b$.

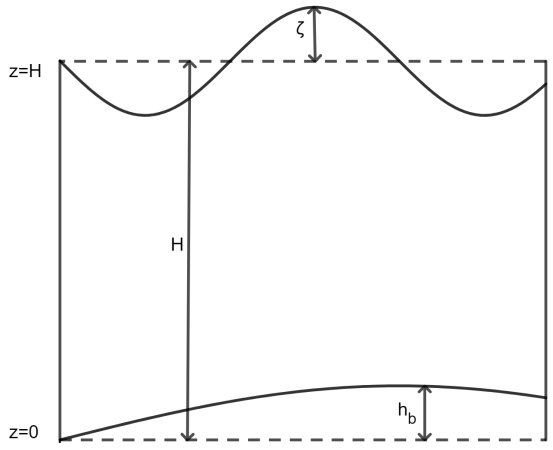


**Fig. 3.2:** Cross-sectional view of the water column showing the vertical boundaries.

### Kinematic boundary conditions

Both at the bottom and at the free surface, so-called kinematic boundary conditions are prescribed. At the bottom, this condition implies that water particles may not penetrate the bottom. Mathematically, this impermeability means that at the bottom boundary, the normal component of the velocity vector must be zero. Since the bottom boundary is defined at $z - h_b(x, y) = 0$, the normal vector is given by

$$\begin{pmatrix} \frac{\partial z - h_b}{\partial x} \\ \frac{\partial z - h_b}{\partial y} \\ \frac{\partial z - h_b}{\partial z} \end{pmatrix} = \begin{pmatrix} -\frac{\partial h_b}{\partial x} \\ -\frac{\partial h_b}{\partial y} \\ 1 \end{pmatrix} \tag{3.13}$$

and the kinematic boundary condition at the bottom reads

$$u_z = u_x \frac{\partial h_b}{\partial x} + u_y \frac{\partial h_b}{\partial y}, \qquad \text{at } z = h_b(x, y). \tag{3.14}$$

Note that the slow changes of the bottom over time are neglected.

At the water surface, water particles may not leave the surface. The difference between this boundary and the bottom boundary is that this boundary moves with the fluid, whereas the bottom is assumed time independent. The location of the top boundary is found at $z = H + \zeta = H + \zeta(x, y, t)$. The kinematic boundary condition at the free surface is then given by

$$u_z = \frac{\partial \zeta}{\partial t} + u_x \frac{\partial \zeta}{\partial x} + u_y \frac{\partial \zeta}{\partial y}, \qquad \text{at } z = H + \zeta(x, y, t). \tag{3.15}$$

### Dynamic boundary conditions

All fluids are subject to internal friction, modelled as viscous forces in the RANS system of equations Eq. (3.12). The dynamic boundary condition requires the tangential shear stress to be continuous at the free surface. Therefore the stress exerted by the atmosphere, the wind stress, must be equal to the viscous movement due to the viscous terms at the boundary. This gives

$$D \nabla u_x \cdot \mathbf{n} = \frac{\tau_{x,\text{wind}}}{\rho}, \tag{3.16a}$$

$$D \nabla u_y \cdot \mathbf{n} = \frac{\tau_{y,\text{wind}}}{\rho}, \tag{3.16b}$$

where $\mathbf{n}$ denotes the normal vector and $\tau_{\text{wind},x}$ and $\tau_{\text{wind},y}$ the components of the wind stress exerted by the atmosphere in the $x-$ and $y-$direction, respectively. In other words,

$$\begin{aligned} \frac{\tau_{\text{wind},x}}{\rho} &= -\mu_h \frac{\partial u_x}{\partial x}\frac{\partial \zeta}{\partial x} - \mu_h \frac{\partial u_x}{\partial y}\frac{\partial \zeta}{\partial y} + \mu_v \frac{\partial u_x}{\partial z}, \\ \frac{\tau_{\text{wind},y}}{\rho} &= -\mu_h \frac{\partial u_y}{\partial x}\frac{\partial \zeta}{\partial x} - \mu_h \frac{\partial u_y}{\partial y}\frac{\partial \zeta}{\partial y} + \mu_v \frac{\partial u_y}{\partial z}, \end{aligned} \qquad \text{at } z = H + \zeta(x, y, t). \tag{3.17}$$

The wind stress components are usually taken as quadratic functions of the wind velocity $\mathbf{u}_{10}$, the wind speed 10 meters above the sea and parameterised using a drag coefficient:

$$\tau_{\text{wind},x} = C_d \rho_{\text{air}} U_{10} u_{x,10}, \qquad \tau_{\text{wind},y} = C_d \rho_{\text{air}} U_{10} u_{y,10},$$

where $\rho_{\text{air}}$ is the air density, $u_{10,x}$ and $u_{10,y}$ are the $x$ and $y$ components of the wind vector $\mathbf{u}_{10}$, $U_{10} = \sqrt{u_{10,x}^2 + u_{10,y}^2}$ is the wind speed, and $C_d$ is a drag coefficient with approximate value of 0.0015 for wind over the sea [14].

For the bottom boundary, we consider the bottom stress, denoted by $\tau_{\text{bed}}, x$ and $\tau_{\text{bed},y}$, and find similar boundary conditions

$$\begin{aligned} \frac{\tau_{\text{bed},x}}{\rho} &= -\mu_h \frac{\partial u_x}{\partial x}\frac{\partial h_b}{\partial x} - \mu_h \frac{\partial u_x}{\partial y}\frac{\partial h_b}{\partial y} + \mu_v \frac{\partial u_x}{\partial z}, \\ \frac{\tau_{\text{bed},y}}{\rho} &= -\mu_h \frac{\partial u_y}{\partial x}\frac{\partial h_b}{\partial x} - \mu_h \frac{\partial u_y}{\partial y}\frac{\partial h_b}{\partial y} + \mu_v \frac{\partial u_y}{\partial z} \end{aligned} \qquad \text{at } z = h_b(x, y). \tag{3.18}$$

The seabed stress depends quadratically on the flow velocity and the components can be parameterised using a quadratic bottom stress law

$$\tau_{\text{bed},x} = C_d \rho U_b u_{b,x} \qquad \tau_{\text{bed},y} = C_d \rho U_b u_{b,y},$$

where $\rho$ is the fluid density, $u_{b,x}$ and $u_{b,y}$ are the $x$ and $y$ components of the flow velocity $\mathbf{u}_b$ at the seabed, $U_b = \sqrt{u_{b,x}^2 + u_{b,y}^2}$ is the flow speed at the seabed, and $C_d$ is a drag coefficient with approximate value of 0.0025 for flows in shallow water [15].
We focus on tidally driven flows and therefore the wind stress is neglected. The nonlinearity of the stresses can be removed by using a Lorentz linearisation and expressing the stresses in terms of a friction coefficient $r$ (see [16] or [17]), resulting in

$$\tau = \tau_{\text{bed}} \approx \rho r u. \tag{3.19}$$

## 3.2 Shallow water

In this section, the focus is on water motion in the coastal regions where the water is shallow. For shallow water, some assumptions may be made that simplify the $z-$component of the RANS equations. In Section 3.2.1, scaling is used to substantiate these assumptions, resulting in the hydrostatic balance. The resulting three dimensional shallow water equations are discussed in Section 3.2.2.

### 3.2.1 The hydrostatic balance

In shallow water, water motion is dominated by horizontal flow. To substantiate this observation and obtain the shallow water equations, some scaling analysis needs to be considered.
The flow velocity in the horizontal direction, denoted by $U$ is assumed to vary over a typical length scale $L$. The same velocity and length scale is used in both horizontal directions, because the flow and length in the horizontal directions are comparable. Due to boundedness of the length scale in the vertical direction by the seabed and the free surface, a different scale for the flow and length is expected in the vertical direction. The flow velocity in the vertical direction is denoted by $W$ and the typical vertical length scale is denoted by $H$, the local water depth. To analyse whether terms may be ignored, we aim to find a dominant balance in the continuity equation. In this balance the terms that are significantly smaller are neglected, resulting in a simpler equation which only considers the most dominant processes. To get insight in the order of magnitude of the various flow components, the continuity equation is used. Three cases can be distinguished:

- $U/L \ll W/H$. In this case the continuity equation is dominated by $\frac{\partial u_z}{\partial z} = 0$. The vertical flow would then be constant in $z$ and due to the no flow boundary conditions, this gives $u_z \equiv 0$ for all $z$.
- $U/L \sim W/H$. In this case all contributions to the continuity equation are considered.
- $U/L \gg W/H$. In this case the continuity equation implies that the water flow in one horizontal direction is compensated by the water flow in the perpendicular horizontal direction. This is feasible if the changes in the seabed are small compared to the water depth. This contradicts the assumption of shallow water.

From now on, we assume that $U/L \sim W/H \Rightarrow W \sim H/L\, U$. Since the horizontal length scale is much larger than the vertical length scale for geophysical flow, it follows that the flow is indeed horizontally dominated.

Consider the x-momentum equation of the RANS equations given by Eq. (3.12), denoting the Coriolis parameters as $\Omega$, the terms of this equation can be scaled as

| $\frac{\partial u_x}{\partial t}$ | $u_x \frac{\partial u_x}{\partial x}$ | $u_y \frac{\partial u_x}{\partial y}$ | $u_z \frac{\partial u_x}{\partial z}$ | $f^* u_z$ | $f u_y$ | $\frac{1}{\rho}\frac{\partial p}{\partial x}$ | $\frac{\partial}{\partial x}\left(\mu_h \frac{\partial u_x}{\partial x}\right)$ | $\frac{\partial}{\partial y}\left(\mu_h \frac{\partial u_x}{\partial y}\right)$ | $\frac{\partial}{\partial z}\left(\mu_v \frac{\partial u_x}{\partial z}\right)$ |
|---|---|---|---|---|---|---|---|---|---|
| $\frac{U}{T}$ | $\frac{U^2}{L}$ | $\frac{U^2}{L}$ | $\frac{UW}{H}$ | $\Omega W$ | $\Omega U$ | $\frac{P}{\rho L}$ | $\frac{\mu_h U}{L^2}$ | $\frac{\mu_h U}{L^2}$ | $\frac{\mu_v U}{H^2}$ |

Since we assumed the flow is horizontally dominated, it immediately follows that the term $f^* u_z$ may be neglected. Note that this assumption may not hold near the equator, where the reciprocal Coriolis

parameter reaches its maximum. We may assume the pressure gradient scales as the Coriolis term due to the fundamental importance of the rotation terms in geophysical fluid dynamics, for more details see [14]. A similar analysis can be done regarding the $y-$component of the RANS equations. Considering the $z-$component of the equation, one finds

$$\begin{array}{cccccccccc} \frac{\partial u_z}{\partial t} & u_x\frac{\partial u_z}{\partial x} & u_y\frac{\partial u_z}{\partial y} & u_z\frac{\partial u_z}{\partial z} & f^*u_x & \frac{1}{\rho}\frac{\partial p}{\partial z} & g & \frac{\partial}{\partial x}\left(\mu_h\frac{\partial u_z}{\partial x}\right) & \frac{\partial}{\partial y}\left(\mu_h\frac{\partial u_z}{\partial y}\right) & \frac{\partial}{\partial z}\left(\mu_v\frac{\partial u_z}{\partial z}\right) \\ \frac{W}{T} & \frac{UW}{L} & \frac{UW}{L} & \frac{W^2}{H} & \Omega U & \frac{P}{\rho H} & g & \frac{\mu_h W}{L^2} & \frac{\mu_h W}{L^2} & \frac{\mu_v W}{H^2} \end{array}$$

Assuming $W \sim H/LU$, the order of magnitude of the velocity in the vertical direction is much smaller than the other terms in the $x$-directional momentum equation. Therefore the terms containing $W$ may be neglected. Furthermore, from the previous analysis, we know that the Coriolis term can be scaled as $\Omega U \sim \frac{P}{\rho L}$ and thus the ratio of Coriolis term and the pressure gradient is given by $\frac{H}{L}$. Since this is much smaller than one, we omit the Coriolis term. The $z-$ component of the Reynold Averaged Navier-Stokes equations can now be reduced to

$$\frac{\partial p}{\partial z} = -\rho g. \tag{3.20}$$

This is called the hydrostatic balance.

### 3.2.2 Three dimensional shallow water equations

The system of equations for the three dimensional shallow water equations becomes

$$\begin{cases} \nabla \cdot \mathbf{u} & = 0, \\ \dfrac{\partial u_x}{\partial t} + \mathbf{u}\cdot\nabla u_x - f u_y & = -\dfrac{1}{\rho}\dfrac{\partial p}{\partial x} + \nabla\cdot(D\nabla u_x), \\ \dfrac{\partial u_y}{\partial t} + \mathbf{u}\cdot\nabla u_y + f u_x & = -\dfrac{1}{\rho}\dfrac{\partial p}{\partial y} + \nabla\cdot(D\nabla u_y), \\ \dfrac{\partial p}{\partial z} & = -\rho g. \end{cases} \tag{3.21}$$

# 4

# Depth-averaged shallow water equations

The derivation of the two dimensional shallow water equations is based on depth-integration of the RANS equations. In Section 4.1 a classical depth-averaging approach is discussed, resulting in the classical two dimensional shallow water equations. In [1] a new set of two-dimensional shallow flow equations was developed to deal with partially wet domains. The bottom irregularities, which in many practical cases strongly affect the dynamics and the continuity, are accounted for statistically. This statistical depth-averaging approach is discussed in Section 4.2, giving two dimensional shallow water equations allowing for partially dry areas.

## 4.1 Classical depth-averaging approach

In this section, assuming the hydrostatic balance, the three-dimensional RANS equations are integrated over the depth. First, the mass balance equation is integrated in Section 4.1.1 and in Section 4.1.2 the momentum balance equation follows. Combining these equations results in the two dimensional shallow water equations, given in Section 4.1.3. In Section 4.1.4 the one dimensional shallow water equations obtained after width-averaging are discussed.

### 4.1.1 Mass balance equation

We start by depth integration of the mass balance equation. We integrate the continuity equation over the depth from the bottom $h_b$ to the free surface $H + \zeta$:

$$\int_{h_b}^{H+\zeta} \left( \frac{\partial u_x}{\partial x} + \frac{\partial u_y}{\partial y} + \frac{\partial u_z}{\partial z} \right) \, dz = 0, \tag{4.1a}$$

$$\int_{h_b}^{H+\zeta} \frac{\partial u_x}{\partial x} \, dz + \int_{h_b}^{H+\zeta} \frac{\partial u_y}{\partial y} \, dz + [u_z]_{h_b}^{H+\zeta} = 0. \tag{4.1b}$$

The first two terms can be rewritten using the Leibniz integration rule as

$$\int_{h_b}^{H+\zeta} \frac{\partial u_x}{\partial x} \, dz = \frac{\partial}{\partial x} \left( \int_{h_b}^{H+\zeta} u_x \, dz \right) - \left[ u_x \frac{\partial h_b}{\partial x} \right]_{h_b} - \left[ u_x \frac{\partial \zeta}{\partial x} \right]_{H+\zeta}. \tag{4.2}$$

Collecting all terms, we find that

$$\frac{\partial}{\partial x} \int_{h_b}^{H+\zeta} u_x dz + \frac{\partial}{\partial y} \int_{h_b}^{H+\zeta} u_y dz + \left[ -u_x \frac{\partial h_b}{\partial x} - u_y \frac{\partial h_b}{\partial y} + u_z \right]_{h_b} + \left[ -u_x \frac{\partial \zeta}{\partial x} - u_y \frac{\partial \zeta}{\partial y} + u_z \right]_{H+\zeta} = 0. \tag{4.3}$$

Note that

$$\left[ -u_x \frac{\partial h_b}{\partial x} - u_y \frac{\partial h_b}{\partial y} + u_z \right]_{h_b} = 0 \quad \text{and} \quad \left[ -u_x \frac{\partial \zeta}{\partial x} - u_y \frac{\partial \zeta}{\partial y} + u_z \right]_{H+\zeta} = \frac{\partial \zeta}{\partial t}, \tag{4.4}$$

due to the kinematic boundary conditions. To further simplify the equation, we define the depth averaged velocities by

$$\langle u \rangle_x = \frac{1}{H+\zeta-h_b}\int_{h_b}^{H+\zeta} u_x dz, \qquad \langle u \rangle_y = \frac{1}{H+\zeta-h_b}\int_{h_b}^{H+\zeta} u_y dz, \tag{4.5}$$

resulting in the following depth integrated continuity equation:

$$\frac{\partial}{\partial x}\left[(H+\zeta-h_b)\langle u \rangle_x\right] + \frac{\partial}{\partial y}\left[(H+\zeta-h_b)\langle u \rangle_y\right] + \frac{\partial \zeta}{\partial t} = 0. \tag{4.6}$$

### 4.1.2 Momentum balance equation

The momentum balance equations are given by the RANS equations. We will work out the depth-averaging for the $x-$ component of these equations, the calculations for the $y-$ component are analogous. First, the equations are integrated over depth:

$$\int_{h_b}^{H+\zeta}\left(\frac{\partial u_x}{\partial t} + \frac{\partial u_x^2}{\partial x} + \frac{\partial u_x u_y}{\partial y} + \frac{\partial u_x u_z}{\partial z} - f u_y\right)\, dz = \int_{h_b}^{H+\zeta}\left(-\frac{1}{\rho}\frac{\partial p}{\partial x} + \nabla\cdot(D\nabla u_x)\right)\, dz. \tag{4.7}$$

Focusing on the terms on the left-hand side, using Leibniz integration rule (Eq. (4.2)) and the kinematic boundary conditions given (Eq. (3.14) and Eq. (3.15)), we find that

$$\begin{aligned}
&\int_{h_b}^{H+\zeta}\left(\frac{\partial u_x}{\partial t} + \frac{\partial u_x^2}{\partial x} + \frac{\partial u_x u_y}{\partial y} + \frac{\partial u_x u_z}{\partial z} - f u_y\right)\, dz = \\
&\int_{h_b}^{H+\zeta}\frac{\partial u_x}{\partial t}\, dz + \int_{h_b}^{H+\zeta}\frac{\partial u_x^2}{\partial x}\, dz + \int_{h_b}^{H+\zeta}\frac{\partial u_x u_y}{\partial y}\, dz + \int_{h_b}^{H+\zeta}\frac{\partial u_x u_z}{\partial z}\, dz - \int_{h_b}^{H+\zeta} f u_y\, dz = \\
&\frac{\partial}{\partial t}\int_{h_b}^{H+\zeta} u_x\, dz + \frac{\partial}{\partial x}\int_{h_b}^{H+\zeta} u_x^2\, dz + \frac{\partial}{\partial y}\int_{h_b}^{H+\zeta} u_x u_y\, dz - f\int_{h_b}^{H+\zeta} u_y\, dz + \\
&\left[-u_x^2\frac{\partial h_b}{\partial x} - u_x u_y\frac{\partial h_b}{\partial y} + u_x u_z\right]_{h_b} + \left[-u_x\frac{\partial \zeta}{\partial t} - u_x^2\frac{\partial \zeta}{\partial x} - u_x u_y\frac{\partial \zeta}{\partial y} + u_x u_z\right]_{H+\zeta} = \\
&\frac{\partial}{\partial t}\int_{h_b}^{H+\zeta} u_x\, dz + \frac{\partial}{\partial x}\int_{h_b}^{H+\zeta} u_x^2\, dz + \frac{\partial}{\partial y}\int_{h_b}^{H+\zeta} u_x u_y\, dz - f\int_{h_b}^{H+\zeta} u_y\, dz.
\end{aligned} \tag{4.8}$$

To average the integrals of $u_x^2$ and $u_x u_y$, we use a decomposition similar tot the Reynolds decomposition (see Section 3.1.4), but now for averaging over the depth instead of over time. We decompose the velocities into a depth-averaged part and a fluctuating part:

$$u = \langle u \rangle + \widetilde{u}, \qquad \langle u \rangle = \frac{1}{H+\zeta-h_b}\int_{h_b}^{H+\zeta} u\, dz, \qquad \int_{h_b}^{H+\zeta}\widetilde{u}\, dz = 0.$$

This results in a closure problem, as now quadratic terms in the depth varying quantities are found. To solve this problem we parameterise the integrals of the fluctuating flow as effective eddy viscosity terms:

$$\int_{h_b}^{H+\zeta}\widetilde{u_x}^2 dz = -\widetilde{\eta_h}(H+\zeta-h_b)\frac{\partial \langle u \rangle_x}{\partial x}, \qquad \int_{h_b}^{H+\zeta}\widetilde{u_x}\,\widetilde{u_y} dz = -\widetilde{\eta_h}(H+\zeta-h_b)\frac{\partial \langle u \rangle_x}{\partial y}.$$

Using these expressions, we find that

$$\begin{aligned}
&\frac{\partial}{\partial t}\int_{h_b}^{H+\zeta} u_x\, dz + \frac{\partial}{\partial x}\int_{h_b}^{H+\zeta} u_x^2\, dz + \frac{\partial}{\partial y}\int_{h_b}^{H+\zeta} u_x u_y\, dz - f\int_{h_b}^{H+\zeta} u_y\, dz = \\
&\frac{\partial}{\partial t}\hat{h}\langle u \rangle_x + \frac{\partial}{\partial x}\left(\hat{h}\langle u \rangle_x^2 - \widetilde{\eta_h}\hat{h}\frac{\partial \langle u \rangle_x}{\partial x}\right) + \frac{\partial}{\partial y}\left(\hat{h}\langle u \rangle_x\,\langle u \rangle_y - \widetilde{\eta_h}\hat{h}\frac{\partial \langle u \rangle_x}{\partial y}\right) - f\hat{h}\langle u \rangle_y = \\
&\hat{h}\left(\frac{\partial \langle u \rangle_x}{\partial t} + \langle u \rangle_x\frac{\partial \langle u \rangle_x}{\partial x} + \langle u \rangle_y\frac{\partial \langle u \rangle_x}{\partial y} - f\langle u \rangle_y\right) - \frac{\partial}{\partial x}\left(\widetilde{\eta_h}\hat{h}\frac{\partial \langle u \rangle_x}{\partial x}\right) - \frac{\partial}{\partial y}\left(\widetilde{\eta_h}\hat{h}\frac{\partial \langle u \rangle_x}{\partial y}\right),
\end{aligned} \tag{4.9}$$

with $\hat{h} = H + \zeta - h_b$.

For the integration of the right-hand side, we start by determining the pressure $p$. Using the hydrostatic balance and continuity of the pressure at the free surface, we can find an expression for the pressure

$$\begin{cases} \dfrac{\partial p}{\partial z} = -\rho g, \\ p = p_{atm} \quad \text{at } z = H + \zeta, \end{cases} \Rightarrow p = p_{atm} - \rho g(\zeta - z), \tag{4.10}$$

where $p_{atm}$ is the pressure of the atmosphere. Considering the Leibniz integration rule (Eq. (4.2)), the dynamic boundary conditions (Eq. (3.17) and Eq. (3.18)), integration of the right hand side results in

$$\begin{aligned} \int_{h_b}^{H+\zeta} -\frac{1}{\rho}\frac{\partial p}{\partial x} + \nabla \cdot (D \nabla u_x) dz = \\ \int_{h_b}^{H+\zeta} -\frac{\partial \zeta}{\partial x} g dz + \int_{h_b}^{H+\zeta} \frac{\partial}{\partial x}\left(\mu_h \frac{\partial u_x}{\partial x}\right) dz + \int_{h_b}^{H+\zeta} \frac{\partial}{\partial y}\left(\mu_h \frac{\partial u_x}{\partial y}\right) dz + \int_{h_b}^{H+\zeta} \frac{\partial}{\partial z}\left(\mu_v \frac{\partial u_x}{\partial z}\right) dz = \\ -\hat{h} g \frac{\partial \zeta}{\partial x} + \frac{\partial}{\partial x}\int_{h_b}^{H+\zeta}\left(\mu_h \frac{\partial u_x}{\partial x}\right) dz + \frac{\partial}{\partial y}\int_{h_b}^{H+\zeta}\left(\mu_h \frac{\partial u_x}{\partial y}\right) dz + \\ \left[-\mu_h \frac{\partial u_x}{\partial x}\frac{\partial h_b}{\partial x} - \mu_h \frac{\partial u_x}{\partial y}\frac{\partial h_b}{\partial y} + \mu_v \frac{\partial u_x}{\partial z}\right]_{h_b} + \left[-\mu_h \frac{\partial u_x}{\partial x}\frac{\partial \zeta}{\partial x} - \mu_h \frac{\partial u_x}{\partial y}\frac{\partial \zeta}{\partial y} + \mu_v \frac{\partial u_x}{\partial z}\right]_{H+\zeta} = \\ -\hat{h} g \frac{\partial \zeta}{\partial x} + \frac{\partial}{\partial x}\left(\hat{h}\mu_h \frac{\partial \langle u \rangle_x}{\partial x}\right) + \frac{\partial}{\partial y}\left(\hat{h}\mu_h \frac{\partial \langle u \rangle_x}{\partial y}\right) + r u_x, \end{aligned} \tag{4.11}$$

where $ru_x$ are the stresses expressed in terms of a friction coefficient $r$ as defined in Eq. (3.19). Define $\widetilde{\mu_h} = \mu_h + \widetilde{\eta_h}$. Combining both sides gives the x-component of the momentum balance equation. Omitting the brackets, this results in

$$\frac{\partial u_x}{\partial t} + u_x \frac{\partial u_x}{\partial x} + u_y \frac{\partial u_x}{\partial y} - f u_y = -g \frac{\partial \zeta}{\partial x} + \frac{1}{\hat{h}}\left(\frac{\partial}{\partial x}\left(\widetilde{\mu_h}\hat{h}\frac{\partial u_x}{\partial x}\right) + \frac{\partial}{\partial y}\left(\widetilde{\mu_h}\hat{h}\frac{\partial u_x}{\partial y}\right) - r u_x\right) \tag{4.12a}$$

$$\frac{\partial u_x}{\partial t} + \mathbf{u} \cdot \nabla u_x - f u_y = -g \frac{\partial \zeta}{\partial x} + \frac{1}{\hat{h}}\left(\nabla \cdot (D_2 \nabla u_x) - r u_x\right), \tag{4.12b}$$

with

$$D_2 = \begin{pmatrix} \widetilde{\mu_h}(H + \zeta - h_b) & 0 \\ 0 & \widetilde{\mu_h}(H + \zeta - h_b) \end{pmatrix}.$$

Similarly, the y-component of the momentum balance equation is given by

$$\frac{\partial u_y}{\partial t} + u_x \frac{\partial u_y}{\partial x} + u_y \frac{\partial u_y}{\partial y} + f u_x = -g \frac{\partial \zeta}{\partial y} + \frac{1}{\hat{h}}\left(\frac{\partial}{\partial x}\left(\widetilde{\mu_h}\hat{h}\frac{\partial u_y}{\partial x}\right) + \frac{\partial}{\partial y}\left(\widetilde{\mu_h}\hat{h}\frac{\partial u_y}{\partial y}\right) - r u_y\right) \tag{4.13a}$$

$$\frac{\partial u_y}{\partial t} + \mathbf{u} \cdot \nabla u_y + f u_x = -g \frac{\partial \zeta}{\partial y} + \frac{1}{\hat{h}}\left(\nabla \cdot (D_2 \nabla u_y) - r u_x\right). \tag{4.13b}$$

### 4.1.3 Two dimensional shallow water equations

The two dimensional shallow water equations are now given by

$$\begin{cases} \dfrac{\partial}{\partial x}\left((H + \zeta - h_b)u_x\right) + \dfrac{\partial}{\partial y}\left((H + \zeta - h_b)u_y\right) + \dfrac{\partial \zeta}{\partial t} = 0, \\ \dfrac{\partial u_x}{\partial t} + \mathbf{u} \cdot \nabla u_x - f u_y = -g \dfrac{\partial \zeta}{\partial x} + \dfrac{1}{H + \zeta - h_b}\left(\nabla \cdot (D_2 \nabla u_x) - r u_x\right), \\ \dfrac{\partial u_y}{\partial t} + \mathbf{u} \cdot \nabla u_y + f u_x = -g \dfrac{\partial \zeta}{\partial y} + \dfrac{1}{H + \zeta - h_b}\left(\nabla \cdot (D_2 \nabla u_y) - r u_y\right), \\ u(t) = 0 \quad \text{at } x, y \in \delta\Omega_c, \\ \zeta(t) = A\cos(\sigma t + \phi) \quad \text{at } x, y \in \delta\Omega_s, \end{cases} \tag{4.14}$$

where $\delta\Omega_c$ denotes the coastal boundary and $\delta\Omega_s$ denotes the seaward boundary.

### 4.1.4 One dimensional shallow water equations

To derive the one dimensional shallow water equations, integration over width can be applied similar to the integration over depth. Assuming $x$ dependent Dirichlet boundary conditions implying stationary and impermeable walls at both sides over a fixed width, and integrating the mass balance and momentum balance equation leads to the final one dimensional or cross sectionally averaged shallow water equations. The Coriolis parameter has been neglected as the rotational effect is very small for a narrow channel [18]. For a more detailed derivation, see [19].

The one dimensional shallow water equations are given by

$$\begin{cases} \dfrac{\partial}{\partial x}\left[(H+\zeta-h_b)u\right]+\dfrac{\partial \zeta}{\partial t}=0 \\ \dfrac{\partial u}{\partial t}+u\dfrac{\partial u}{\partial x}=-g\dfrac{\partial \zeta}{\partial x}+\dfrac{1}{H+\zeta-h_b}\left(\dfrac{\partial}{\partial x}\left[\widetilde{\mu_h}(H+\zeta-h_b)\dfrac{\partial u}{\partial x}\right]-ru\right), \\ u(t,L)=0, \\ \zeta(t,0)=A\cos(\sigma t+\phi). \end{cases} \tag{4.15}$$

## 4.2 Statistical depth-averaging approach

The previous approach gives a basic idea of modelling the water motion with variable seabed. For this thesis, we want a method that can also model the water motion over tidal flats. The water depth in these areas varies between very shallow water and dry areas. Delfina et al. [1] proposed a model, redefining some parameters and the momentum balance equations such that the model can account for partially dry areas. They describe new momentum and mass balance equations for two dimensional free surface flows which account for the bathymetrical variations that allow for a realistic description of flooding and drying phenomena [20].

Similar to the approach described in the previous section, they start with the continuity equation and three dimensional RANS equations given by:

$$\begin{cases} \nabla\cdot\mathbf{u} & =0, \\ \dfrac{\partial u_x}{\partial t}+\mathbf{u}\cdot\nabla u_x & =-\dfrac{1}{\rho}\dfrac{\partial p}{\partial x}+\nabla\cdot(D\nabla u_x), \\ \dfrac{\partial u_y}{\partial t}+\mathbf{u}\cdot\nabla u_y & =-\dfrac{1}{\rho}\dfrac{\partial p}{\partial y}+\nabla\cdot(D\nabla u_y), \\ 0 & =-\dfrac{1}{\rho}\dfrac{\partial p}{\partial z}-g. \end{cases} \tag{4.16}$$

They define a few new variables and parameters. In Fig. 4.1 a sketch is given of these variables and parameters within the one dimensional domain. They redefine the free surface or water height variable $\zeta^*$ to the free surface elevation $\zeta$ plus the constant reference water height $H$, such that $\zeta^*=\zeta+H$. This new variable gives the absolute water height, from now on the subscript asterisk will be omitted. They set the minimum water height to be equal to zero. The bottom elevation, defined as $h_b$ is greater than zero. Previously, the entire domain was assumed to be wet, but in the new formulation domains are allowed to be partially dry. Therefore, they define the water volume per unit area $Y$ and the equivalent water depth $H_k$. They let $\overline{h_f}$ be the mean bottom height per element in the domain. Furthermore, a phase function $\phi(\mathbf{x})$ is defined to determine whether the area is wet or dry. It is given by

$$\phi(x,y)=\begin{cases} 1 & \text{if } z>h_b \\ 0 & \text{if } z\le h_b, \end{cases} \tag{4.17}$$

where $h_b$ is the local bottom elevation. The fraction of area higher than the bottom elevation $h_b$ is then given by the average of the phase function: $\nu=\overline{\phi(\mathbf{x},h_b)}$. The parameter $\eta$ defined as the wetted percentage of the domain is given by $\eta=\nu(x,y,\zeta)$. Note that $\eta$ can be interpreted as a storativity coefficient of the water.

Analogous to Section 4.1.1, the three dimensional equations are integrated over depth and an averaging

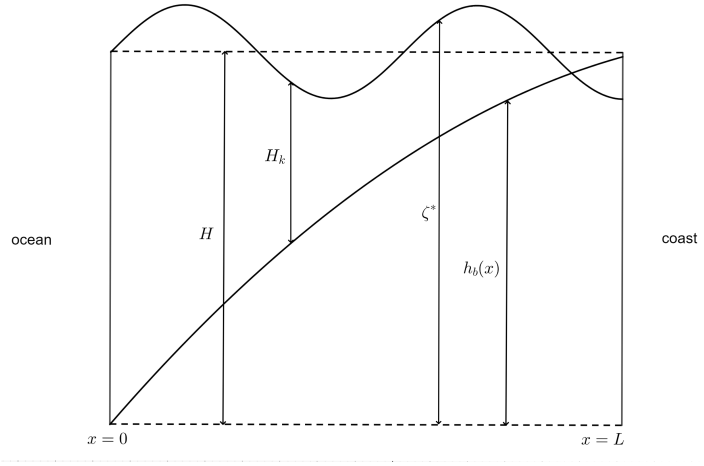


**Fig. 4.1:** A sketch of a one dimensional domain for the statistical depth-averaged shallow water equations.

procedure is applied. However, to define the total flow rates, denoted by $q$, they consider the phase-averaged velocities $U$. This results in the following continuity equation:

$$\eta \frac{\partial \zeta}{\partial t} + \frac{\partial q_x}{\partial x} + \frac{\partial q_y}{\partial y} = S, \tag{4.18}$$

where $q_x$ and $q_y$ are the total flow rates per unit width in $x$ and $y$ directions defined by

$$q_x = \int_{-\infty}^{\zeta} U_x \, dz \quad \text{and} \quad q_y = \int_{-\infty}^{\zeta} U_y \, dz,$$

and $U_x$ and $U_y$ are the phase-averaged velocities in the $x$ and $y$ directions, respectively. $S$ describes a source term which we will set to zero. Note that except for the extra parameter $\eta$ and an extra averaging procedure of the velocities, this continuity equation is equal to the one of our previous model. They apply a similar procedure to the momentum equations, but they use the effective water depth and correct the nonuniform vertical velocities due to the bottom irregularities. We combine the stresses and viscosities to the free surface shear stress $\tau_s$ and bottom shear stress $\tau_b$ and neglect the free surface shear stress. This results in the following equations

$$\begin{cases} \dfrac{\partial q_x}{\partial t} + \dfrac{\partial}{\partial x}\left(\epsilon_{xx}\dfrac{q_x^2}{Y}\right) + \dfrac{\partial}{\partial y}\left(\epsilon_{xy}\dfrac{q_x q_y}{Y}\right) + \dfrac{\tau_{bx}}{\rho} + gY\dfrac{\partial \zeta}{\partial x} = 0, \\ \dfrac{\partial q_y}{\partial t} + \dfrac{\partial}{\partial x}\left(\epsilon_{xy}\dfrac{q_x q_y}{Y}\right) + \dfrac{\partial}{\partial y}\left(\epsilon_{yy}\dfrac{q_y^2}{Y}\right) + \dfrac{\tau_{by}}{\rho} + gY\dfrac{\partial \zeta}{\partial y} = 0, \end{cases} \tag{4.19}$$

where the $\epsilon$'s are correction factors for the nonuniform vertical velocity defined by:

$$\epsilon_{xy} = \frac{Y}{q_x q_y} \int_{-\infty}^{\zeta} \frac{U_x U_y}{\nu} \, dz. \tag{4.20}$$

Let us compare these new equations to our previously used equations given in Eq. (4.14), with $ru = \tau_{bx}/\rho$. Assuming there are no dry areas, the water volume can be simplified to the water depth, resulting in $Y = H - \zeta - h_b$. Furthermore, assuming all areas are wet gives $\eta = 1$ and the correction terms for the bottom irregularities can also be assumed to be equal to one. By rescaling the velocity $q$

to the water depth times the velocity, we can write Eqns. (4.14) as

$$\frac{\partial u_x}{\partial x} + \frac{\partial u_y}{\partial y} + \frac{\partial \zeta}{\partial t} = 0, \tag{4.21a}$$

$$\frac{\partial u_x}{\partial t} + \mathbf{u} \cdot \nabla \frac{u_x}{Y} + gY\frac{\partial \zeta}{\partial x} + \frac{\tau_{bx}}{\rho} = 0, \tag{4.21b}$$

$$\frac{\partial u_y}{\partial t} + \mathbf{u} \cdot \nabla \frac{u_y}{Y} + gY\frac{\partial \zeta}{\partial y} + \frac{\tau_{by}}{\rho} = 0. \tag{4.21c}$$

Note that the nonlinear terms in the new system are in conservative form and for $\epsilon = 1$ these terms are equal to the nonlinear terms in the old system. So assuming the domain has no partially dry areas, our new system reduces to the classical shallow water equations.

Before continuing, we need to find an expression for the new parameters $\eta$ and $Y$. For this we need to analyse the characteristics of the bottom. We define the amplitude of the bottom elevations $a_r$. As defined earlier, $\nu(\mathbf{x})$ represents the fraction of area lying above the ground surface. Statistically, $\nu$ can also be seen as the probability that the local bottom elevation does not exceed the water elevation: if this fraction is 1, the entire area is wet and the probability of no drying occurring is 1, and vice versa if this fraction is 0. The probability density function of bottom elevations per element is therefore given by $\frac{\partial \nu}{\partial z}$. Furthermore, the bottom elevations can be assumed to be distributed as a Gaussian pdf [21]. A proper measure of ground irregularities is the standard deviation $\sigma_b$ of the bottom elevations. $a_r$ is therefore given by $a_r = 2\sigma_b$. This results in

$$\frac{\partial \nu}{\partial z} = \frac{2}{a_r\sqrt{\pi}} e^{-\varepsilon^2}, \tag{4.22}$$

where $\varepsilon(\mathbf{x}) = 2(z - \overline{h_b})/a_r$. Integration with respect to $z$ results in an analytical expression for $\nu$:

$$\nu(x) = \frac{1}{2}\left[1 + \mathrm{erf}(\varepsilon)\right], \tag{4.23}$$

where erf is the error function defined by

$$\mathrm{erf}(x) = \frac{2}{\sqrt{\pi}} \int_0^x e^{-t^2} dt. \tag{4.24}$$

Recalling that $\eta$ is the wetted percentage of the domain, this results in

$$\eta = \frac{1}{2}\left[1 + \mathrm{erf}\left(\frac{2(\zeta - \overline{h_b})}{a_r}\right)\right]. \tag{4.25}$$

Note that, assuming $a_r$ is finite for a wet domain such that $\zeta > h_b$ for all $\mathbf{x}$ and $t$, one finds that $\eta = 1$, while for a dry domain this leads to $\eta = 0$. If $\zeta = h_b$, $\eta = \frac{1}{2}$ which is consistent with drying and flooding of the domain. Furthermore, $Y$ was defined as the water volume per unit area and can be expressed as

$$Y = \int_{-\infty}^{\zeta} \nu dz = a_r\left(\eta\frac{\zeta - h_b}{a_r} + \frac{1}{4\sqrt{\pi}} exp\left[-4\left(\frac{\zeta - \overline{h_b}}{a_r}\right)^2\right]\right). \tag{4.26}$$

Ground unevenness in small water depths produces energy losses and the dissipation term in the momentum balance equations becomes dominant. This is used to find an approximation of the bottom shear stress. As a first approximation, the convective acceleration is neglected and we focus on the energy loss term. Considering a small uniform subdomain and defining $Q$ as the discharge and $M$ the cross sectional width, a steady uniform flow gives

$$u = \frac{Q}{M}. \tag{4.27}$$

To estimate the value of $Q$, the mean water depth and the mean energy slope can be used and the Strickler coefficient $K_s$, indicating the resistance to flow of the surface, is introduced. This results in

$$q = gY\frac{K_s\sqrt{J}}{M}\int_M Y(\zeta, x, y)^{5/3}\, ds, \tag{4.28}$$

where $J$ is the mean energy slope and the coefficient $\frac{5}{3}$ is derived from the Manning law (with $\alpha = \frac{2}{3}$ and $\beta = \frac{1}{2}$). The energy loss per unit length is given by

$$J = \frac{q^2}{K_s^2 H_k^{10/3}}, \tag{4.29}$$

where $H_k$ is an equivalent water depth. An expression for this depth can be given by

$$\begin{aligned} H_k &= \left( \frac{1}{M} \int_M Y(\zeta, x, y)^{5/3} \, ds \right)^{3/5} \\ &= a_r \left[ \int_{-\infty}^{Y/a_r} \left( \frac{Y}{a_r} - \varepsilon \right)^{5/3} \frac{\partial \nu}{\partial \varepsilon} \, d\varepsilon \right]^{3/5}. \end{aligned} \tag{4.30}$$

For more details on the derivation, see [22]. Using numerical integration, a suitable analytical approximation of Eq. (4.30) is given by [23]:

$$H_k = Y + 0.27 a_r \sqrt{\frac{Y}{a_r}} exp\left( -\frac{2Y}{a_r} \right). \tag{4.31}$$

The bottom shear stress can then be approximated by

$$\frac{\tau_b x}{\rho} = gY \frac{|\mathbf{q}|}{K_s^2 H_k^{10/3}} q_x, \tag{4.32}$$

with $H_k$ as defined in Eq. (4.31). This approximation can be confirmed by considering uniform flow in the $x$- direction, since the momentum equation then reduces to

$$\tau_{bx} = -\rho g Y \frac{\partial \zeta}{\partial x} = \rho g Y J_x. \tag{4.33}$$

### 4.2.1 Two dimensional shallow water equations for partially dry areas

The two dimensional system of equations is now given by

$$\begin{cases} \eta \dfrac{\partial \zeta}{\partial t} + \dfrac{\partial u_x}{\partial x} + \dfrac{\partial u_y}{\partial y} = 0, \\ \dfrac{\partial u_x}{\partial t} + \dfrac{\partial}{\partial x}\left( \epsilon_{xx} \dfrac{u_x^2}{Y} \right) + \dfrac{\partial}{\partial y}\left( \epsilon_{xy} \dfrac{u_x u_y}{Y} \right) + gY \dfrac{|\mathbf{u}|}{K_s^2 H_k^{10/3}} u_x + gY \dfrac{\partial \zeta}{\partial x} = 0, \\ \dfrac{\partial u_y}{\partial t} + \dfrac{\partial}{\partial x}\left( \epsilon_{xy} \dfrac{u_x u_y}{Y} \right) + \dfrac{\partial}{\partial y}\left( \epsilon_{yy} \dfrac{u_y^2}{Y} \right) + gY \dfrac{|\mathbf{u}|}{K_s^2 H_k^{10/3}} u_y + gY \dfrac{\partial \zeta}{\partial y} = 0, \\ u(t) = 0 \qquad \text{at } x, y \in \delta\Omega_c, \\ \zeta(t) = H_r + A\cos(\sigma t + \phi) \quad \text{at } x, y \in \delta\Omega_s, \end{cases} \tag{4.34}$$

where $H_r$ is the constant reference water depth, $\zeta$ is the water height, $u$ is the depth integrated velocity, $K_s$ is the Strickler friction coefficient, $t$ is time and $\eta$ is the local percentage of wetted domain, and $H_k$ the equivalent depth, given by Eq. (4.25) and Eq. (4.31), respectively.
An earlier version of this system of equations neglects the second nonlinear term in the momentum balance equations (essentially setting $\epsilon$ to zero), and is given in [20]. The effectiveness and the restrictions of this model are discussed along a model application in [22].

### 4.2.2 One dimensional shallow water equations for partially dry areas

The model in one dimension is given by:

$$\begin{cases} \eta \dfrac{\partial \zeta}{\partial t} + \dfrac{\partial u}{\partial x} = 0, \\ \dfrac{\partial u}{\partial t} + \dfrac{\partial}{\partial x}\left( \epsilon_{xx} \dfrac{u^2}{Y} \right) + gY \dfrac{|\mathbf{u}|}{K_s^2 H_k^{10/3}} u + gY \dfrac{\partial \zeta}{\partial x} = 0, \\ \zeta(t, 0) = H_r + A\cos(\sigma t + \phi), \\ \dfrac{\partial \zeta}{\partial x}(t, L) = 0, \end{cases} \tag{4.35}$$

where $H_r$ is the constant reference water depth, $\zeta$ is the water height, $u$ is the depth integrated velocity, $K_s$ is the Strickler friction coefficient, $t$ is time and $\eta$ is the local percentage of wetted domain, and $H_k$ the equivalent depth, given by Eq. (4.25) and Eq. (4.31), respectively.

# 5

# Analysis of the classical shallow water equations

In this chapter the shallow water equations obtained by the classical depth-averaging approach are analysed. The one dimensional equations are simplified to obtain a linear system of equations in Section 5.1. First, assuming a flat bed, this linearised system is solved and the results are discussed in Section 5.2. Three solution techniques are employed: analytical, numerical using a forward Euler and centered space scheme, and a solution method in the frequency domain. This system allows for an analytical solution and hence an in-depth analysis of the underlying physics. This is discussed in Section 5.2.2. Since an analytical solution is obtained, the accuracy of the numerical methods can be assessed. In Section 5.3 the linearised system with variable seabed is solved using the numerical solution methods. The results are discussed in Section 5.4.

## 5.1 Linearisation

We start with the one dimensional shallow water equations given by Eqns. (4.15), obtained by the classical depth-averaging approach as discussed in Section 4.1. Scaling analysis allows for the neglect of the nonlinear terms, for more details see Appendix C. For now, the total water depth is assumed large, such that the free surface deviation may also be neglected (i.e. $\zeta \ll H$). This results in the following system of equations:

$$\begin{cases} \dfrac{\partial}{\partial x}[(H-h_b)u] + \dfrac{\partial \zeta}{\partial t} = 0, \\ \dfrac{\partial u}{\partial t} + g\dfrac{\partial \zeta}{\partial x} + \dfrac{r}{H-h_b}u = 0, \\ u(t,L) = 0, \\ \zeta(t,0) = A\cos(\sigma t + \phi), \end{cases} \tag{5.1}$$

where $H$ is the constant reference depth, $h_b = h_b(x)$ is the known bottom deviation, $u$ is the depth-averaged flow velocity and $\zeta$ the free surface elevation.

## 5.2 One dimensional shallow water system

In this section, the linearised one dimensional shallow water equations without any bottom deviations (i.e. $h_b \equiv 0$) is solved and discussed. In Section 5.2.1, an analytical solution is obtained. Section 5.2.2 discusses some insight in the underlying physics that this solution provides. In Section 5.2.3 and Section 5.2.4, a numerical method and a solution method in the frequency domain are discussed. The results of all three methods are compared and discussed in Section 5.4.

Fig. 5.1 shows a sketch of our simplified one dimensional model. The following boundary conditions are assumed; the coastline is defined at $x = L$, the assumption is that there is no water transport there thus $u(t, L) = 0$. At $x = 0$, the sea surface elevation is prescribed.

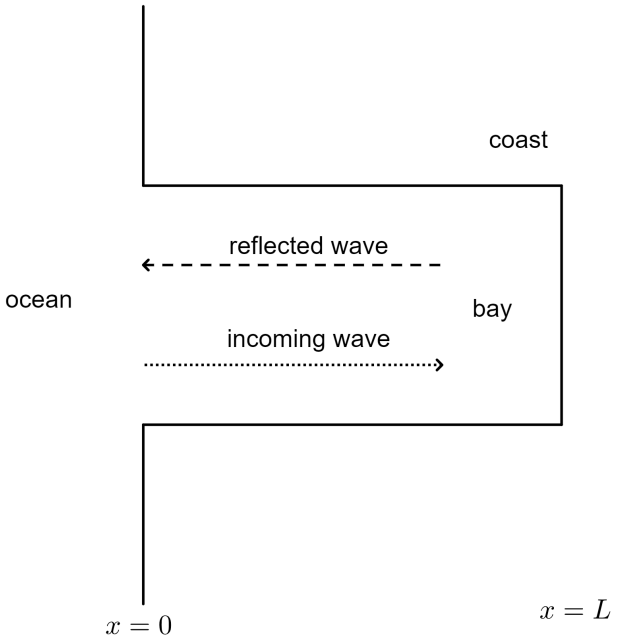


**Fig. 5.1:** The domain of our simplified one dimensional system: a rectangular embayment.

### 5.2.1 Analytical solution

The analytical solution to this system of equations consists of a particular solution due to the forcing at the seaward boundary, and a homogeneous solution. In this case, all the eigenvalues of the homogeneous solution have a negative real part and therefore the homogeneous solution converges to zero for $t \to \infty$. Since we are interested in the long-term behaviour, this transient behaviour is neglected and only the particular solution will be discussed. For more details we refer to Appendix D.
To find the particular solution, first we combine the equations to obtain a second order partial differential equation for the free surface elevation $\zeta(t, x)$. Using $\zeta$, the velocity $u$ can be obtained. To obtain this equation, we let the operator $(\partial/\partial t + r/H)$ act on the mass balance equation and substitute the momentum balance equation in this equation. This results in

$$\begin{cases} \dfrac{\partial^2 \zeta}{\partial t^2} - gH\dfrac{\partial^2 \zeta}{\partial x^2} + \dfrac{r}{H}\dfrac{\partial \zeta}{\partial t} = 0, \\ \zeta(t,0) = A\cos(\sigma t + \phi), \\ \dfrac{\partial \zeta}{\partial x}(t, L) = 0. \end{cases} \tag{5.2}$$

Note that the boundary conditions for $\zeta$ at $x = L$ follows directly from the boundary condition $u(t, L) = 0$ for all $t$. If $u(t, L) = 0$, it follows that $\frac{\partial u}{\partial t}(t, L) = 0$ and thus $\frac{\partial \zeta}{\partial x}(t, L) = 0$ as well.

Using the seaward boundary condition and the linearity of Eq. (5.2), we assume a solution of the form $\zeta(t, x) = Re\left(Z(x)e^{-i\sigma t}\right)$. We take $\phi = 0$. Substitution gives an ordinary differential equation and we find

$$\begin{cases} Z''(x) + \left(\dfrac{\sigma^2}{gH} + \dfrac{ir\sigma}{gH^2}\right) Z(x) = 0, \\ Z(0) = A, \\ Z'(L) = 0. \end{cases} \tag{5.3}$$

We define the complex wavenumber $K$ such that $K^2 = \frac{\sigma^2}{gH} + \frac{ir\sigma}{gH^2}$. The general solution solution of $Z(x)$ is an exponential function with complex exponents $iKx$ and $-iKx$. Using the boundary conditions, this results in the following solution:

$$Z(x) = \frac{A}{2\cos(KL)}\left[e^{iK(L-x)} + e^{-iK(L-x)}\right]. \tag{5.4}$$

The analytical solution of the free surface elevation can now be given by

$$\zeta(t,x) = Re\left(\frac{A}{2\cos(KL)}\left[e^{iK(L-x)}e^{-i\sigma t} + e^{-iK(L-x)}e^{-i\sigma t}\right]\right). \tag{5.5}$$

For the velocity $u$ we assume a solution of the form $u(t,x) = Re\left(U(x)e^{-i\sigma t}\right)$. Substitution of the analytical solution of $\zeta$ in the mass balance equation gives the analytical solution of the velocity

$$u(t,x) = Re\left(\frac{-\sigma A}{2HK\cos(KL)}\left[e^{iK(L-x)}e^{-i\sigma t} - e^{-iK(L-x)}e^{-i\sigma t}\right]\right). \tag{5.6}$$

### 5.2.2 Physical interpretation

To interpret the solutions, we consider the positive and negative complex exponents separately. Using the amplitude-phase formulation, we write the complex amplitude $Z(x)$ as $Z(x) = \hat{Z}e^{i\theta x}$, with $\hat{Z}$ the amplitude and $\theta$ the phase of $Z(x)$. See Appendix E for more details on the amplitude-phase formulation. The complex wavenumber $K$ consists of an imaginary part $K_i$ and a real part $K_r$, such that $K = K_r + iK_i$. These components read $K_r = \sqrt{\frac{\sigma}{2gH}(\sigma + \sqrt{\sigma^2 + g^2r^2})}$ and $K_i = \sqrt{\frac{\sigma}{2gH}(-\sigma + \sqrt{\sigma^2 + g^2r^2})}$. We define $K_i$ as the friction scale; for a frictionless case (i.e. $r \ll 0$) $K_i = 0$, when increasing the friction $K_i$ also increases.

$$\zeta(t,x) = Re\left(\frac{A}{2\cos(KL)}\left[e^{K_i(L-x)}e^{i(K_rx-\sigma t-K_rL)} + e^{-K_i(L-x)}e^{-i(K_rx+\sigma t-K_rL)}\right]\right). \tag{5.7}$$

The water height in Eq. (5.7) is described by the incoming, right moving wave given by the positive exponent, and the reflected, left moving wave given by the negative exponent. The exponent $e^{\pm K_i(L-x)}$ describes a decrease in amplitude of the waves with respect to the friction scale. Fig. 5.2 shows the amplitudes of the incoming and reflected waves as a function of $x$. The figure shows that both the incoming and the reflected wave is attenuated due to the bottom friction effects.

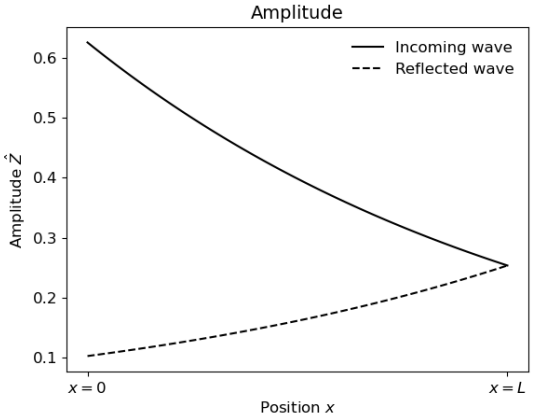


**Fig. 5.2:** The amplitudes of incoming and reflected waves. The values of the used parameters can be found in Tab. 5.1.

As expected from the definition of $K_i$, the larger the bottom friction $r$ the larger the reduction of the wave amplitudes. Fig. 5.3 gives a visualisation of the influence of friction on the solutions.

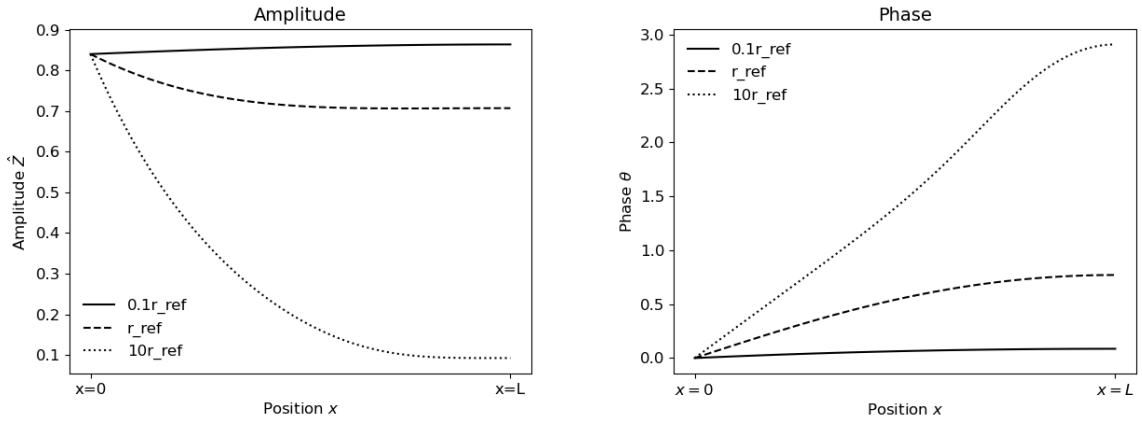


**(a)** Amplitude **(b)** Phase

**Fig. 5.3:** The amplitude and phase of $Z(x)$ for different values of the friction coefficient. The reference friction $r_{ref} = 4 \cdot 10^{-4}$ rad/s, see parameters in Tab. 5.1.

Fig. 5.3a shows that a larger friction leads to smaller amplitudes, indicating attenuation of the wave, whereas Fig. 5.3b illustrates that a larger friction results in larger phases, as was expected from the definition of the wavenumber. Furthermore, the figures show that in case of weak friction, the largest sea surface elevations occur at the coast. Therefore, for weak friction, the wave is amplified at the coast. For all friction, the phase increases from the sea towards the coast. This increase is larger in case of strong friction, while in case of weak friction the increase is barely visible.
Similar results can be found for the amplitude and phase functions of the velocity shown in Fig. 5.4.

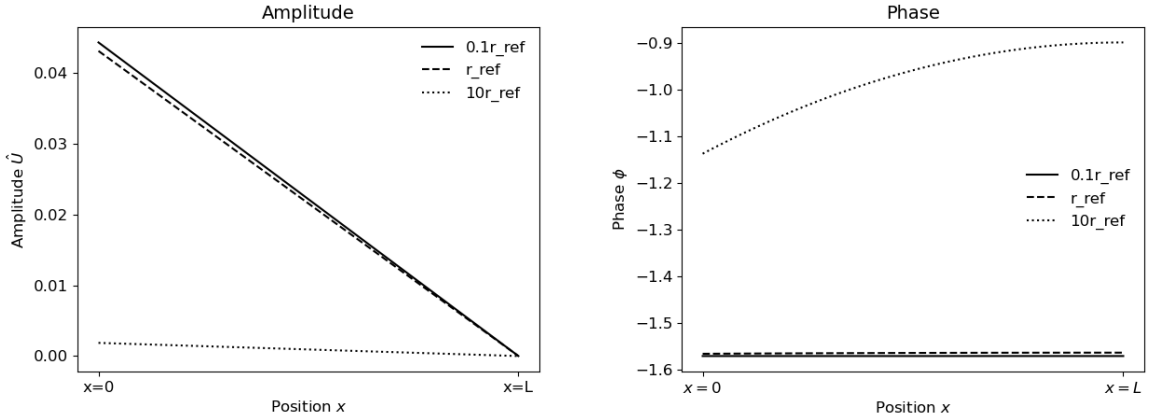


**(a)** Amplitude **(b)** Phase

**Fig. 5.4:** The amplitude and phase of $U(x)$ for different values of the friction coefficient. The reference friction $r_{ref} = 4 \cdot 10^{-4}$ rad/s, see parameters in Tab. 5.1.

The velocity amplitude is largest at the seaward boundary and decreases to zero at the coast. Furthermore, Fig. 5.4a shows that the amplitude of the tidal velocity is larger for a smaller friction coefficient. From the phase of the velocity function shown in Fig. 5.4b, we see that for weak friction the phases are almost constant and the tide behaves like a pumping mode. For increasing friction values of the friction coefficient, there are clear phase differences in the basin.

For more analysis on the behaviour of the waves, we consider the dimensionless amplitudes, by dividing by $A$ the amplitude at the seaward boundary. We change the basin length and make it dimensionless, by dividing by $\frac{1}{\sigma}\sqrt{gH}$. To study the effect of bottom friction on the resonance characteristics of the tidal embayment, we analyse the influence of the frictionless tidal wavelength $\sigma L/\sqrt{gH}$ on the amplitudes of the waves. Since the Figs. 5.3a and 5.4a show that the largest sea surface elevation occurs at the coast and the largest velocity occurs at the seaward boundary, we expect amplification

for the sea surface at the coast and for the velocity at the seaward boundary. We study the amplitudes at these boundaries respectively. Consider the dimensionless sea surface amplitude $\widetilde{Z} = \frac{Z(\hat{L})}{A}$ and the dimensionless velocity amplitude $\widetilde{U} = \frac{\hat{U}(0)\sqrt{gH}}{gA}$ versus the parameter $y = \sigma L/\sqrt{gH}$.

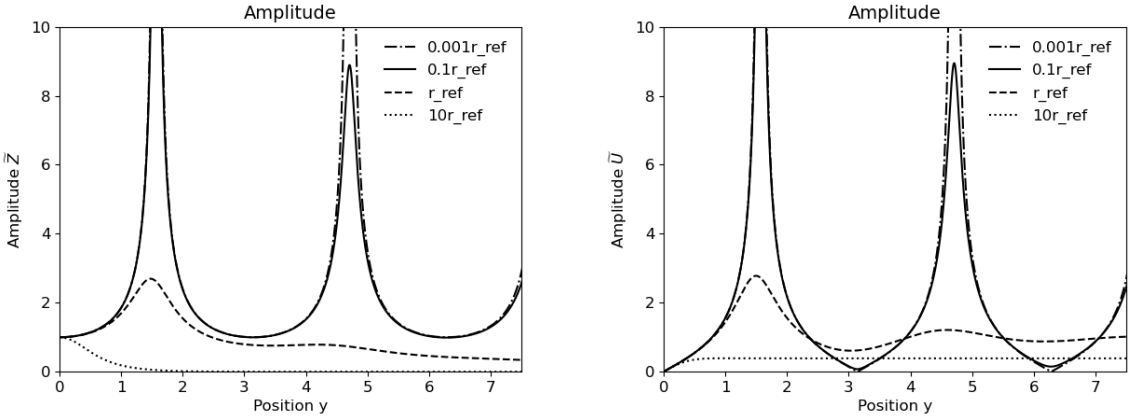


**(a)** $\widetilde{Z}$ **(b)** $\widetilde{U}$

**Fig. 5.5:** The dimensionless amplitudes versus the frictionless parameter for different amounts of friction.The reference friction $r_{ref} = 4 \cdot 10^{-4}$ rad/s, see parameters in Tab. 5.1.

Fig. 5.5a shows that the amplification for the sea surface elevation at the coast, and Fig. 5.5b shows the amplification for the velocity at the seaward boundary. Both figures show that small friction coefficients lead to tidal amplification for both the sea surface elevation and the velocity. The reference friction leads to a more realistic results, with a slight amplification. Increasing friction coefficients decrease the amplification.

### 5.2.3 Fully numerical solution

Since the analytical solution is restricted to simple problems, this section provides a numerical method which can be expanded to more complex problems. The numerical solution will be tested by comparing the results to the analytical solution, this will be discussed in Section 5.4. The numerical method used is called the forward time centered space (FTCS) scheme. We start with discretisation in space using a central difference scheme. Let $i$ denote the index of the spatial points in the discretised domain with stepsize $\Delta x$, then

$$\begin{cases} \dfrac{du_i}{dt} &= -g\dfrac{\zeta_{i+1} - \zeta_{i-1}}{2\Delta x} - \dfrac{r}{H}u_i, \\ \dfrac{d\zeta_i}{dt} &= -H\dfrac{u_{i+1} - u_{i-1}}{2\Delta x}. \end{cases} \tag{5.8}$$

A forward time or forward Euler scheme is used for the time discretisation. Let k denote the space in time with timestep $\Delta t$. The forward Euler scheme is given by

$$\frac{du}{dt} = \frac{u^{k+1} - u^k}{\Delta t},$$

combining this with the discretisation in space gives

$$\begin{cases} u_i^{k+1} &= u_i^k - \Delta t\ g\dfrac{\zeta_{i+1}^k - \zeta_{i-1}^k}{2\Delta x} - \dfrac{\Delta t\ r}{H}u_i^k, \\ \zeta_i^{k+1} &= \zeta_i^k - \Delta t\ H\dfrac{u_{i+1^k} - u_{i-1}^k}{2\Delta x}. \end{cases} \tag{5.9}$$

For the resulting system, the CFL condition $\left|\frac{\Delta t H}{\Delta x}\right| \leq 1$ (or $\left|\frac{\Delta t g}{\Delta x}\right| \leq 1$) is a necessary condition for stability but not sufficient. In fact, the FTCS scheme is unconditionally unstable [24]. To derive a stable solution, the forward Euler scheme is combined with the Lax-Friedrich's method. The system

now becomes conditionally stable, with the condition being the CFL condition. Lax-Friedrich's method simply replaces the term $u_i^k$ or $\zeta_i^k$ with its spatial average. This results in the following scheme

$$\begin{cases} u_i^{k+1} &= \left(\frac{1}{2} - \frac{\Delta t\ r}{2H}\right)\left(u_{i+1}^k + u_{i-1}^k\right) - \frac{\Delta t\ g}{2\Delta x}\left(\zeta_{i+1}^k - \zeta_{i-1}^k\right), \\ \zeta_i^{k+1} &= \frac{1}{2}\left(\zeta_{i+1}^k + \zeta_{i-1}^k\right) - \frac{\Delta t\ H}{2\Delta x}\left(u_{i+1}^k - u_{i-1}^k\right). \end{cases} \tag{5.10}$$

The scheme is $O(\Delta t)$ accurate in time and $O(\Delta x^2)$ in space. Note that by using the spatial average, the method introduces viscosity. The dissipation term decreases faster than the truncation error of the method and therefore the method converges to the correct solution. Note that attention needs to be paid to the choice of the timestep. For the method to be stable the timestep must be smaller than the step in space divided by $H$. For a timestep much smaller than the step in space, however, the dissipation term increases and the amplitude decreases resulting in stable but inaccurate results. Therefore, For accurate and stable results we consider a large number of discretisation steps in space and set the timestep equal to the CFL condition $\Delta = 0.99\Delta x/H$.
We rewrite the system to matrix-vector notation as

$$\begin{cases} \mathbf{u}^{k+1} = V_1\mathbf{u}^k + W_1\zeta^{k+1}, \\ \zeta^{k+1} = V_2\mathbf{u}^k + W_1\zeta^k. \end{cases} \tag{5.11}$$

with matrices $V_1$, $V_2$, $W_1$ and $W_2$ defined by

$$V_1 = \left(\frac{1}{2} - \frac{\Delta t r}{2H}\right)\begin{pmatrix} 0 & 2 & 0 & 0 & \cdots & 0 \\ 1 & 0 & 1 & 0 & \cdots & 0 \\ 0 & 1 & 0 & 1 & \cdots & \vdots \\ \vdots & & \ddots & \ddots & \ddots & \vdots \\ 0 & \cdots & 0 & 1 & 0 & 1 \\ 0 & \cdots & \cdots & 0 & 0 & 1 \end{pmatrix}, \qquad W_1 = \frac{\Delta t g}{2\Delta x}\begin{pmatrix} 2 & -2 & 0 & 0 & \cdots & 0 \\ 1 & 0 & -1 & 0 & \cdots & 0 \\ 0 & 1 & 0 & -1 & \cdots & \vdots \\ \vdots & & \ddots & \ddots & \ddots & \vdots \\ 0 & \cdots & 0 & 1 & 0 & -1 \\ 0 & \cdots & \cdots & 0 & 0 & 0 \end{pmatrix},$$

$$V_2 = \frac{\Delta t H}{2\Delta x}\begin{pmatrix} 0 & 0 & 0 & 0 & \cdots & 0 \\ 1 & 0 & -1 & 0 & \cdots & 0 \\ 0 & 1 & 0 & -1 & \cdots & \vdots \\ \vdots & & \ddots & \ddots & \ddots & \vdots \\ 0 & \cdots & 0 & 1 & 0 & -1 \\ 0 & \cdots & \cdots & 0 & 2 & -2 \end{pmatrix}, \qquad W_2 = \frac{1}{2}\begin{pmatrix} 1 & 0 & 0 & 0 & \cdots & 0 \\ 1 & 0 & 1 & 0 & \cdots & 0 \\ 0 & 1 & 0 & 1 & \cdots & \vdots \\ \vdots & & \ddots & \ddots & \ddots & \vdots \\ 0 & \cdots & 0 & 1 & 0 & 1 \\ 0 & \cdots & \cdots & 0 & 2 & 0 \end{pmatrix},$$

$$\mathbf{u}^0 = \begin{pmatrix} u_0 \\ u_1 \\ u_2 \\ \vdots \\ u_{n-1} \\ 0 \end{pmatrix}, \qquad \zeta^0 = \begin{pmatrix} A\cos(\sigma t) \\ \zeta_1 \\ \zeta_2 \\ \vdots \\ \zeta_{n-1} \\ \zeta_n \end{pmatrix}.$$

### 5.2.4 Solution in the frequency domain, combined with a centered space discretisation

Since the system of equations is forced periodically, it seems appropriate to solve the sea surface elevation and velocity in the frequency domain. Just like for the analytical solution, we assume the solution is of the form $e^{-i\sigma t}$ due to the boundary condition. However, to solve more complex problems like a variable

sea bottom, the spatial part of the variables is obtained using space discretisation. Substitution of the assumed frequency $e^{-i\sigma t}$ into the system of equations 5.1 gives

$$U(x) = \frac{-igH}{\sigma H + ir} Z'(x) \quad \text{and} \quad Z(x) = \frac{H}{i\sigma} U'(x).$$

Now we discretise in space using a central difference scheme and substitute the first equation into the second equation, this resulting scheme is given by

$$\begin{cases} U_j &= \dfrac{-igH}{2\Delta x(\sigma H + ir)} \left(Z_{j+1} - Z_{j-1}\right), \\ Z_j &= \dfrac{-iH}{2\Delta x\ \sigma} \left(U_{j+1} - U_{j-1}\right). \end{cases} \tag{5.12}$$

We rewrite to matrix vector notation as

$$\begin{cases} I\mathbf{U} + X\mathbf{Z} = \tilde{\mathbf{U}}, \\ Y\mathbf{U} + I\mathbf{Z} = \tilde{\mathbf{Z}}, \end{cases} \tag{5.13}$$

with $I$ the identity matrix,

$$X = \begin{pmatrix} -2x & 2x & 0 & 0 & \cdots & 0 \\ -x & 0 & x & 0 & \cdots & 0 \\ 0 & -x & 0 & x & \cdots & \vdots \\ \vdots & & \ddots & \ddots & \ddots & \vdots \\ 0 & \cdots & 0 & -x & 0 & x \\ 0 & \cdots & \cdots & 0 & 0 & 0 \end{pmatrix}, \qquad Y = \begin{pmatrix} 0 & 0 & 0 & 0 & \cdots & 0 \\ -y & 0 & y & 0 & \cdots & 0 \\ 0 & -y & 0 & y & \cdots & \vdots \\ \vdots & & \ddots & \ddots & \ddots & \vdots \\ 0 & \cdots & 0 & -y & 0 & y \\ 0 & \cdots & \cdots & 0 & -2y & 2y \end{pmatrix},$$

$$\tilde{\mathbf{U}} = \begin{pmatrix} 0 \\ 0 \\ 0 \\ \vdots \\ 0 \\ 0 \end{pmatrix}, \quad \tilde{\mathbf{Z}} = \begin{pmatrix} A \\ 0 \\ 0 \\ \vdots \\ 0 \\ 0 \end{pmatrix}, \qquad x = \frac{igH}{2\Delta x(\sigma H + ir)} \text{ and } y = \frac{iH}{2\Delta x\ \sigma}.$$

The solutions in the frequency domain are now given by

$$\begin{cases} u(x,t) &= Re\left(\mathbf{U}e^{-i\sigma t}\right), \\ \zeta(t,x) &= Re\left(\mathbf{Z}e^{-i\sigma t}\right). \end{cases} \tag{5.14}$$

## 5.3 One dimensional shallow water system with arbitrary seabed

In the previous example, the seabed deviations were neglected. Now we consider the same situation with a variable seabed. This way we can account for the water becoming more shallow closer to the coast. Fig. 5.6 shows a sketch of the domain of the simplified one dimensional system with variable seabed.

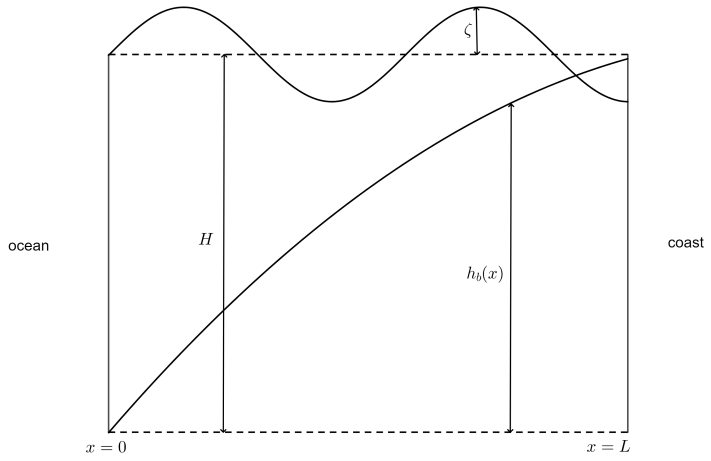


**Fig. 5.6:** The domain of the simplified one dimensional system with variable seabed $h_b = h(x)$.

Assuming the bottom deviation is known and continuously differentiable, the system of equations given by Eq. (5.1) can be written as

$$\begin{cases} [H - h_b(x)] \dfrac{\partial u}{\partial x} - \dfrac{\partial h_b}{\partial x}\dfrac{\partial u}{\partial x} + \dfrac{\partial \zeta}{\partial t} = 0, \\ \dfrac{\partial u}{\partial t} + g\dfrac{\partial \zeta}{\partial x} + \dfrac{r}{H - h_b(x)}u = 0, \\ u(t, L) = 0, \\ \zeta(t, 0) = A\cos(\sigma t + \phi). \end{cases} \tag{5.15}$$

To generalise these equations, we aim to find a method that does not require differentiation of the bottom. Therefore, we define a new variable $\hat{u} = \frac{1}{g}(H - h(x))u$, this variable is a product of distance and time and represents the displacement. Note that this choice both leads to a simplified equation as well as ensuring maximum accuracy of a stable numerical scheme. A more obvious choice would have been $\hat{u} = (H - h(x))u$. In this case the CFL condition is given by $|\frac{gH\Delta t}{\Delta x}| \leq 1$. The order of accuracy of the Lax-Friedrich method is given by $O(\Delta t + \Delta x^2/\Delta t)$. This condition ensures that $\Delta t$ is $O(gH)$ smaller than $\Delta x$, which with the parameter values given in Tab. 5.1 gives an approximate accuracy of $O(100\Delta x)$ while the previous results had an approximate accuracy of $O(10\Delta x)$. Therefore, to increase accuracy back to approximately $O(10\Delta x)$, we rewrite the system such that $\hat{u} = \frac{1}{g}(H - h(x))u$. Omitting the overline, this leads to

$$\begin{cases} \dfrac{\partial \zeta}{\partial t} = -g\dfrac{\partial u}{\partial x}, \\ \dfrac{\partial u}{\partial t} = -(H - h_b(x))\dfrac{\partial \zeta}{\partial x} - \dfrac{r}{H - h_b(x)}u, \\ u(t, L) = 0, \\ \zeta(t, 0) = A\cos(\sigma t + \phi). \end{cases} \tag{5.16}$$

### 5.3.1 Fully numerical solution

Similar as before, we combine a FTCS scheme with Lax-Friedrich's method, resulting in

$$\begin{cases} u_i^{k+1} = \dfrac{1}{2}\left(1 - \dfrac{\Delta t\ r}{H - h_i}\right)(u_{i+1}^k + u_{i-1}^k) - \dfrac{\Delta t}{2\Delta x}(H - h_i)(\zeta_{i+1}^k - \zeta_{i-1}^k), \\ \zeta_i^{k+1} = \dfrac{1}{2}(\zeta_{i+1}^k + \zeta_{i-1}^k) - \dfrac{\Delta t\ g}{2\Delta x}(u_{i+1}^k - u_{i-1}^k). \end{cases} \tag{5.17}$$

The CFL condition is given by $|\frac{H\Delta t}{\Delta x}| \leq 1$ and it is a necessary and sufficient condition for the solution to be stable.

### 5.3.2 Frequency approximation and centered space discretisation

We assume the solutions are of the form $u,\ \zeta \sim Re\left(\hat{U}(x)e^{-i\sigma t}\right),\ Re\left(Z(x)e^{-i\sigma t}\right)$. Substitution gives

$$\begin{cases} \hat{U}(x) = \dfrac{-i(H-h(x))^2}{\sigma(H-h(x))+ir} Z'(x) \\ Z(x) = \dfrac{-ig}{\sigma}\hat{U}'(x) \end{cases} \tag{5.18}$$

Using central differences for discretisation in space and substitution, we find the following scheme

$$\begin{cases} U_j = \dfrac{-i(H-h(x))^2}{2\Delta x[\sigma\,(H-h\,(x))+ir]}\,(Z_{j+1}-Z_{j-1}) \\ Z_j = \dfrac{-ig}{2\Delta x\ \sigma}\,(U_{j+1}-U_{j-1}) \end{cases} \tag{5.19}$$

## 5.4 Results

The analytical solution obtained in Section 5.2.1 allows the accuracy of the numerical solutions to be tested. For the initial conditions for the fully numerical solution method, the analytical solutions with a deviation of order $10^{-2}$ is employed. The friction ensures that the solution converges. The parameter values used in the calculations are given in Tab. C.1, the values are provided by [25]. To ensure stability,

| Variables | | Parameters | |
|---|---|---|---|
| H | 12 m | f | $10^{-4}$ rad/s |
| L | $1.9 \cdot 10^4$ m | g | 9.81 m/s$^2$ |
| U | 0.19 m/s | r | $4 \cdot 10^{-4}$ m/s |
| A | 0.84 m | $\widetilde{\mu_h}$ | 10 m$^2$/s |
| $\sigma$ | $1.4 \cdot 10^{-4}$ rad/s | | |

**Table 5.1:** Parameter values of the Ameland system, provided by [25].

the CFL condition is used such that $\Delta t = 0.99\frac{\Delta x}{H}$. The solutions for $n = 100$ and $\Delta x \approx 188$ and $\Delta t \approx 16$ are illustrated in Fig. 5.7. Fig. 5.7 suggest that both the fully numerical method and the numerical method in the frequency domain, can be used to predict water motion using the classical shallow water equations. In the fully numerical solution a slight phase shift can be observed, this is the biggest cause of the error as can be seen by the periodicity of the error. Since the analytical solution consists of only one frequency, the solution in the frequency domain is straightforward and its accuracy is solely dependent on the discretisation in space. The centered space scheme should result in an accuracy of $O\left(\Delta x^2\right)$. The time discretisation in the fully numerical method reduces the accuracy, it uses Lax-Friedrich's method which has an accuracy of order $O\left(\Delta t + \frac{\Delta x^2}{\Delta t}\right)$. The CFL condition used for the time step, reduces this to $O\left(\frac{\Delta x}{H} + H\Delta x\right)$. Indeed, Fig. 5.7 shows that for both the velocity and the water height, the solution in the frequency domain is more accurate than the fully numerical solution. To study the accuracy of both methods, we consider the error dependent on the discretisation in the space. For a fair comparison, while ensuring the numerical solution is no longer affected by the initial condition, we consider the solutions at a set time of $t = 12$ hours. Comparing the dashed lines in Fig. 5.8 it is found that the errors of the fully numerical method have the expected order of accuracy. The corresponding errors are given in Tab. 5.2. These values can be used to calculate the rate of convergence. Using the

| N | Numeric, u | Numeric, z | Harmonic, u | Harmonic, z |
|---|---|---|---|---|
| 8 | 2.02E-02 | 7.11E-02 | 3.77E-04 | 2.99E-03 |
| 16 | 1.15E-02 | 4.09E-02 | 8.92E-05 | 7.80E-04 |
| 32 | 6.18E-03 | 2.20E-02 | 2.17E-05 | 1.99E-04 |
| 64 | 3.20E-03 | 1.14E-02 | 5.35E-06 | 5.03E-05 |
| 128 | 1.63E-03 | 5.82E-03 | 1.33E-06 | 1.27E-05 |
| 256 | 8.23E-04 | 2.94E-03 | 3.31E-07 | 3.17E-06 |
| 512 | 4.14E-04 | 1.48E-03 | 8.25E-08 | 7.95E-07 |
| 1024 | 2.07E-04 | 7.40E-04 | 2.06E-08 | 1.99E-07 |

**Table 5.2:** Mean absolute errors of the fully numerical solution (numeric) and the solution in the frequency domain (harmonic), over different number steps in space.

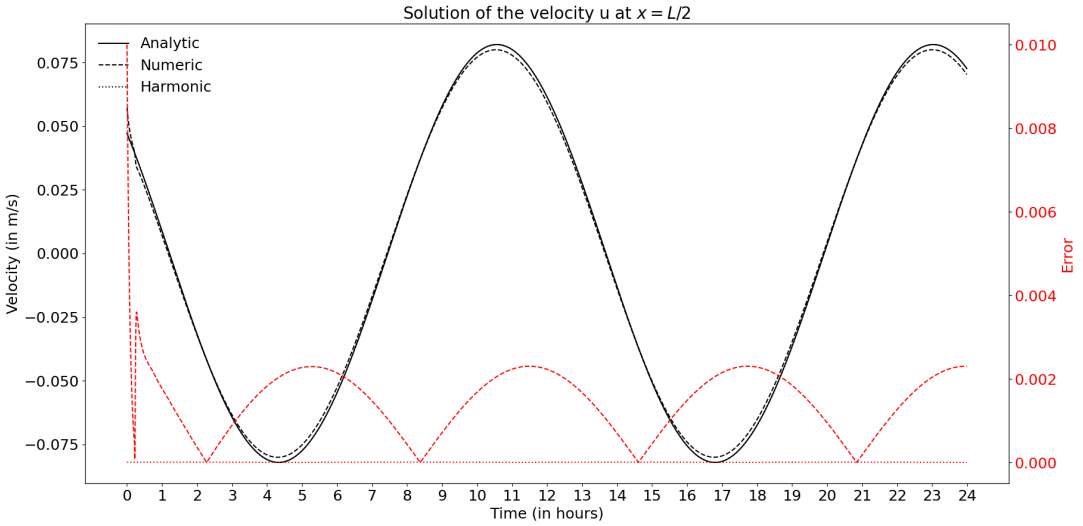


**(a)** Solutions of the velocity $u$.

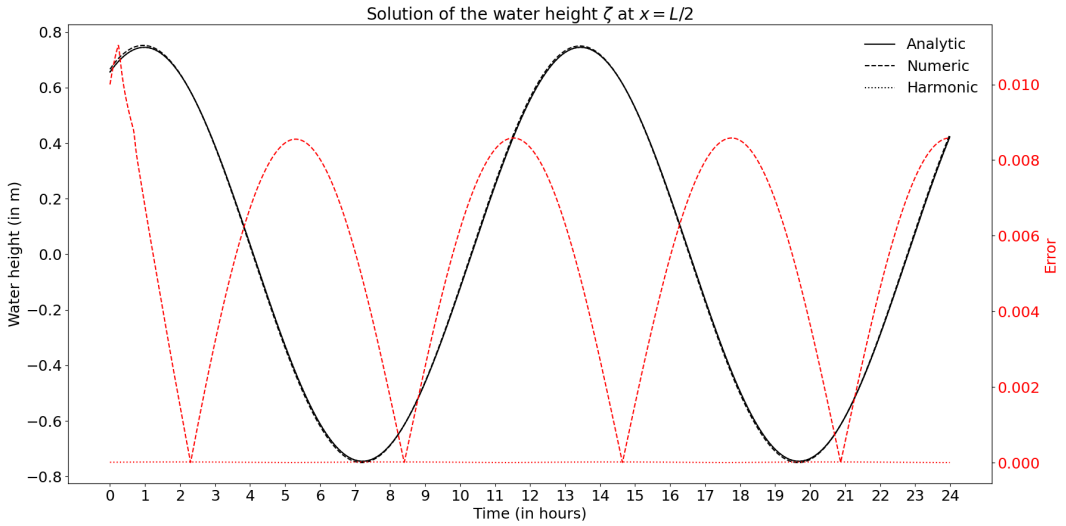


**(b)** Solutions of the water height $\zeta$.

**Fig. 5.7:** Solutions of the velocity and the water height at $x = L/2$ over time for the period of one day. The solid line is the analytical solution (analytic), the dashed line the fully numerical solution (numeric) and the dotted line the solution in the frequency domain (harmonic). The black lines are the solutions and the red lines are the errors.

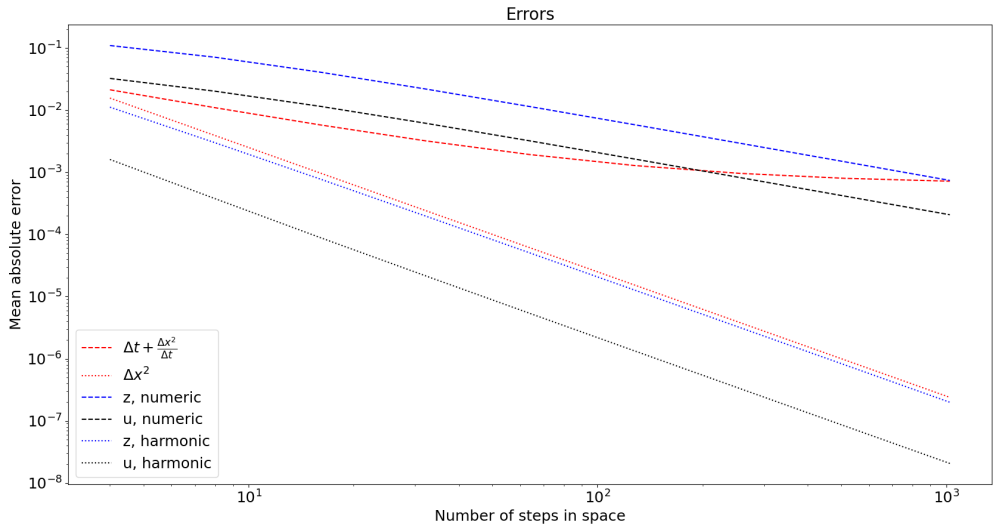


**Fig. 5.8:** Errors of the solutions for the velocity and the water height at $x = L/2$ over the number of discretisation steps in space. The dashed line is the fully numerical solution (numeric) and the dotted line the solution in the frequency domain (harmonic). The black lines are the errors of the velocity, the blue lines are the errors of the water height and the red lines are the expected accuracies.

most accurate solutions of the smallest $\Delta x$, the rates of convergence are determined by

$$P_{numeric,u} \approx \frac{E_{512}}{E_{1024}} \approx \frac{4.14 \cdot 10^{-4}}{2.07 \cdot 10^{-4}} \approx 2.0,$$
$$P_{numeric,z} \approx \frac{E_{512}}{E_{1024}} \approx \frac{1.48 \cdot 10^{-3}}{7.40 \cdot 10^{-4}} \approx 2.0,$$
$$P_{harmonic,u} \approx \frac{E_{512}}{E_{1024}} \approx \frac{8.25 \cdot 10^{-8}}{2.06 \cdot 10^{-8}} \approx 4.0,$$
$$P_{harmonic,z} \approx \frac{E_{512}}{E_{1024}} \approx \frac{7.95 \cdot 10^{-7}}{1.99 \cdot 10^{-7}} \approx 4.0,$$

where $E$ denotes the mean absolute errors of the solution at the given number of steps in space. These rates show that the fully numerical solution converges linearly and the solution in the frequency domain converges quadratically. This is in line with the analytically determined order of accuracies.
Next, we consider different seabeds. First, the solutions for a constant very shallow water depth are obtained. For very shallow water, the timestep becomes smaller to satisfy the CFL condition and ensure stable solutions. This decreases the accuracy of the solutions and therefore a larger number if steps in space is required for accurate results. Therefore, the water motion prediction with very small water depth is done over a smaller domain $L = 593.75$. Fig. 5.10 shows the solutions of the velocity and the water height for a constant water depth $H = 10$ and $H = 1$.

As can be seen in Fig. 5.9 and Fig. 5.10, the water height deviation remains approximately the same for various water depths. This is due to the forcing boundary condition. The error of the water height deviation is larger for shallower water. Furthermore, it can be observed that the velocity increases for decreasing water depths. As expected, the numerical solution is more accurate for larger constant water depths. The fully numerical solution has a large error in the amplitude of the velocity. This is confirmed in the amplitude convergence illustrated in Fig. 5.11. Additionally, the solutions are less dependent on the initial condition for shallower water since the friction increases.
Fig. 5.11 illustrates the slow convergence of the amplitudes for both the velocity and the water height deviation for the fully numerical solution, compared to the analytical solution and the solution in the frequency domain. Even for a fine grid, a slight under- and overestimation remains for the amplitudes of the velocity and water height deviation, respectively.

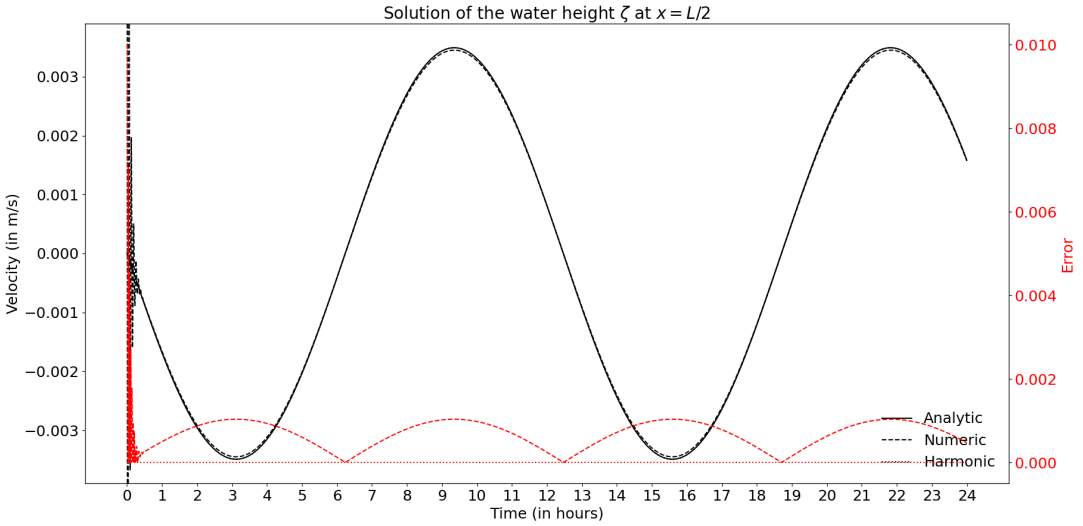


**(a)** Solutions of the velocity $u$ for $H = 10$.

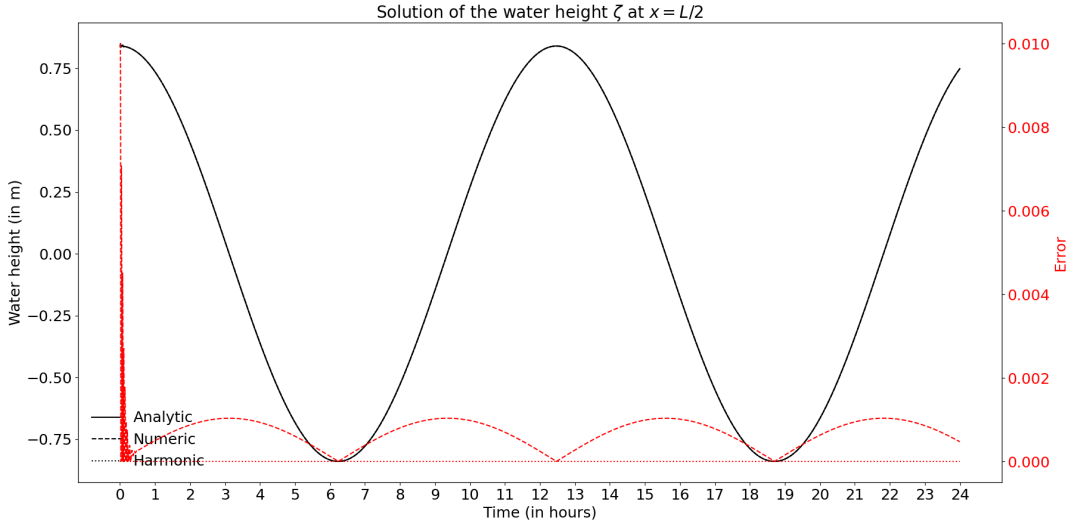


**(b)** Solutions of the water height $\zeta$ for $H = 10$.

**Fig. 5.9:** Solutions of the velocity and the water height at $x = L/2$ for water depth $H = 10$, over time for the period of one day.

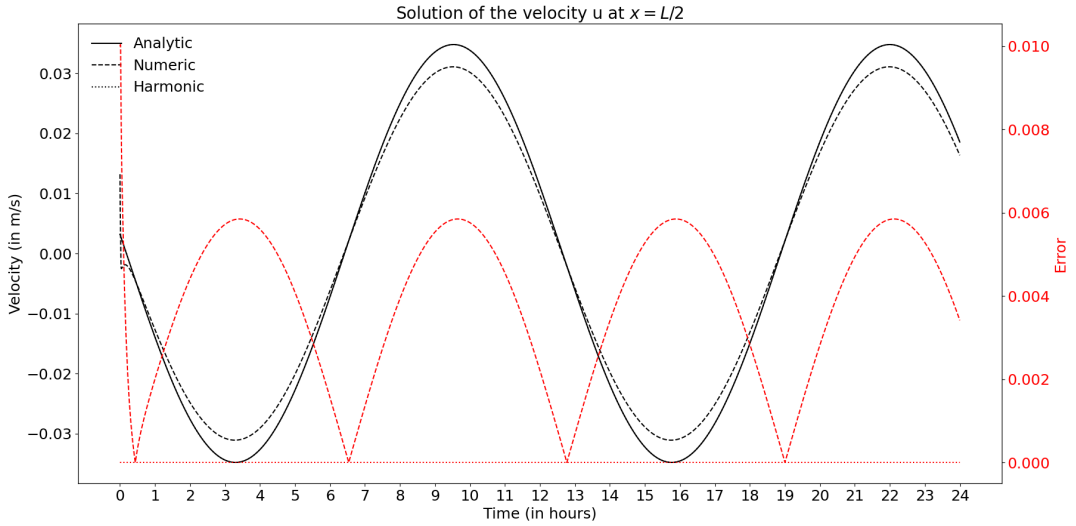


**(a)** Solutions of the velocity $u$ for $H = 1$.

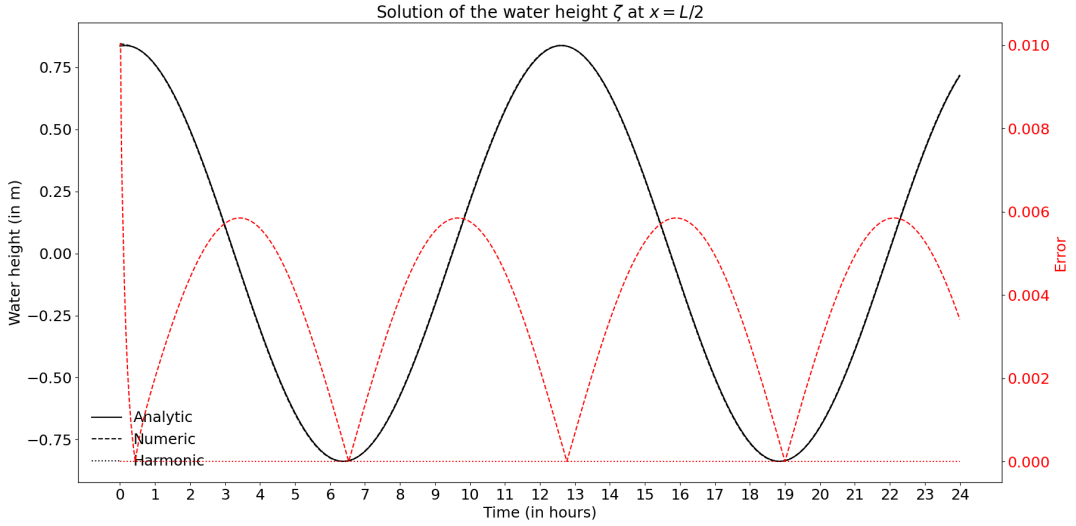


**(b)** Solutions of the water height $\zeta$ for $H = 1$.

**Fig. 5.10:** Solutions of the velocity and the water height at $x = L/2$ for water depth $H = 1$, over time for the period of one day.

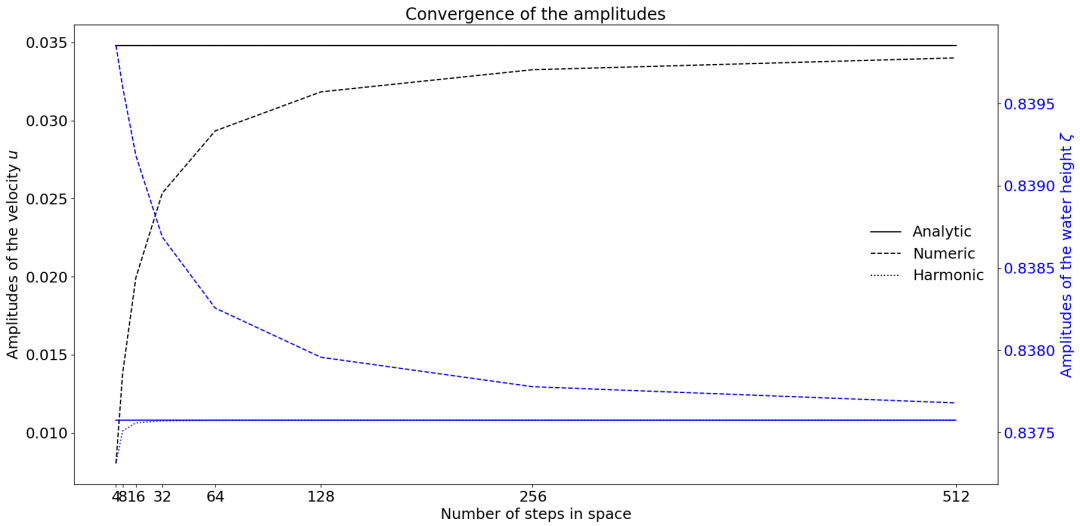


**Fig. 5.11:** Amplitude convergence of the velocity on the right-hand axis and the water height deviation on the left-hand axis, for water depth $H = 1$m.

Finally, three variable seabeds are considered: a linear, a quadratic and a square root seabed where the water depth decreases near the coast. These seabeds have been chosen to illustrate the basic influence of the bottom.

Similarly to the constant small water depth, the bottom had little influence on the water height

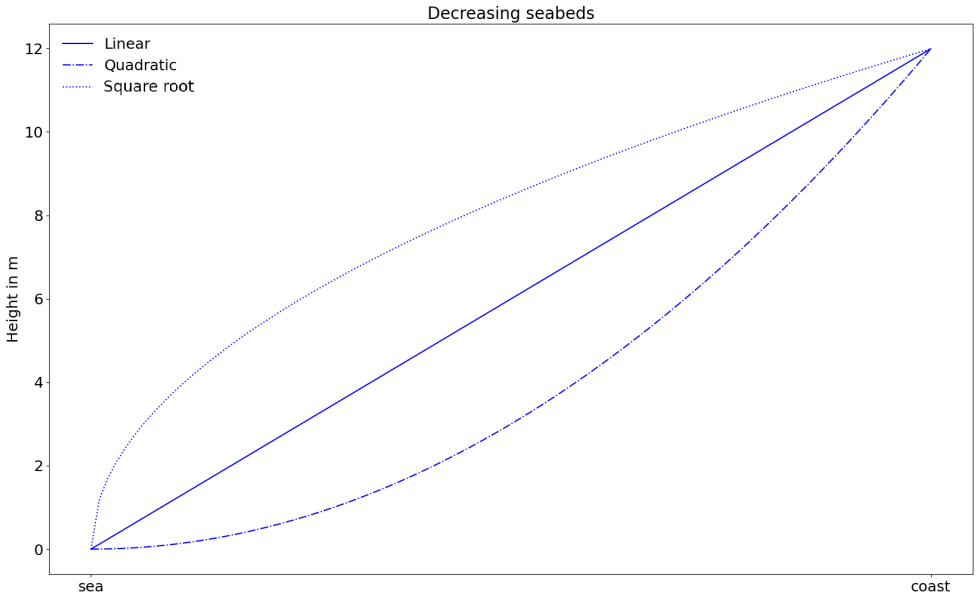


**Fig. 5.12:** A linear, quadratic and square root decreasing seabed.

elevation due to the forcing boundary. The velocity solutions for the different seabeds are given in Fig. 5.13. The water depth starts at $H = 12$ and decreases to $H = 0.01$. The solutions are plotted near the coast at $x = L - \Delta x$ where the water depth should be close to zero for all bottoms. Fig. 5.13 shows that the solutions in the frequency domain are similar, while the fully numerical solutions differ much more. The fully numerical solutions suggest a larger velocity for slower decreasing water depth, however these solutions differ only due to inaccuracy. Similar to the constant smaller water depth, solutions for fast decreasing water depth need a finer grid for accurate results. The solutions

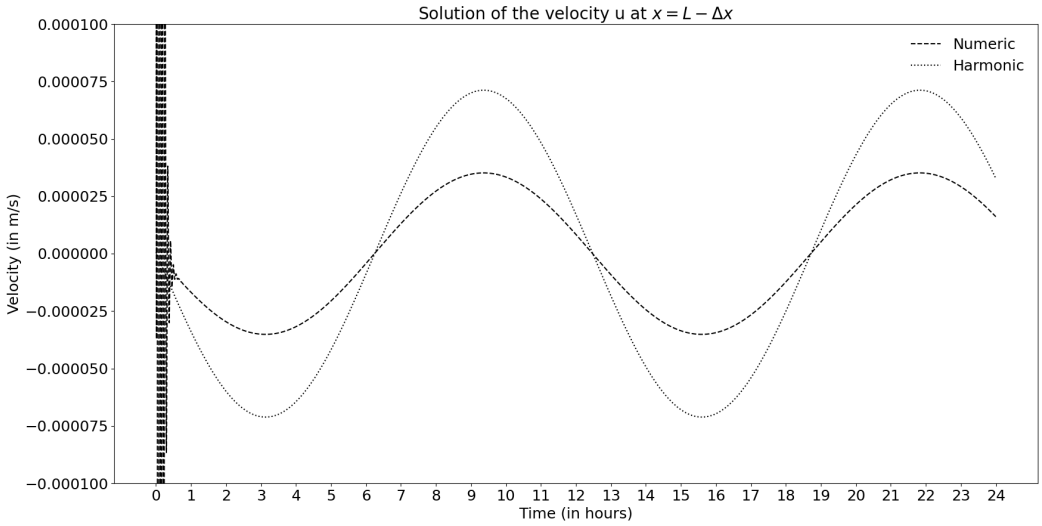


**(a)** Solutions of the velocity $u$ for a linear seabed.

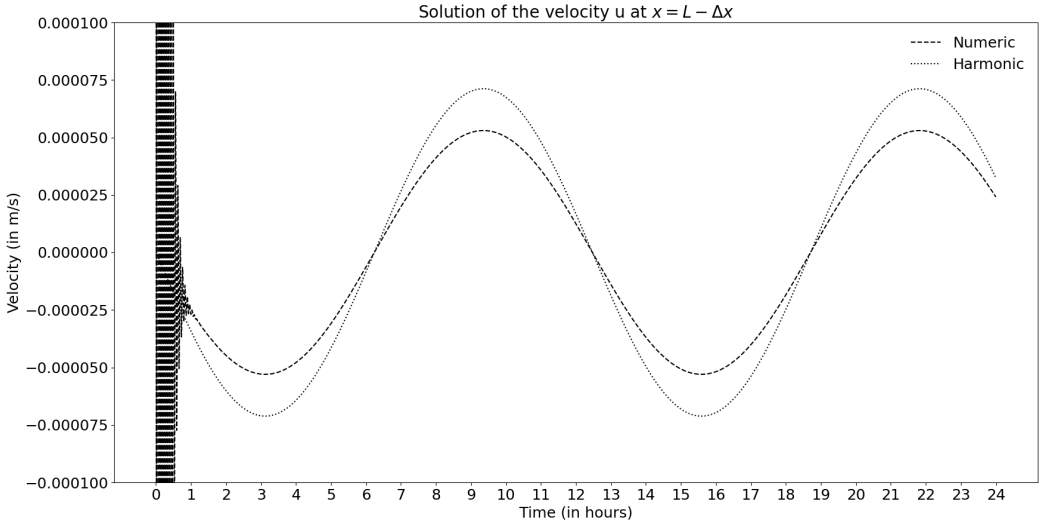


**(b)** Solutions of the velocity $u$ for a quadratic seabed.

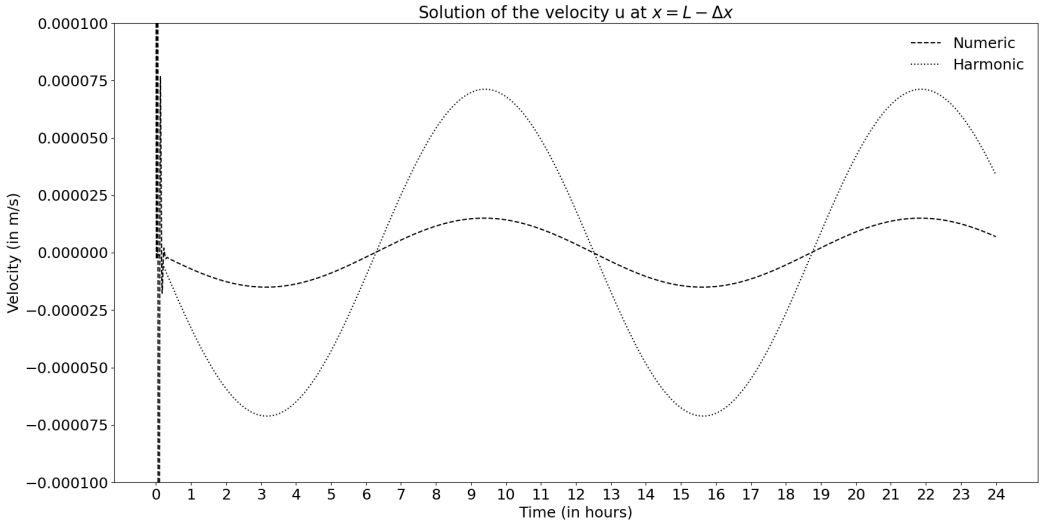


**(c)** Solutions of the velocity $u$ for a square root seabed.

**Fig. 5.13:** Solutions of the velocity at $x = L - \Delta x$ for decreasing water depth, over time for the period of one day. The dashed line is the fully numerical solution (numeric) and the dotted line is the solution in the frequency domain (harmonic).

for the square root seabed show little dependence on the initial condition and underestimation of the amplitude of the velocity. The solution for the quadratic seabed are quite different, with more influence from the initial condition and much more accurate amplitudes. Meanwhile the solutions for the linear seabed appear to be an average of the two other seabeds. The square root seabed decreases to a small water depth fastest whereas the quadratic seabed decreases much slower and the linear seabed is in between the two, explaining the results. To substantiate that the amplitudes of the fully numerical solution do convergence to the amplitudes of the solution in the frequency domain, we perform an amplitude convergence analysis given in Fig. 5.14 The amplitudes convergence for all variable seabeds.

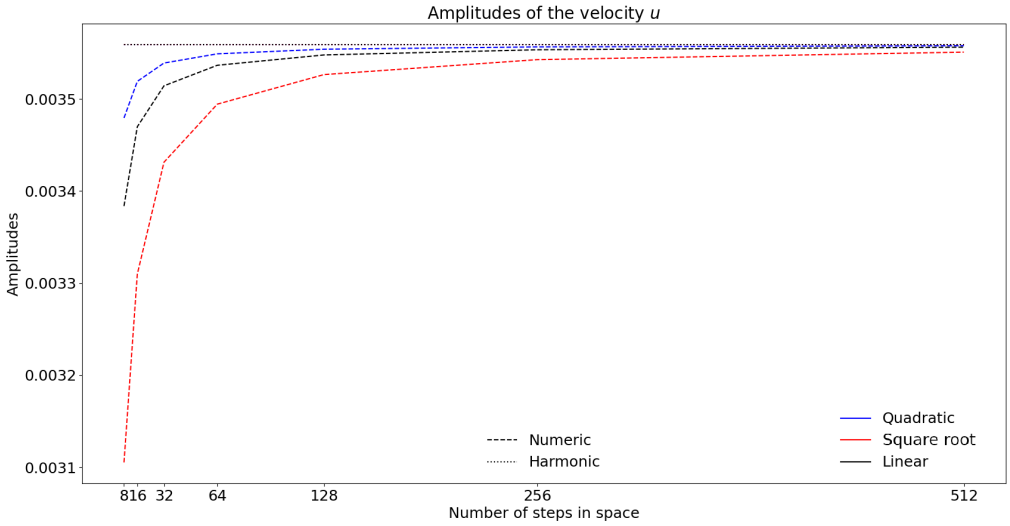


**(a)** Amplitude convergence of the velocity $u$ for variable seabeds.

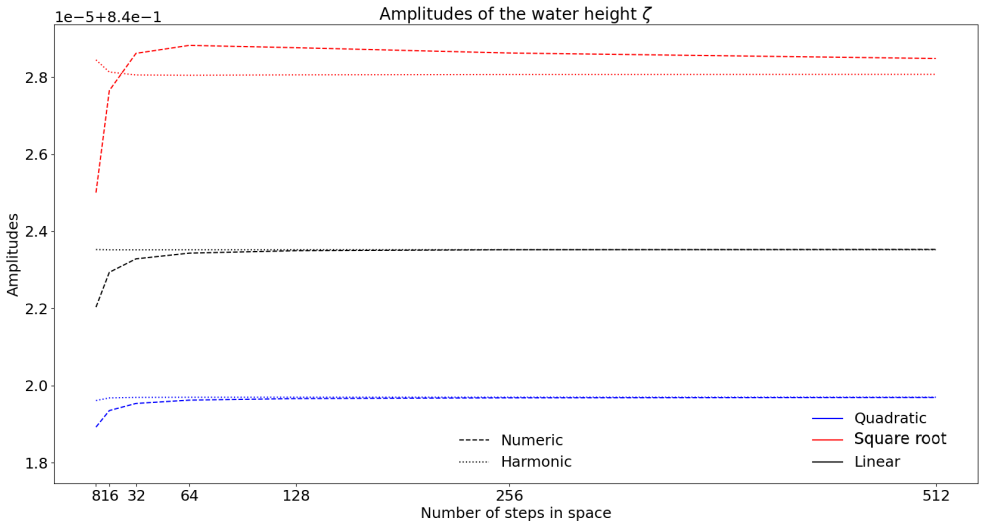


**(b)** Amplitude convergence of the water height deviation $\zeta$ for variable seabeds.

**Fig. 5.14:** Amplitude convergence for variable seabeds.

As expected, the convergence of the amplitude of the fully numerical solution is slower for the square root seabed. For this case, there is no analytical solution to compare the solutions with. Therefore, the rates of convergence are determined by considering previous iterations. The solutions are compared halfway across the domain at $x = L/2$.

| N | u, linear | z, linear | u, quadratic | z, quadratic | u, square root | z, square root |
|---|---|---|---|---|---|---|
| 8-16 | 2.32E-04 | 3.41E-04 | 3.58E-04 | 4.54E-04 | 2.20E-04 | 2.45E-04 |
| 16-32 | 1.40E-04 | 1.99E-04 | 2.47E-04 | 2.97E-04 | 1.27E-04 | 1.44E-04 |
| 32-64 | 8.22E-05 | 1.12E-04 | 1.58E-04 | 1.89E-04 | 7.08E-05 | 8.07E-05 |
| 64-128 | 4.56E-05 | 6.20E-05 | 9.56E-05 | 1.16E-04 | 4.33E-05 | 4.84E-05 |
| 128-256 | 2.50E-05 | 3.31E-05 | 5.62E-05 | 6.95E-05 | 2.77E-05 | 3.16E-05 |
| 256-512 | 1.43E-05 | 1.85E-05 | 3.24E-05 | 3.96E-05 | 1.80E-05 | 2.16E-05 |

**Table 5.3:** Mean absolute errors between the fully numerical solutions of an increasing amount of discretisation steps, for the linear, quadratic and square root seabed.

This

| N | u, linear | z, linear | u, quadratic | z, quadratic | u, square root | z, square root |
|---|---|---|---|---|---|---|
| 8-16 | 3.464E-07 | 4.19E-06 | 6.91E-08 | 2.27E-06 | 1.45E-06 | 1.22E-05 |
| 16-32 | 1.78E-07 | 1.10E-06 | 4.08E-08 | 5.88E-07 | 7.21E-07 | 2.52E-06 |
| 32-64 | 8.80E-08 | 2.78E-07 | 2.17E-08 | 1.48E-07 | 3.40E-07 | 3.75E-07 |
| 64-128 | 4.15E-08 | 6.97E-08 | 1.08E-08 | 3.72E-08 | 1.49E-07 | 6.26E-08 |
| 128-256 | 1.81E-08 | 1.75E-08 | 5.14E-09 | 9.30E-09 | 5.73E-08 | 3.43E-08 |
| 256-512 | 6.99E-09 | 4.39E-09 | 2.25E-09 | 2.33E-09 | 1.79E-08 | 2.06E-08 |

**Table 5.4:** Mean absolute errors between the solutions in the frequency domain of an increasing amount of discretisation steps, for the linear, quadratic and square root seabed.

This gives average convergence rates $P_{numeric} = 1.68$ and $P_{harmonic} = 3.16$. It is important to note that the convergence rates of the solutions in the frequency domain (harmonic) are much smaller for the velocities than for the water height deviations.
For this simple linear case, the solution method in the frequency domain is much more accurate than the numerical method, with a twice as large order of accuracy. Furthermore, this method does not require an initial condition. Most importantly, the solution in the frequency domain is computationally more efficient than the fully numerical method. One iteration of the fully numerical method requires the same amount of matrix vector multiplication as the entire method in the frequency domain. The solution in the frequency domain is therefore computationally much more efficient than the fully numerical solution.

## 5.5 Conclusion

In this chapter, it has been shown that the linearised classical shallow water equations can easily be solved using the frequency domain and that this method is favourable compared to the fully numerical method. For more complex problems, more frequencies need to be considered increasing the complexity of the method or, using an approximation of a finite amount of frequencies, decreasing the accuracy of the solution. This will be tested using the statistical shallow water equations in Chapter 6.

# 6

# Analysis of the statistical shallow water equations

In this chapter the shallow water equations obtained by the statistical depth-averaging approach are solved and discussed. At first, the time-dependecies are overleooked as the derivative with respect to time is set to zero. The resulting stationary equations are first discretised in space using a Galerkin approach in Section 6.1, before applying time discretisation for the fully numerical method in Section 6.2 and frequency approximation in Section 6.3. The new equations are tested by considering a purely wet domain for varying seabeds, the results are discussed in Section 6.4

## 6.1 Discretisation in space

We start by discretising the one dimensional statistical shallow water equations (given in Eqns. (4.35)) in space. To do so, we consider the stationary system of equations. Furthermore, we assume $\epsilon \cong 1$, since convective inertia is usually negligible at small water depths [1]. Note that for a wet domain, $\eta = 1$ and the water volume per unit area $Y$ for the one dimensional system is simply given by $\zeta - h_f$. This leads to the following stationary system of equations

$$\begin{cases} \dfrac{\partial u}{\partial x} = 0, \\ -\dfrac{\partial}{\partial x}\left(\dfrac{\widetilde{u}}{Y}u\right) + gY\dfrac{|\widetilde{u}|}{K_s^2 H_k^{10/3}}u + gY\dfrac{\partial \zeta}{\partial x} = 0, \\ \zeta(0) = H_r + A, \quad \dfrac{\partial u}{\partial x}(0) = 0, \\ \dfrac{\partial \zeta}{\partial x}(L) = 0, \qquad u(L) = 0. \end{cases} \tag{6.1}$$

Now we can apply centered space discretisation, but to generalise the results a finite element method with a Galerkin approach is used.

### 6.1.1 Finite element method

The nonlinear convection term and the nonlinear friction are linearised by using the Picard iteration such that $u \approx \widetilde{u}$ can be considered constant for each time step and over each element.

Multiplying by the test function $v$ and integrating over the domain results in the weak formulation

$$\int_0^L \frac{\partial u}{\partial x} v dx = 0, \tag{6.2a}$$

$$-\int_0^L \frac{\widetilde{u}}{Y} u \frac{\partial v}{\partial x} + gY\frac{|\widetilde{u}|}{K_s^2 H_k^{10/3}} uv + gY\frac{\partial \zeta}{\partial x} v dx = 0. \tag{6.2b}$$

To obtain the Galerkin equations, the variables are approximated using the basis function for the elements $\varphi$. The velocity $u$ and the water height $\zeta$ can be approximated by $u(x) \approx \sum_{j=0}^{n} u_j \varphi_j(x)$ and $\zeta(x) \approx \sum_{j=0}^{n} z_j \varphi_j(x)$, and the test function is taken as $v = \varphi_i$. The Galerkin equations are

$$\sum_{j=0}^{n} u_j \int_0^L \frac{\partial \varphi_j}{\partial x} \varphi_i dx = 0, \tag{6.3a}$$

$$-\sum_{j=0}^{n} u_j \int_0^L \frac{\widetilde{u}}{Y} \varphi_j \frac{\partial \varphi_i}{\partial x} + gY \frac{|\widetilde{u}|}{K_s^2 H_k^{10/3}} \varphi_j \varphi_i dx + \sum_{j=0}^{n} z_j \int_0^L gY \frac{\partial \varphi_j}{\partial x} \varphi_i dx = 0. \tag{6.3b}$$

To write the solution in matrix vector notation, we define

$$M_{ij} = \int_0^L \varphi_i \varphi_j dx, \tag{6.4}$$

$$S_{ij} = \int_0^L \varphi_i \frac{\partial \varphi_j}{\partial x} dx, \tag{6.5}$$

$$\widetilde{S_{ij}} = \int_0^L \frac{\partial \varphi_i}{\partial x} \varphi_j dx, \tag{6.6}$$

$$\tag{6.7}$$

and compute the three element matrices

$$M^{e_k} = \begin{pmatrix} M^{e_k}_{k-1k-1} & M^{e_k}_{k-1k} \\ M^{e_k}_{kk-1} & M^{e_k}_{kk} \end{pmatrix}, \quad S^{e_k} = \begin{pmatrix} S^{e_k}_{k-1k-1} & S^{e_k}_{k-1k} \\ S^{e_k}_{kk-1} & S^{e_k}_{kk} \end{pmatrix}, \quad \widetilde{S^{e_k}} = \begin{pmatrix} S^{e_k}_{k-1k-1} & S^{e_k}_{k-1k} \\ S^{e_k}_{kk-1} & S^{e_k}_{kk} \end{pmatrix}. \tag{6.8}$$

The linear Lagrangian polynomials are chosen as basis function, such that by using Holand & Bel's theorem the element matrices can be computed and are given by [26]

$$M^{e_k} = \begin{pmatrix} \frac{\Delta x}{3} & \frac{\Delta x}{6} \\ \frac{\Delta x}{6} & \frac{\Delta x}{3} \end{pmatrix}, \qquad S^{e_k} = \begin{pmatrix} -\frac{1}{2} & \frac{1}{2} \\ -\frac{1}{2} & \frac{1}{2} \end{pmatrix}, \qquad \widetilde{S^{e_k}} = \begin{pmatrix} -\frac{1}{2} & -\frac{1}{2} \\ \frac{1}{2} & \frac{1}{2} \end{pmatrix}. \tag{6.9}$$

Assuming $\widetilde{u}$ and vectors $Y$ and $H$ are constant over each element, the stationary system can now be written in matrix vector notation as

$$S\mathbf{u} = 0, \tag{6.10a}$$

$$-\frac{\widetilde{\mathbf{u}}}{Y} \widetilde{S}\mathbf{u} + gY \frac{|\widetilde{\mathbf{u}}|}{K_s^2 H_k^{10/3}} M\mathbf{u} + gYS\mathbf{z} = 0. \tag{6.10b}$$

## 6.2 Fully numerical solution

Finally, we apply forward Euler to the full system. We define $\widetilde{\mathbf{u}} = \mathbf{u}^k$ as the solution of the velocity in the previous time step and let $LF$ be a matrix that applies Lax-Friedrich relaxation. This results in

$$\mathbf{u}^{k+1} = \left( I + \Delta t \frac{\mathbf{u}^k}{Y} M^{-1} \widetilde{S} - \Delta t \frac{|\mathbf{u}^k|}{K_s^2 H_k^{10/3}} \right) LF\mathbf{u}^k - \Delta t g Y M^{-1} S\mathbf{z}^k, \tag{6.11a}$$

$$\mathbf{z}^{k+1} = LF\mathbf{z}^k - \Delta t \eta^{-1} M^{-1} S\mathbf{u}^k. \tag{6.11b}$$

Before moving to the solution in the frequency domain, the new equations are tested using the fully numerical solution. This provides insight to the behaviour of the nonlinear terms. The solution is compared to the previous results. The absolute water depth is set to 10, the bottom elevation is defined as a Gaussian distribution with mean 0.5 with a standard deviation of 1. Since the new equations have been applied to a domain without any partially dry areas, the results can be compared to our previously obtained results of the numerical method given in Section 5.3.1. To compare these methods

we let $\frac{r}{H_r} \sim \frac{Y|\mathbf{u}|}{K_s^2 H_k^{10/3}} \sim 10^{-8}$. We plot the solutions of both methods along with the equivalent depth $H_k$ and effective water depth $Y$, to analyse their behaviour. The results are given in Fig. 6.1.

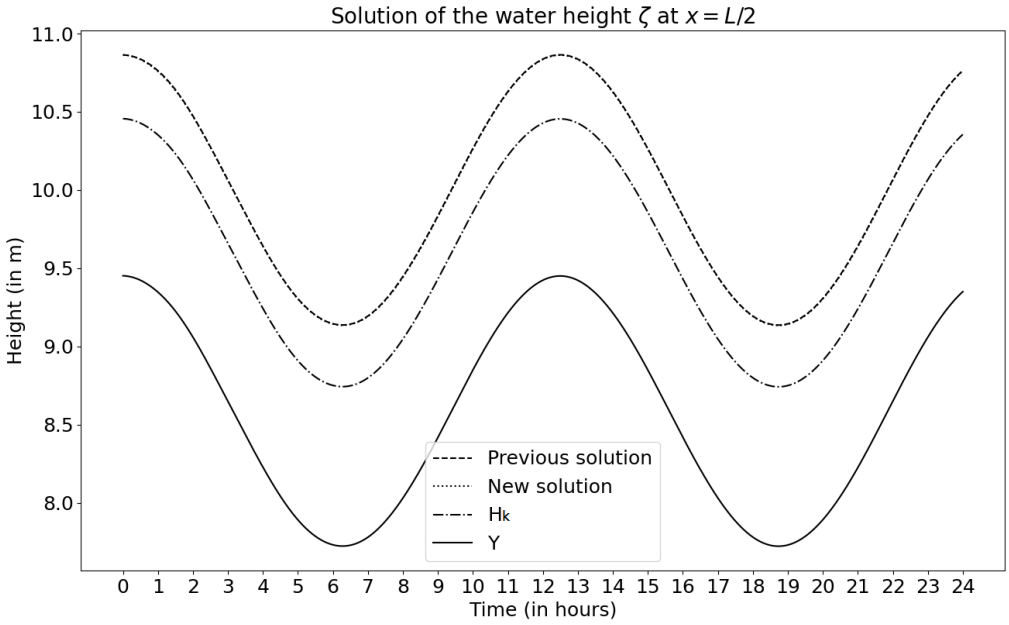


**Fig. 6.1:** Fully numerical solutions of the water height

Fig. 6.1 shows the fully numerical solutions of the water height and the corresponding equivalent water depth $H_k$ and effective water depth $Y$. As expected, the new solution is nearly identical to the previous solution obtained in Chapter 5. The solutions of the water depths over time indicate that the variables and parameters can be approximated as infinite sums over frequencies within the same frequency domain.

## 6.3 Solution in the frequency domain

From the results of the numerical method, it follows that $u$, $\zeta$, $Y$ and $H$ can all be approximated as an infinite sum over frequencies that are a multiple of the forcing frequency.

Applying FEM and substituting the approximations based on the frequency domain, we get:

$$\sum_{n=-N}^{N} -in\sigma\eta M z_n e^{-in\sigma t} + \sum_{n=-N}^{N} S u_n e^{-in\sigma t} = 0, \tag{6.12a}$$

$$\begin{aligned} &\sum_{n=-N}^{N} -in\sigma M u_n e^{-in\sigma t} - \sum_{m=-N}^{N} \alpha_m e^{-im\sigma t} \sum_{n=-N}^{N} \widetilde{S} u_n e^{-in\sigma t} + \\ &\sum_{m=-N}^{N} \beta_m e^{-im\sigma t} \sum_{n=-N}^{N} M u_n e^{-in\sigma t} + \sum_{m=-N}^{N} \gamma_m e^{-im\sigma t} \sum_{n=-N}^{N} S z_n e^{-in\sigma t} = 0, \end{aligned} \tag{6.12b}$$

where $M$, $S$ and $\widetilde{S}$ are the finite element matrices and the coefficients $\alpha_n$, $\beta_n$ and $\gamma_n$ are the Fourier

coefficients corresponding to the projections of the functions

$$\begin{aligned}\frac{u}{Y} &\approx \sum_{n=-N}^{N} \alpha_n(x) e^{-in\sigma t},\\ g\frac{|u|Y}{K_s^2 H_k^{10/3}} &\approx \sum_{n=-N}^{N} \beta_n(x) e^{-in\sigma t},\\ gY &\approx \sum_{n=-N}^{N} \gamma_n(x) e^{-in\sigma t},\end{aligned}$$

on the various frequencies. $N$ is the number of tidal constituents taken into account. These coefficients are determined at a previous iteration using a Fast Fourier transform.
For $N = 1$, this results in six unknown variables: $u_{-1}, u_0, u_1, z_{-1}, z_0, z_1$ and since Eqns. (6.12) must hold for all $t$, six equations:

$$\begin{aligned}i\sigma\eta M z_{-1} + S u_{-1} &= 0,\\ S u_0 &= 0,\\ -i\sigma\eta M z_1 + S u_1 &= 0,\\ i\sigma M u_{-1} - \alpha_{-1}\widetilde{S}u_0 - \alpha_0\widetilde{S}u_{-1} + \beta_{-1}Mu_0 + \beta_0 M u_{-1} + \gamma_{-1}Sz_0 + \gamma_0 S z_{-1} &= 0,\\ -\alpha_{-1}\widetilde{S}u_1 - \alpha_0\widetilde{S}u_0 - \alpha_1\widetilde{S}u_{-1} + \beta_{-1}Mu_1 + \beta_0 M u_0 + \beta_1 M u_{-1} + \gamma_{-1}Sz_1 + \gamma_0 S z_0 + \gamma_1 S z_{-1} &= 0,\\ -i\sigma M u_1 - \alpha_0\widetilde{S}u_1 - \alpha_1\widetilde{S}u_0 + \beta_0 M u_1 + \beta_1 M u_0 + \gamma_0 S z_1 + \gamma_1 S z_0 &= 0.\end{aligned}$$

This can be extended to more frequency components, leading to a larger system of equations.

## 6.4 Results

To compare the solution to the previous results discussed in Chapter 5, the solutions are derived for a water motion over a purely wet domain with a constant seabed. The domain is divided into a grid of $n = 100$ for a period of 24 hours, for the fully numerical solution the CFL condition is used to derive the timestep and for the solution in the frequency domain, the number of frequency components considered is set to $N = 5$. Fig. 6.2 shows the solution for water motion in a domain with a reference water depth $H = 11$ with a constant bottom $h_b = 1$. As expected, the solutions are dominated by the linear terms and therefore very close to the linear analytical solutions. The influence of the nonlinear terms increases for more shallow water. In Fig. 6.3 the solutions of the water motion over a domain with the same reference water depth and a constant bottom of $h_b = 10$ are shown. The fully numerical solution of the velocity indicates nonlinearities, whereas the solution in the frequency domain appears to be predominantly linear. Fourier analysis of the solutions allows analysis of the amplitudes of the velocity solutions. These are given in Fig. 6.4.
As can be seen in Fig. 6.4c, the fully numerical velocity solution in very shallow water is dominated by the forcing frequency and one multiple of the forcing frequency. For larger water depths, the solution is dominated solely by the forcing frequency. The solution in the frequency domain shows no other frequencies than the forcing frequency, indicating it does not adequately address the nonlinearities.
Next, a linearly varying seabed is considered. The seabed starts at $h_b = 6$ and linearly increases to a partially dry domain at $h_b = 12$, with a reference height $H_r = 11$. The amplitude of the bottom elevations is chosen as $a_r = 4$. The Fig. 6.5 shows the fully numerical solutions and Fig. 6.6 gives the corresponding frequencies of the velocity solution. The fully numerical velocity solution shows some slight nonlinearities and a small dependence on one multiple of the forcing frequency. The numerical solution method works well for the partially dry domain and indicates that a small number of frequencies is sufficient to approximate a solution.

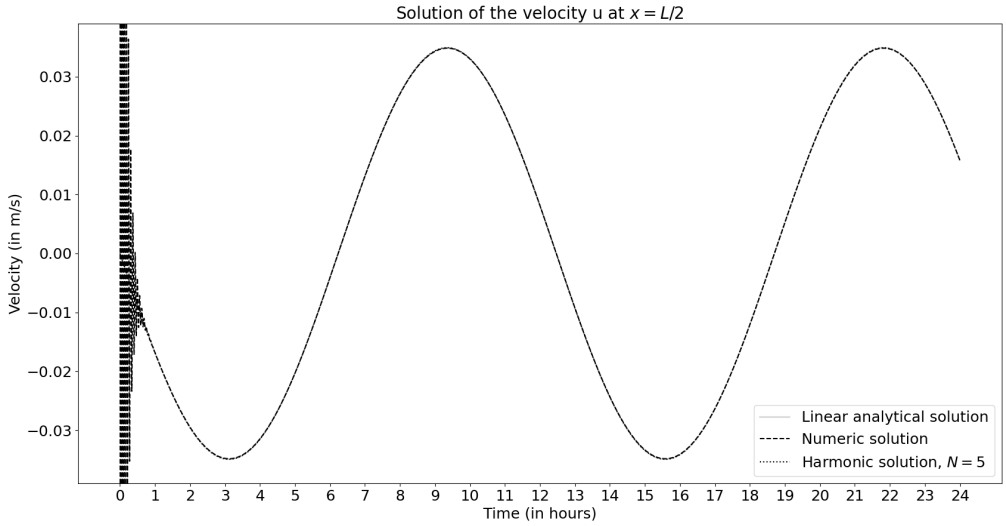


**(a)** Solutions of the velocity $u$ for $H = 10$.

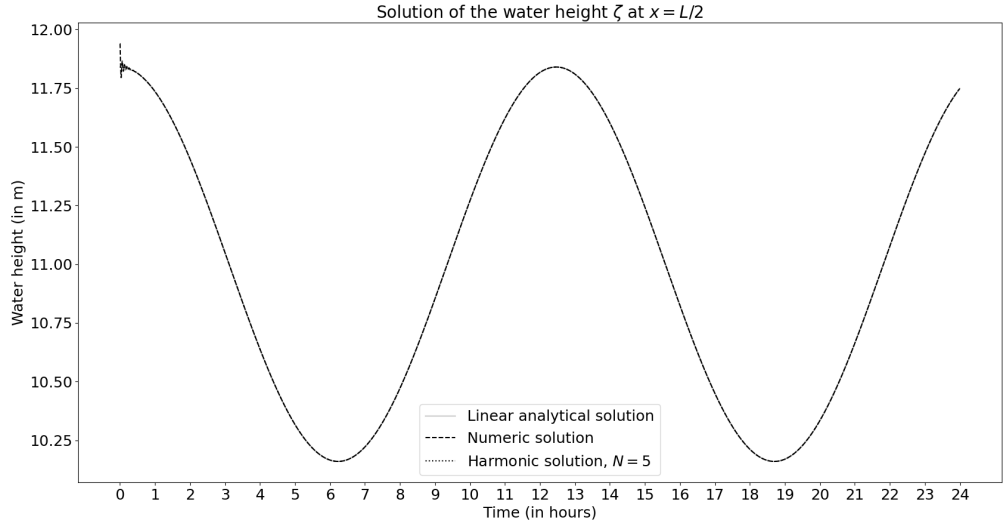


**(b)** Solutions of the water height $\zeta$ for $H = 10$.

**Fig. 6.2:** Solutions of the velocity and the water height at $x = L/2$ for water depth $H = 10$, over time for the period of one day.

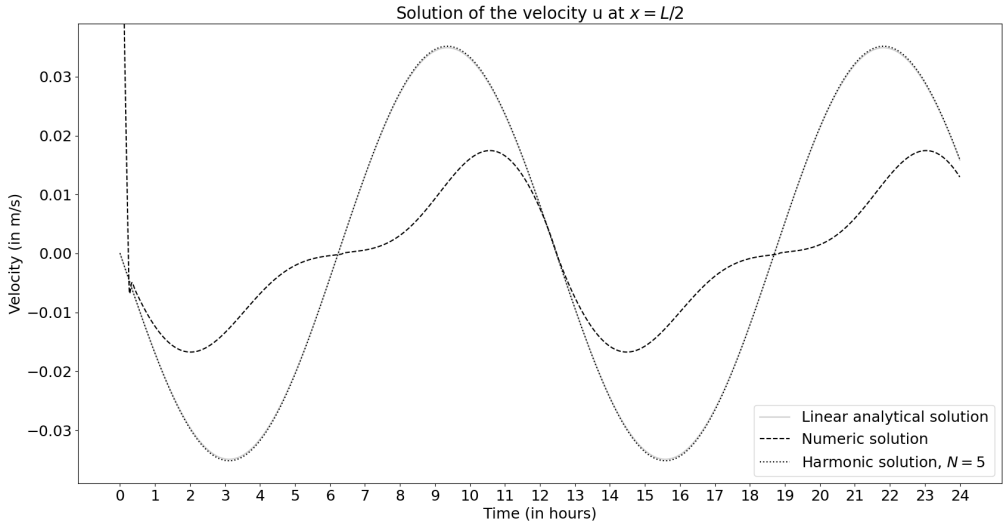


**(a)** Solutions of the velocity $u$ for $H = 1$.

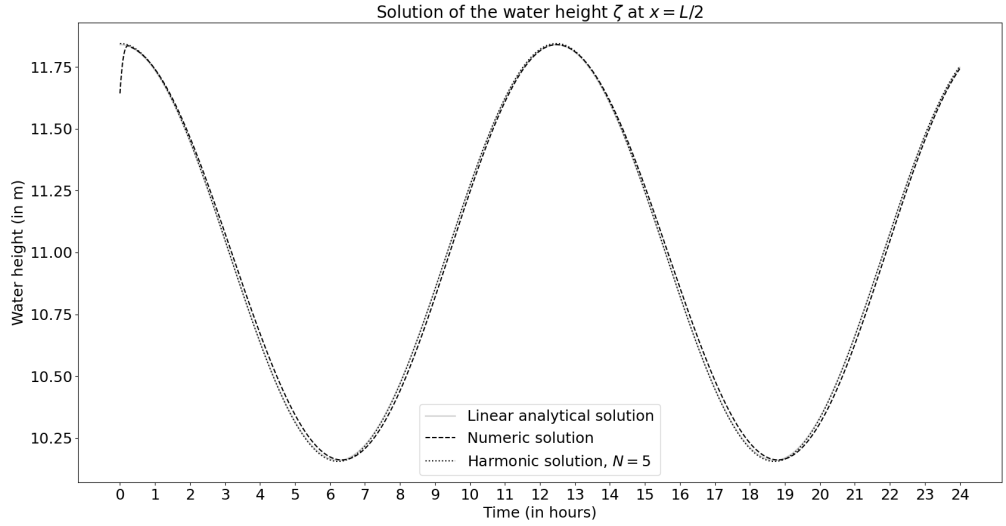


**(b)** Solutions of the water height $\zeta$ for $H = 1$.

**Fig. 6.3:** Solutions of the velocity and the water height at $x = L/2$ for water depth $H = 1$, over time for the period of one day.

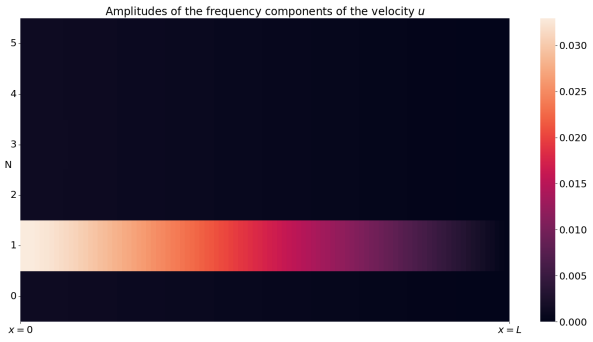


**(a)** Amplitudes of the frequency components $N$ of the fully numerical solutions of the velocity $u$ for $H = 1$.

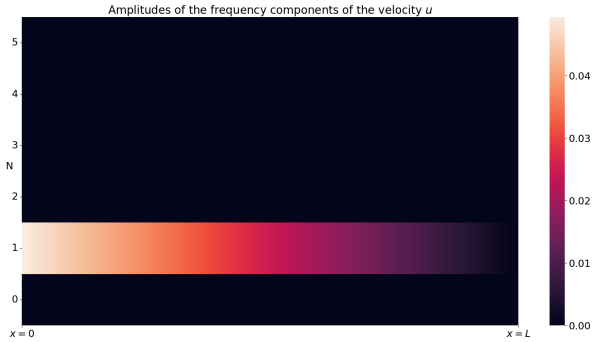


**(b)** Amplitudes of the frequency components $N$ of the solution in the frequency domain of the velocity $u$ for $H = 1$for $H = 1$.

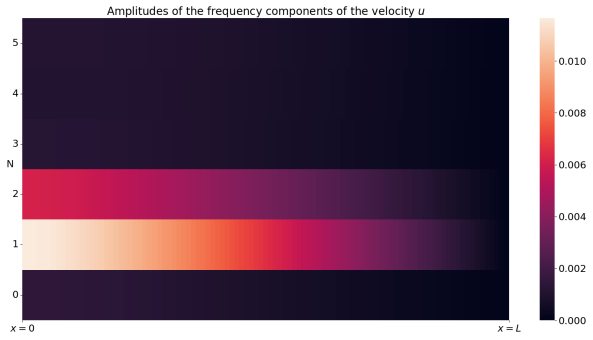


**(c)** Amplitudes of the frequency components $N$ of the fully numerical solution of the velocity $u$ for $h_b = 10$.

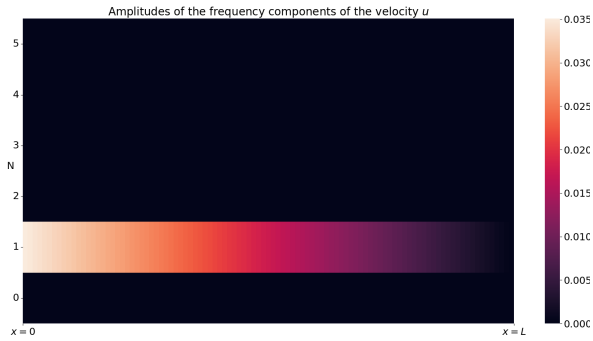


**(d)** Amplitudes of the frequency components $N$ of the solution in the frequency domain of the velocity $u$ for $h_b = 10$.

**Fig. 6.4:** Amplitudes of the frequency components $N$ of the solutions of the velocity $u$ for two different constant bottoms $h_b = 1$ and $h_b = 10$.

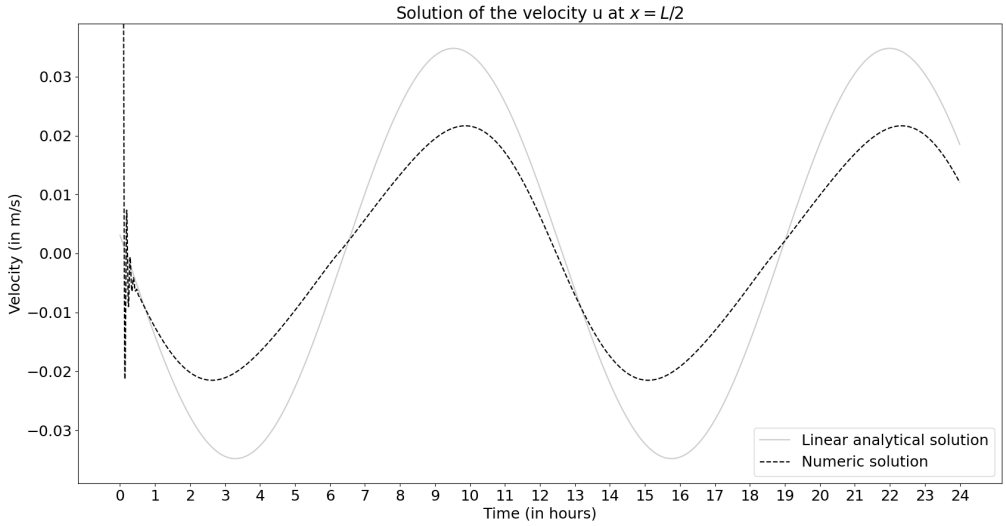


**(a)** Solutions of the velocity $u$ for $H = 1$.

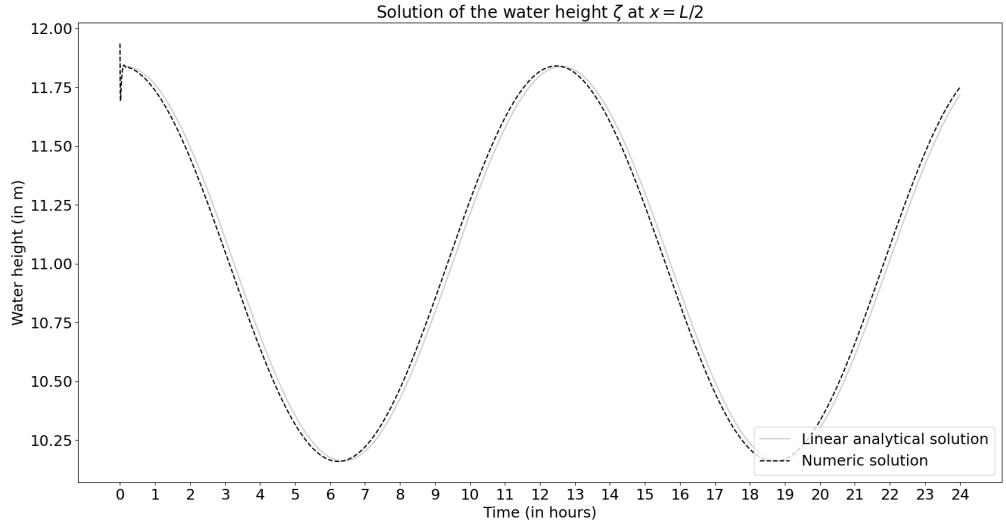


**(b)** Solutions of the water height $\zeta$ for $H = 1$.

**Fig. 6.5:** Solutions of the velocity and the water height at $x = L/2$ for water depth $H = 1$, over time for the period of one day.

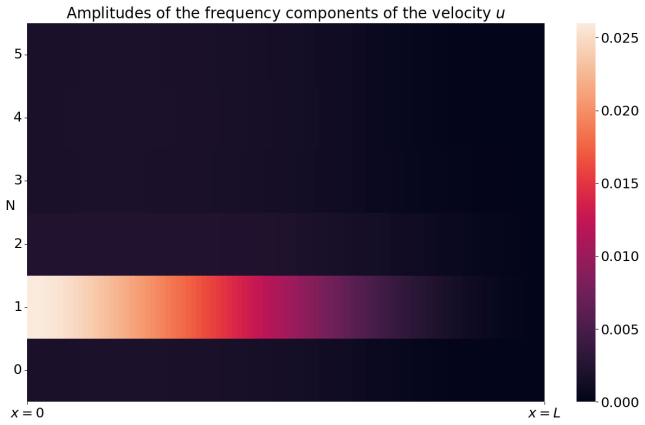


**Fig. 6.6:** Caption

## 6.5 Conclusion

While the solutions in the frequency domain give an accurate indication of the water height $\zeta$, the expected nonlinearities are neglected where they should not be. The linear terms describing the first frequencies appear to be dominate the solution, whereas the fully numerical solutions show dependence on the first multiple of the forcing frequency. Similar results are found for varying seabeds. In contrast to the results of the classical shallow water equations, the fully numerical solution is better equipped to handle the nonlinearities that arise in very shallow waters and tidal flats. The fully numerical solution indicates the solutions can be approximated by the sum of a small number of frequencies.

# 7

# Conclusion

This thesis focuses on the prediction of water motion over tidal flats in the frequency domain. Most existing research focuses on numerical methods which are computationally expensive and require high-quality input data. Furthermore, the classical shallow water equations are only equipped to handle purely wet domains. This thesis presents a water motion solution in the frequency domain. Promising results are found for the classical shallow water equation and future research is needed for the statistical shallow water equations that allow partially dry domains.

As is explained in Chapter 2, tides are generated by tidal forces and result in various tidal constituents. Each constituent has its own frequency. The amplitudes and phases can be found by data analysis. These amplitudes, frequencies and phases are all that are needed for water motion prediction. Tidal analysis shows that a few constituents are enough for accurate water motion prediction. This provides the motivation of water motion prediction in the frequency domain.

For shallow water over a purely wet domain, the classical shallow water equations are derived and linearised. For not too shallow water, the nonlinear terms may be neglected. The new solution method in the frequency domain is compared to a fully numerical solution. The solution in the frequency domain gives more accurate results and faster convergence while being less computationally intensive. The fully numerical solution needs a large number of steps in space for accurate results. This result could be improved using a combination of a coarse and refined mesh. Furthermore, larger domains should be tested for a larger number of steps in space. This is too computationally expense for the scope of this thesis.
Another way to improve the accuracy of the fully numerical solution, is using a different time scheme. It is challenging to find a stable and accurate fully numerical method for a system of equations with first order derivatives in space and time. More research on the available methods should be done.
The challenges of the fully numerical method give extra motivation for a new method. Frequency approximation turns the system of equations to a system of first order ordinary differential equations. The solutions are stable and accurate and computationally much faster than the fully numerical solutions. While the solutions have only been tested for one dimensional cases, this can easily be extended to two dimensional cases. Two dimensional domains would allow for more interesting domains and the approximation of existing tidal inlets. Future research should consider this for more elaborate results.

More research is required for water motion prediction in the frequency domain over tidal flats. The results of the method are less promising for more complex problems, such as the statistical shallow water equations discussed in Chapter 6. The nonlinearities arising in very shallow and partially dry areas, impose some challenges. First of all, in order to derive a solvable problem the nonlinear terms need to be approximated using projections of a previous iteration. Since this requires input data and more extensive computations as well as more iterations, some of the attractive qualities of the new method are hereby lost. Future research should consider a different solution for dealing with the nonlinear terms. Furthermore, considering multiple frequencies requires more computations. While the method can easily be extended to consider any finite amount of frequencies, each frequency adds four variables

and equations. This complicates the computations. The method is not yet able to distinguish multiple frequencies.

In conclusion, this thesis presents a new method for predicting water motion over tidal flats in the frequency domain. For simple problems, this approach provides accurate results with faster convergence and less computational cost compared to existing numerical methods. The method cannot yet be used for water motion prediction over tidal flats due to nonlinearities arising in very shallow and partially dry areas. Further research is required to address these challenges.

# References


1. Defina, A. Two-dimensional shallow flow equations for partially dry areas. *Water Resources Research* **36,** 3251–3264. ISSN: 00431397 (2000).
2. Withers, K. & Tunnell, J. W. J. *Identification of Tidal Flat Alterations and Determination of Effects on Biological Productivity of These Habitats Within the Coastal Bend Corpus Christi Bay National Estuary Program* tech. rep. (1998).
3. Unesco, W. H. C. *Wadden Sea* `https://whc.unesco.org/en/list/1314/`.
4. Department of Oceanography, N. p. s. *Basic Concepts in Physical Oceanography: Tides*
5. Blumberg, A. F. & Bruno, M. S. in *The Urban Ocean* 52–71 (Cambridge University Press, 2018). `https://www.cambridge.org/core/product/identifier/9781108123839%23CN-bp-6/type/book_part`.
6. Gerkema, T. *An Introduction to Tides* ISBN: 9781316998793 (Cambridge University Press, July 2019).
7. Lopes, A. M. & Tenreiro Machado, J. Tidal Analysis Using Time–Frequency Signal Processing and Information Clustering. *Entropy* **19,** 390. ISSN: 1099-4300 (July 2017).
8. Cox, S. *Pytides* `https://github.com/sam-cox/pytides`.
9. Fox, R. W. & McDonald, A. T. *Introduction to Fluid Mechanics* Fourth edition (John Wiley & Sons, 1994).
10. Batchelor, G. K. *An Introduction to Fluid Dynamics* ISBN: 9780521663960 (Cambridge University Press, Feb. 2000).
11. Kundu, P. K., Cohen, I. M. & Dowling, D. R. Geophysical Fluid Dynamics. *Fluid Mechanics,* 621–690. `https://linkinghub.elsevier.com/retrieve/pii/B9780123821003100137` (Jan. 2012).
12. *Lecture material-Environmental Hydraulic Simulation* tech. rep. (2006). `http://daad.wb.tu-harburg.de`.
13. Vreugdenhil, C. B. *Numerical Methods for Shallow-Water Flow* ISBN: 978-90-481-4472-3 (Springer Netherlands, Dordrecht, 1994).
14. Cushman-Roisin, B. & Beckers, J.-M. *Introduction to geophysical fluid dynamics* ISBN: 9780080916781 (Academic press, 2009).
15. Burchard, H., Hetland, R. D., Schulz, E. & Schuttelaars, H. M. Drivers of Residual Estuarine Circulation in Tidally Energetic Estuaries: Straight and Irrotational Channels with Parabolic Cross Section. *Journal of Physical Oceanography* **41,** 548–570. ISSN: 1520-0485 (Mar. 2011).
16. Terra, G. M., Jan van de Berg, W. & Maas, L. R. M. Experimental verification of Lorentz' linearization procedure for quadratic friction. *Fluid Dynamics Research* **36,** 175–188. ISSN: 0169-5983 (Mar. 2005).
17. Roos, P. C. *et al.* Unsteady Linearisation of Bed Shear Stress for Idealised Storm Surge Modelling. *Journal of Marine Science and Engineering* **9,** 1160. ISSN: 2077-1312 (Oct. 2021).
18. Pedlosky, J. *Geophysical Fluid Dynamics* ISBN: 978-0-387-96387-7 (Springer New York, New York, NY, 1987).
19. Rozendaal, M. P. *An Idealised Morphodynamic Model of a Tidal Inlet and the Adjacent Sea* tech. rep. (2018). `https://repository.tudelft.nl/`.
20. Defina, A., D'Alpaos, L. & Matticchio, B. *A new set of equations for very shallow water and partially dry areas suitable to 2d numerical models* in *Proceedings of the speciality conference on "Modelling of flood propagation over initially drya areas"* (eds Molinaro, P. & Natale, L.) (American society of civil engineers, New York, 1994), 72–81.

21. Mandelbrot, B. B. & Wheeler, J. A. The Fractal Geometry of Nature. *American Journal of Physics* **51,** 286–287. ISSN: 0002-9505 (Mar. 1983).

22. D'Alpaos, L., Defina, A. & Matticchio, B. *2D finite element modelling of flooding due to river bank collapse* in *Proceeding of the speciality conference on "Modelling of flood propagation over initially dry areas"* (eds Molinaro, P. & Natale, L.) (American society of civil engineers, New York, 1994), 60–71.

23. Defina, A. Appendix to: Two-dimensional shallow flow equations for partially dry areas. *Water Resources Research,* 3261–3263 (2000).

24. Rezzolla, L. *Numerical Methods for the Solution of Partial Differential Equations* tech. rep. (2020).

25. Ter Brake, M. C. *Tidal embayments : modelling and understanding their morphodynamics.* ISBN: 9789461130334 ([s.n.], 2011).

26. Van Kan, J., Segal, A. & Vermolen, F. *Numerical methods in scientific computing* second edition (Delft Academic Press, 2014).

27. Godin, G. *The analysis of tides* (University of Toronto Press, 1972).

28. Luijendijk, A. P. *Validation, calibration and evaluation of Delft3D-FLOW model with ferry measurements* tech. rep. (2001).

# A

# Rayleigh criterion

Many of the tidal constituents have relatively similar frequencies. This can complicate tidal analysis, making it difficult to distinguish constituents. To do so Godin discovered a requirement for the minimum length of the time series known as the Rayleigh criterion [27]. This criterion requires that all the constituents included in the harmonic analysis of a given time series must be separated by at least one complete period from their neighbouring constituents over the length of data record. In other words:

$$\|f_2 - f_1\| = \frac{1}{T}, \tag{A.1}$$

where $f_1$ and $f_2$ are the frequencies of the constituents and $T$ is the record length of the data set. Tab. A.1 below shows the minimum required observation period or record length to distinguish some important diurnal and semidiurnal constituents.

| | $O_1$ | $P_1$ | $K_1$ | $mu_2$ | $N_2$ | $nu_2$ | $M_2$ | $\lambda_2$ | $L_2$ | $S_2$ | $K_2$ | $M_4$ | $MS_4$ | $M_6$ |
|---|---|---|---|---|---|---|---|---|---|---|---|---|---|---|
| $O_1$ | | 14.8 | 13.7 | 1.1 | 1 | 1 | 1 | 1 | 1 | 0.9 | 0.9 | 0.3 | 0.3 | 0.2 |
| $P_1$ | | | 183 | 1.1 | 1.1 | 1.1 | 1.1 | 1 | 1 | 1 | 1 | 0.3 | 0.3 | 0.2 |
| $K_1$ | | | | 1.2 | 1.1 | 1.1 | 1.1 | 1 | 1 | 1 | 1 | 0.3 | 0.3 | 0.2 |
| $mu_2$ | | | | | 31.8 | 27.6 | 14.8 | 10.1 | 9.6 | 7.4 | 7.1 | 0.5 | 0.5 | 0.3 |
| $N_2$ | | | | | | 206 | 27.6 | 14.8 | 13.8 | 9.6 | 9.1 | 0.5 | 0.5 | 0.3 |
| $nu_2$ | | | | | | | 31.8 | 15.9 | 14.8 | 10.1 | 9.6 | 0.5 | 0.5 | 0.3 |
| $M_2$ | | | | | | | | 31.8 | 27.6 | 14.8 | 13.7 | 0.5 | 0.5 | 0.3 |
| $\lambda 2$ | | | | | | | | | 206 | 27.6 | 23.9 | 0.5 | 0.5 | 0.3 |
| $L_2$ | | | | | | | | | | 31.7 | 27.1 | 0.5 | 0.5 | 0.3 |
| $S_2$ | | | | | | | | | | | 183 | 0.5 | 0.5 | 0.3 |
| $K_2$ | | | | | | | | | | | | 0.5 | 0.5 | 0.3 |
| $M_4$ | | | | | | | | | | | | | 14.8 | 0.5 |
| $MS_4$ | | | | | | | | | | | | | | 0.5 |
| $M_6$ | | | | | | | | | | | | | | |

**Table A.1:** Periods in days needed to distinguish two constituents, provided by [28].

# B

# Derivation of the Reynolds Averaged Navier Stokes equations

The convective terms follow from:

$$\frac{\partial}{\partial x}\left(\nu\frac{\partial\overline{u_x}}{\partial x}-\overline{u_x'^2}\right)+\frac{\partial}{\partial y}\left(\nu\frac{\partial\overline{u_x}}{\partial y}-\overline{u_x'u_y'}\right)+\frac{\partial}{\partial z}\left(\nu\frac{\partial\overline{u_x}}{\partial z}-\overline{u_x'u_z'}\right)=$$
$$\frac{\partial}{\partial x}\left(\nu\frac{\partial\overline{u_x}}{\partial x}+2\eta_h\frac{\partial\overline{u_x}}{\partial x}\right)+\frac{\partial}{\partial y}\left(\nu\frac{\partial\overline{u_x}}{\partial y}+\eta_h\frac{\partial\overline{u_x}}{\partial y}+\eta_h\frac{\partial\overline{u_y}}{\partial x}\right)+\frac{\partial}{\partial z}\left(\nu\frac{\partial\overline{u_x}}{\partial z}+\eta_h\frac{\partial\overline{u_x}}{\partial z}+\eta_h\frac{\partial\overline{u_z}}{\partial x}\right)=$$
$$\frac{\partial}{\partial x}\left((\nu+\eta_h)\frac{\partial\overline{u_x}}{\partial x}\right)+\frac{\partial}{\partial x}\left(\eta_h\frac{\partial\overline{u_x}}{\partial x}\right)+\frac{\partial}{\partial y}\left((\nu+\eta_h)\frac{\partial\overline{u_x}}{\partial y}\right)+$$
$$\frac{\partial}{\partial y}\left(\eta_h\frac{\partial\overline{u_y}}{\partial x}\right)+\frac{\partial}{\partial z}\left((\nu+\eta_v)\frac{\partial\overline{u_x}}{\partial z}\right)+\frac{\partial}{\partial z}\left(\eta_h\frac{\partial\overline{u_z}}{\partial x}\right)=$$
$$\frac{\partial}{\partial x}\left((\nu+\eta_h)\frac{\partial\overline{u_x}}{\partial x}\right)+\frac{\partial}{\partial y}\left((\nu+\eta_h)\frac{\partial\overline{u_x}}{\partial y}\right)+\frac{\partial}{\partial z}\left((\nu+\eta_v)\frac{\partial\overline{u_x}}{\partial z}\right)+\frac{\partial}{\partial x}\eta_h\left(\frac{\partial\overline{u_x}}{\partial x}+\frac{\partial\overline{u_y}}{\partial y}+\frac{\partial\overline{u_z}}{\partial z}\right)=$$
$$\frac{\partial}{\partial x}\left((\nu+\eta_h)\frac{\partial\overline{u_x}}{\partial x}\right)+\frac{\partial}{\partial y}\left((\nu+\eta_h)\frac{\partial\overline{u_x}}{\partial y}\right)+\frac{\partial}{\partial z}\left((\nu+\eta_v)\frac{\partial\overline{u_x}}{\partial z}\right)$$

# C

# Scaling

The resulting shallow water equations contain many nonlinear terms complicating analysis of the system. Therefore, scaling analysis is applied to determine which terms may be neglected under certain circumstances.

The physical variables and parameters are made dimensionless by

$$t = \frac{1}{\sigma}t', \qquad \zeta = A\zeta',$$
$$x = Lx', \qquad u = Uu'.$$

. Since the seabed varies between zero and the water depth $H$, we define the dimension of the variable seabed by $h_b = Hh'$.
Substitution of the dimensionless variables and parameters in the mass balance equation gives

$$\frac{UH}{L}\frac{\partial}{\partial x'}((1+\frac{A\zeta'}{H}-h')u'_x) + \frac{UH}{L}\frac{\partial}{\partial x'}((1+\frac{A\zeta'}{H}-h')u'_y) + \sigma A\frac{\partial \zeta'}{\partial t'} = 0$$

It follows that for this balance to hold, the orders of magnitude of all terms must be of the same order thus $\sigma A \sim \frac{UH}{L}$. The values of the parameters for the Ameland system are given in Tab. C.1, the values are provided by [25]. These estimations of the parameters provide the order of magnitude of the parameters needed for the analysis.

| Variables | | Parameters | |
|---|---|---|---|
| H | 12 m | f | $10^{-4}$ rad/s |
| L | $1.9 \cdot 10^4$ m | g | 9.81 m/s$^2$ |
| U | 0.19 m/s | r | $4 \cdot 10^{-4}$ m/s |
| A | 0.84 m | $\widetilde{\mu_h}$ | 10 m$^2$/s |
| $\sigma$ | $1.4 \cdot 10^{-4}$ rad/s | | |

(C.1)

Substitution of the scaling and the dimensionless parameters and variables in the momentum equation in the $x$-direction gives

$$\sigma U\frac{\partial u'_x}{\partial t} + \frac{U^2}{L}\mathbf{u}'\nabla u'_x - fUu'_y = -\frac{gA}{L}\frac{\partial \zeta'}{\partial x'} + \frac{U}{H(1+A\zeta'/H-h')}\left[\frac{HD}{L^2}\nabla\cdot(1+A\zeta'/H-h')\nabla u'_x) - ru'_x\right],$$
$$\frac{\partial u'_x}{\partial t} + \frac{U}{\sigma L}\mathbf{u}'\nabla u'_x - \frac{f}{\sigma}u'_y = -\frac{gA}{\sigma UL}\frac{\partial \zeta'}{\partial x'} + \frac{1}{\sigma H(1+A\zeta'/H-h')}\left[\frac{HD}{L^2}\nabla\cdot(1+A\zeta'/H-h')\nabla u'_x) - ru'_x\right].$$

The order of magnitude of all the terms are given by

| $\frac{\partial u'_x}{\partial t}$ | $\mathbf{u}'\nabla u'_x$ | $fu'_y$ | $\frac{\partial \zeta'}{\partial x'}$ | $\frac{1}{H+\zeta-h_b}\nabla\cdot(D_2\nabla u'_x)$ | $ru'_x$ |
|---|---|---|---|---|---|
| 1 | $\frac{U}{\sigma L}$ | $\frac{f}{\sigma}$ | $-\frac{gA}{\sigma UL}$ | $\frac{\widetilde{\mu_h}}{\sigma L^2}$ | $\frac{r}{H\sigma}$ |
| 1 | $7.1 \cdot 10^{-2}$ | 0.71 | 16 | $2.0 \cdot 10^{-4}$ | 0.24 |

(C.2)

The order of magnitude for the y-directional terms are assumed equal. Furthermore $A/H \sim 7 \cdot 10^{-2}$, thus all nonlinear terms may be neglected and assuming $h(x)$ known, this leads to a simple linear system.

# D

# Homogeneous solution

Solutions to partial differential equations can be divided into the homogeneous solution and the particular solution. For the simplified one dimensional system, the homogeneous solution converges to zero and is therefore neglected. This will be shown here.
We start with the homogeneous system

$$\begin{cases} H\dfrac{\partial u}{\partial x} + \dfrac{\partial \zeta}{\partial t} = 0, \\ \dfrac{\partial u}{\partial t} = -g\dfrac{\partial \zeta}{\partial x} - \dfrac{r}{H}u, \\ u(t, L) = 0, \\ \zeta(t, 0) = 0. \end{cases} \tag{D.1}$$

For the homogeneous problem, we can apply the method of separation of variables. First, we rewrite the system to two independent system by applying the operator $\partial/\partial t + r/H$ to the mass balance equation and the operator $\partial/\partial t$ to the momentum balance equation and substitution of the other equation. This gives two similar independent systems

$$\begin{cases} \dfrac{\partial^2 u}{\partial t^2} - gH\dfrac{\partial^2 u}{\partial x^2} + \dfrac{r}{H}\dfrac{\partial u}{\partial t} = 0, \\ \dfrac{\partial u}{\partial x}(t, 0) = 0, \\ u(t, L) = 0, \end{cases} \qquad \begin{cases} \dfrac{\partial^2 \zeta}{\partial t^2} - gH\dfrac{\partial^2 \zeta}{\partial x^2} + \dfrac{r}{H}\dfrac{\partial \zeta}{\partial t} = 0, \\ \zeta(t, 0) = 0, \\ \dfrac{\partial \zeta}{\partial x}(t, L) = 0. \end{cases} \tag{D.2}$$

Separation of variables gives

$$\begin{aligned} F(x)G''(t) - gHF''(x)G(t) + \frac{r}{H}F(x)G'(t) = 0 \\ \frac{1}{G(t)}G''(t) - gH\frac{1}{F(x)}F''(x) + \frac{r}{H}\frac{1}{G(t)}G'(t) = 0 \\ gH\frac{1}{F(x)}F''(x) = \frac{1}{G(t)}G''(t) + \frac{r}{H}\frac{1}{G(t)}G'(t) = -\lambda \end{aligned} \tag{D.3}$$

which give the following general solutions

$$F(x) = a_1 e^{i\sqrt{\lambda/gH}x} + a_2 e^{-i\sqrt{\lambda/gH}x}, \quad G(t) = b_1 e^{(-r/2H + \sqrt{r^2/4H^2 - \lambda})t} + b_2 e^{(-r/2H - \sqrt{r^2/4H^2 - \lambda})t}. \tag{D.4}$$

The eigenvalue $\lambda$ follows from the boundary conditions, while $u$ and $\zeta$ have different solution the resulting eigenvalue is the same. We find

$$\lambda = \frac{gH}{L^2}\left(\frac{\pi}{2} + \pi k\right)^2, \quad \text{with } k \in \mathbb{Z}.$$

Thus all eigenvalues are real and positive. We analyse the behaviour of the time-dependent solution $G(t)$. There are two cases to study:

Case 1

$$r^2/4H^2 + \lambda \geq 0. \tag{D.5}$$

Since $\lambda > 0$, it follows that $\sqrt{r^2/4H^2 - \lambda} \leq r/2H$ and thus

$$G(t) \leq b_1 + b_2 e^{(-r/H)t} \tag{D.6}$$

Case 2

$$r^2/4H^2 + \lambda \leq 0. \tag{D.7}$$

It follows that $\sqrt{r^2/4H^2 - \lambda}$ gives imaginary results and thus

$$Re\left[G(t)\right] = be^{(-r/2H)t} \tag{D.8}$$

Both cases result in the solution $G(t)$ converging to zero as $t \to \infty$.

# E

# Amplitude-phase formulation

As described in chapter 2, waves and tides are described by amplitudes and phases. So we are looking for solutions of the form $Ae^{i\theta(x)}$, where $A$ is the amplitude and $\theta$ is the phase. The amplitude and phase from complex solutions $Z(x)$ can be computed in the following way.

$$\begin{cases} \text{amplitude } A & = \sqrt{Re[Z(x)]^2 + Im[Z(x)]^2}, \\ \text{phase } \theta & = Arg[Z(x)], \end{cases} \tag{E.1}$$

where $Arg[Z(x)]$ is the principal argument of a complex number given by

$$Arg[Z(x)] = \begin{cases} \arctan\left(\dfrac{Im[Z(x)]}{Re[Z(x)]}\right) & \text{if } Re[Z(x)] > 0, \\ \arctan\left(\dfrac{Im[Z(x)]}{Re[Z(x)]}\right) + \pi & \text{if } Re[Z(x)] < 0 \text{ and } Im[Z(x)] \geq 0, \\ \arctan\left(\dfrac{Im[Z(x)]}{Re[Z(x)]}\right) - \pi & \text{if } Re[Z(x)] < 0 \text{ and } Im[Z(x)] < 0, \\ \dfrac{\pi}{2} & \text{if } Re[Z(x)] = 0 \text{ and } Im[Z(x)] > 0, \\ -\dfrac{\pi}{2} & \text{if } Re[Z(x)] = 0 \text{ and } Im[Z(x)] < 0, \\ undefined & \text{if } Re[Z(x)] = 0 \text{ and } Im[Z(x)] = 0. \end{cases} \tag{E.2}$$

We will use these definitions to rewrite the solutions into amplitude-phase formulation.